AD722029

ON THE TRANSMISSION OF SOUND FROM A MONOPOLE SOURCE THROUGH A FINITE, CORRUGATED BOUNDARY BETWEEN FLUID MEDIA

By J. A. Macaluso

The Pennsylvania State University
Institute for Science and Engineering
ORDNANCE RESEARCH LABORATORY
University Park, Pennsylvania

NAVY DEPARTMENT · NAVAL ORDNANCE SYSTEMS COMMAND

ABSTRACT

This investigation was undertaken with the objective of developing
techniques for solving the problem of sound transmission from a
harmonic monopole source through a finite, corrugated boundary between
fluid media and to corroborate these techniques by means of laboratory
data obtained for the important case of air-to-water sound transmission.

Using a form of the Kirchoff radiation integral, expressions were
derived describing both the refected and transmitted acoustic
potentials due to the scattering of monopole sound at a corrugated
boundary between fluids. For the case of sound transmission through
the boundary the integral expression was reduced to an approximate
closed-form solution which is valid in the limit of geometrical optics
and for extended interface geometries for which the tangent plane
approximation is applicable.

Empirical data was obtained using four different laboratory models
of corrugated (sinusoidal) surface sections designed to float on the
surface of an anechoic tank so as to simulate different corrugated air-
water boundaries. Numerous comparisons of theoretical results with
experimental data obtained by loudspeaker insonification of these
model surfaces demonstrated the suitability of the theory and illu-
strated the inaccuracies which arise in cases for which the tangent
plane approximation is unsuitable.

TABLE OF CONTENTS

TABLE OF CONTENTS (cont.)

TABLE OF CONTENTS (cont.)

LIST OF TABLES

LIST OF FIGURES

LIST OF FIGURES (cont.)

LIST OF FIGURES (cont.)

LIST OF FIGURES (cont.)

LIST OF FIGURES (cont.)

LIST OF SYMBOLS

Symbol	Description
c_1	Velocity of propagation in medium one
c_2	Velocity of propagation in medium two
d	Receiver depth
f	excitation frequency
H	Corrugation waveheight
h	y coordinate of source
i	$\sqrt{-1}$, except when used as a subscript
k_1	ω/c_1, magnitude of propagation vector, $\vec{k}_1$
k_2	ω/c_2, magnitude of propagation vector, $\vec{k}_2$
k_{1x}, k_{1y}, k_{1z}	Rectangular components of $\vec{k}_1$
k_{2x}, k_{2y}, k_{2z}	Rectangular componets of $\vec{k}_2$
n	c_2/c_1
p_i	Source acoustic pressure at unit distance
p_t	Transmitted acoustic pressure
R_0	Distance from source to interface

LIST OF SYMBOLS (cont.)

Symbol	Description
R_1	Distance from interface to receiver in medium 1
R_2	Distance from interface to receiver in medium 2
r_c	Radius of curvature of interface
r_{cm}	Minimum radius of curvature of corrugation
S	Reflection coefficient
T	Transmission coefficient
t	Time parameter
x,y,z	General field point corrdinates
x_i, y_i, z_i	Receiver ccordinates, i=1 cr 2
x_m, z_m	Coordinates of stationary phase point
y_0	Height of ccrrugaticn abcve xz plane
α	Local angle of incidence
γ	Initial corrugaticn displacement angle
θ_1	Angle of incidence
θ_2	Angle of transmission
λ_a	Acoustic wavelength in air

LIST OF SYMBOLS (cont.)

Symbol	Description
λ_ω	Acoustic wavelength in water
λ_s	Wavelength of corrugated surface
λ_1	Acoustic wavelength in source medium
ρ_1	Mass density of medium 1
ρ_2	Mass density of medium 2
$\bar{\phi}$	Space variation of the potential
ϕ_r	Reflected acoustic potential
ϕ_t	Transmitted acoustic potential
ϕ_{tm}	Transmitted potential due to stationary phase point at x_m, z_m
ω	Source radian frequency
ω_s	$2\pi/\lambda_s$

CHAPTER I

INTRODUCTION

General Introduction to the Problem Area

In recent years, a considerable amount of interest has evolved
regarding changes which occur in the characteristics of acoustic
signals which are transmitted within or between two media of different
characteristic impedances which share a common boundary. Of
particular interest is the problem of predicting the influence of
various rough boundary surface configurations on the characteristics
of these signals. Until very recently, such studies have been almost
entirely devoted to the problem of sound scattering (reflection) from
such boundaries by various classes of rough surfaces. Evidently,
this interest in acoustic signal scattering was motivated principally
by the need to understand the effects of rough surfaces such as that
of the sea surface or ocean bottom on various echo-ranging signals
transmitted in the ocean. However, with the development of more
sophisticated underwater acoustics equipment, it has become obvious
that reception of acoustic signals passing between air and water is
practicable. Hence, in order to more fully exploit this capability,
renewed interest has been shown in studies related to the problem
of sound transmission through various classes of rough surfaces
separating fluid media. Moreover, in addition to problems involving
sound transmission between different fluids separated by rough

boundaries, various related problems abound involving the transmission
of vibrational waves between fluid-solid and solid-solid interfaces
in such fields as oceanography and seismology. Hence, basic studies
which enhance our knowledge of vibrational wave transmission between
media separated by arbitrary boundary geometries can be expected to
contribute significantly to the advancement of technology even in
diciplines not directly involved with the transmission of sound waves,
per se.

Need for the Study

Present theoretical literature contains but scant reference to
the problem of sound transmission through a rough interface separating
two media of different characteristic impedances. That which does
exist deals in various approximate ways with the transmission of a
perfectly planar incident wave at the surface of an infinite boundary
described as a general periodic uneven surface or a boundary·comprised
of a corrugated surface extending to infinity in two directions. No
reference whatever has been found which relates to the point-source
rough interface transmission problem. Evidently, one of the reasons
that this latter problem has been virtually neglected to date is that
the mathematical difficulties encountered in the development of a
rigorous theoretical treatment have proven to be intractable. In fact,
Lysanov (1958) points out that it is impossible to use the method of
separation of variables to obtain a solution of the wave equation
which satisfies the boundary conditions specified on the uneven

surface. Denied the use of this powerful method for solving the
relevant system of equations, it is not difficult to appreciate the
mathematical complexities which result.

For the specific case of a simple (monopole) source in one medium,
both (wave) integral equations and geometrical optics-type (ray theory)
solutions exist which can be used to compute the sound field developed
in the adjacent medium, but only for the case of a smooth (flat)
boundary geometry. Much still remains to be done to extend these
techniques, or develop new ones, which will permit one to compute the
sound field in the adjacent media for rough boundary geometries.

Finally, no empirical data of any consequence appears to be
available for the case of sound transmitted between fluid media
separated by rough boundaries.

Specific Statement of the Problem

The objective of this study is to advance our understanding of
the processes involved in acoustic transmission between fluid media
which are separated by an uneven boundary surface. In this context,
the specific problem herein chosen for study concerns the description
of the steady-state sound field which arises in a fluid medium due to
the transmission of acoustic energy from a point (monopole) harmonic
source located in a second (adjacent) fluid medium sharing a common,
limited time-invariant corrugated boundary with the first.

Scope and Limitations of the Study

In order to advance our understanding of acoustic transmission between media separated by rough boundary surfaces this study was initiated to:

(1) Develop a mathematical model and computational procedure to predict the acoustic field in a fluid medium due to the operation of a point (monopole) harmonic source in a second fluid medium of different acoustic impedance. Each of the two homogeneous isotropic media are assumed to occupy its own infinite half-space. Transmission of acoustic energy is assumed to take place only through a finite portion of the common boundary between the two media. Further, the cross-section of the acoustically transparent interface between the media is assumed to be composed of regular corrugations (sinusoidal undulations).

(2) Obtain empirical data on the transmission of sound from air to water through a finite corrugated boundary surface with excitation frequency and source angle as parameters.

(3) Establish the suitability of the mathematical model by comparing predicted results with the empirical data obtained during the laboratory tests.

(4) Investigate various relationships between the physical parameters of the surface and source with the objective of defining the conditions under which the accuracy of the theoretical procedures will be maintained.

To facilitate the manipulation and evaluation of the expressions to be developed herein, it was necessary to introduce certain specific assumptions in the course of the mathematical analysis. Actually, these restrictions have become familiar in studies of this type and most, if not all of them, have been used, either implicitly or explicity, in all of the studies on scattering and refraction reported to date. These limitations include the following suppositions:

1. Multiple reflections in either medium can be ignored.

2. The source and receiver are restricted to positions not in the immediate vicinity of the interface in the sense that $k_1 R_0$ and $k_2 R_2$ are large.

3. Masking (shadowing) of one portion of the surface by adjacent ones need not be considered.

4. Transient effects are not included.

5. The tangent plane approximation is valid.

6. The spatial rate of change of the phase of the incident wave changes much more rapidly than that of the transmission or reflection coefficients in the region of the interface.

Note that no specific restriction on the height of the surface is made, providing the above assumptions remain valid.

Previous Related Studies

Apparently, the earliest and certainly the best known approximate approach to solving the problem of reflection and transmission of harmonic waves at a rough interface is that described by Rayleigh in

his "Theory of Sound" published in 1877 (See Reference 8). For a normally incident plane harmonic wave and an infinite sinusoidal surface, Rayleigh formulated a solution to the problem in terms of an equivalent problem in which the solution of an infinite set of linear equations must be found. Inverting this system, he obtained a solution to the transmitted wave in the form of an infinite series made up of individual terms representing distinct planar waves (the spectra) which are scattered in various directions. In order to evaluate the coefficients in the series, it is necessary to assume that the acoustic wavelength is much smaller than the wavelength of the surface undulations, observer and source are in the far field of the surface and the slope of the uneven surface is small.

A noteworthy extension of Rayleigh's basic treatment has been reported by Asano (1966). He assumes that a general periodic surface can be decomposed into a Fourier series composed of elementary corrugations and then proceeds to fit boundary conditions at a representative corrugated interface, much in the same way as Rayleigh. However, in addition to considering purely longitudinal vibrations, he includes transverse vibrations (shear waves) in his formulation for several cases of interest in seismology. Although his work is, for the most part, restricted to the case of plane normally incident elastic waves, he does include the subject of oblique incidence when the incident wave is of the plane longitudinal (P) type. Again, to facilitate application of the boundary conditions, both the amplitude and slope of the corrugations were assumed to be small.

By numerically evaluating the first two coefficients of the
resulting series solution, Asano reached several important conclusions
regarding the effects of corrugation amplitude and wavelength on the
strengths of the lower order spectral components. The most striking
observation noted was the presence of large, rapid fluctuations in
the values of the series coefficients as the ratio of the corrugation
wavelength to the wavelength of the incident P-wave (λ_S/λ_1) was varied
in the range of about one-half to two. Especially rapid changes were
frequently encountered for values of (λ_S/λ_1) just slightly less than
one. On the other hand, for values of (λ_S/λ_1) in excess of two, the
amplitude coefficients tended to remain reasonably constant. Although
his numerical evaluation was limited to velocity contrasts less than
two to one, Asano noted a tendancy toward greater fluctuation in the
amplitudes of all low order coefficients as the velocity contrast was
increased. He also noted a tendency for the regularly refracted
P-wave to gain energy at the expense of the regularly reflected P-wave
as the corrugation amplitude was increased. For the case of an
obliquely directed incident P-wave, the angle of incidence appeared to
have little effect on the regularly reflected and refracted P-waves
but a somewhat more significant (although still moderate) influence
on the irregularly reflected and refracted P-waves.

A particularly illuminating study of a related problem in the
field of electricity and magnetism is that of Park and Erteza (1969).
Undertaking to solve the problem of radiation from an arbitrarily
oriented electromagnetic dipole source in the presence of a rough,

imperfectly conducting earth, they present a form of the vector
Helmholtz integral which is suited for their application. By means of
this formulation, they proceed to express the reflected and transmitted
Hertz potentials in terms of the dyadic reflection and transmission
coefficients of the boundary. Applying themselves to a mathematical
model of a slightly rough surface described by a random process with
a stationary Gaussian height distribution, they obtain solutions of
the geometrical optics type for the expected Hertz potentials and
expected power arising from steady state excitation of an elementary
dipole. In addition to being a worthwhile exposition of an application
of the mathematics of geometrical optics to transmission in the
presence of a rough boundary, this recent contribution is apparently
the first significant work to be reported on the problem of scattered
electromagnetic transmission through a rough interface.

Mashashvili and Urusovskii (1969) report an extension of work
previously reported by Urusovskii (1965) in which they consider the
problem of plane wave diffraction by an extended periodically uneven
interface between two homogeneous media. Using the Green's formula,
together with the Hankel function representation of the incident wave
field, they make use of the periodicity of the integral kernels to
develop a solution for the reflected and transmitted pressure fields
in terms of a set of algebraic equations.

THEORETICAL DEVELOPMENT

Kirchoff Radiation Integral

Due to the similarity in the development of the integral equations for scattering (reflection) and transmission (refraction) arising from point source insonification of a corrugated boundary, it is useful to carry through the general theoretical development for both cases. However, methods for evaluating the resulting integral expressions as well as application of corroborative experimental work will be restricted to the case of transmission through the boundary. as indicated previously. However, it is important to emphasize that only minor modifications are required to adapt the computational procedures developed for sound transmission to the case of sound scattering (reflection).

An integral equation for the portion of the incident sound field scattered back into the original medium by the corrugations, as well as an expression for the field transmitted into the adjacent medium, may be found with the aid of the Kirchoff integral. In order to develop a form of the Kirchoff integral suited for use in the present study, we begin by consideration of Green's Theorem in the form (Reference 4, Page 15):

$$\int_V (\phi \nabla^2 \psi - \psi \nabla^2 \phi) dv = \oint_S (\phi \frac{\partial \psi}{\partial n} - \psi \frac{\partial \phi}{\partial n}) ds, \tag{2.1}$$

where ϕ and ψ are arbitrary scalar fields, dv is the differential element of volume, and ds the differential element of surface area. The partial derivative $\frac{\partial}{\partial n}$ denotes differentiation with respect to the unit normal directed outward from the volume under consideration.

For the solution of the Hyperbolic (wave) equation relevant to the present case, we require specification of Cauchy boundary conditions (the potential and its normal derivative) on an "open" surface (Reference 4, Page 17). Here, the open surface is the three-dimensional half-space at a fixed-time. We can manipulate Equation (2.1) to obtain an integral expression for the velocity potential at any point within the particular medium to be used in Equation (2.1) and for any time, t, greater than the fixed initial instant chosen. However, it is expedient to restrict ourselves to the steady-state time periodic case from the outset and, with this understanding, we can develop the pertinent form of the Kirchoff equation with minimal effort. Refer to the geometry depicted by Figure 1. Then using the subscript, i, to denote the numerals 1 or 2 (which refer to medium 1 or 2) and the subscript, j, to indicate the letters r or t for reflection or transmission, we let

$$\psi = \frac{e^{-i(\omega t - k_i R_i)}}{R_i} \quad . \tag{2.2}$$

Separating the time variation from the potential, we can write

$$\phi_j = \bar{\phi}_j \, e^{-i\omega t} \quad . \tag{2.3}$$

Now, the physics of the problem requires that the scattered potentials satisfy a homogeneous wave equation, i.e.,

$$\nabla^2 \phi_j - \frac{1}{c_i^2} \frac{\partial^2}{\partial t^2} \phi_j = 0, \tag{2.4}$$

or, using Equation (2.3),

$$\nabla^2 \bar{\phi}_j + k_i^2 \bar{\phi}_j = 0 \quad ; \quad k_i^2 \equiv \frac{\omega^2}{c_i^2} \quad . \tag{2.5}$$

Further, since ψ in Equation (2.2) is Green's function for the medium containing the observation point, it satisfies the equation

$$\nabla^2 \psi - \frac{1}{c_i^2} \frac{\partial^2}{\partial t^2} \psi = -4\pi \, \delta(\bar{R}_i) \, e^{-i\omega t} \tag{2.6}$$

or

$$\nabla^2 \left(\frac{e^{ik_i R_i}}{R_i}\right) + k_i^2 \left(\frac{e^{ik_i R_i}}{R_i}\right) = -4\pi \, \delta(\bar{R}_i). \tag{2.7}$$

Using Equations (2.2), (2.3), (2.5) and (2.7), it is easy to show that Equation (2.1) becomes:

$$\bar{\phi}_j (x_i, y_i, z_i) = \frac{1}{4\pi} \oint_S \frac{e^{ik_i R_i}}{R_i} \left[\frac{\partial \bar{\phi}_j}{\partial n} + ik_i \left(1 + \frac{i}{k_i R_i}\right)\bar{\phi}_j\right] ds. \tag{2.8}$$

Since we need consider only the space variation of the potential, we will henceforth dispense with the bar over the symbol for the potential. In addition, for observation points in the far field of the surface Equation (2.8) simplifies to:

$$\phi_j (x_i, y_i, z_i) = \frac{1}{4\pi} \oint_S \frac{e^{ik_i R_i}}{R_i} \left[\frac{\partial \phi_j}{\partial n} + ik_i \phi_j\right] ds \quad . \tag{2.9}$$

Geometrical Optics Result for the Surface Potential

To determine the value of the potential required by Equation (2.9), it is convenient to express the monopole source at (0, h, 0) in a double Fourier series in much the same fashion as for instance, Brekhovskikh (1960). For $y \leq h$, the unity amplitude velocity potential due to the source is:

$$\frac{e^{ik_1 R_0}}{R_0} = \frac{i}{2\pi} \iint\limits_{-\infty}^{\infty} \exp\left\{ i[k_{1x}x + k_{1z}z - k_{1y}(y-h)] \right\} \frac{dk_{1x}dk_{1z}}{k_{1y}} ,$$

(2.10)

where

$$k_{1y} = (k_1^2 - k_{1x}^2 - k_{1z}^2)^{1/2}$$

and

$$R_0 = [x^2 + z^2 + (y-h)^2]^{1/2} .$$

(2.11)

Since the phase of the potential does not change upon transmission into the second medium, use of the tangent plane approximation permits us to write the potential for the transmitted wave, evaluated at the point P on the interface, as

$$\phi_t(x, y_0, z) = \frac{i}{2\pi} \iint\limits_{-\infty}^{\infty} T \exp\left\{ i[k_{1x}x + k_{1z}z - k_{1y}(y_0 - h)] \right\} \frac{dk_{1x}dk_{1z}}{k_{1y}} ,$$

(2.12)

where

$$T = \frac{2\rho_1 c_2 \cos\theta_1}{\rho_2 c_2 \cos\theta_1 + \rho_1 c_1 \cos\theta_2}$$

(2.13)

is the (plane wave) transmission coefficient evaluated at point P on the interface. Of course, we relate θ_2 to θ_1 by means of Snell's law; i.e.,

$$k_1 \sin \theta_1 = k_2 \sin \theta_2 \qquad . \tag{2.14}$$

To evaluate the potential at the interface, using Equation (2.12), apply the geometrical optics approximation and restrict the location of the source point such that the quantity $k_1 R_1$ remains large. In this instance, the integral may be evaluated by the method of stationary phase in much the same way as that employed by Park and Erteza (1969). To illustrate the use of this method, we seek to find the points at which the phase term in Equation (2.12) takes on stationary values. That is, defining the phase function as

$$\psi = k_{1x} x + k_{1z} z + k_{1y}(h-y_0) \quad , \tag{2.15}$$

we seek values for k_{1x}, k_{1y} and k_{1z} at which

$$\frac{\partial \psi}{\partial k_{1x}} = \frac{\partial \psi}{\partial k_{1z}} = 0 \quad . \tag{2.16}$$

Using Equations (2.11) and (2.15), and the condition (2.16), the points of stationary phase are found as

$$k_{1x}' = k_1 \frac{x}{R_0}$$

$$k_{1y}' = \frac{k_1}{R_0} (h-y_0)$$

$$k_{1z}' = k_1 \frac{z}{R_0} \qquad . \tag{2.17}$$

In the vicinity of the stationary phase points, the phase function may be expanded in a power series; i.e.,

$$\psi = [\psi]_0 + \frac{1}{2}[\frac{\partial^2 \psi}{\partial k_{1x}^2}]_0 (k_{1x} - k_{1x}')^2 + \frac{1}{2}[\frac{\partial^2 \psi}{\partial k_{1z}^2}]_0 (k_{1z} - k_{1z}')^2$$

$$+ [\frac{\partial^2 \psi}{\partial k_{1x} k_{1z}}]_0 (k_{1x} - k_{1x}') (k_{1z} - k_{1z}') + \ldots, \qquad (2.18)$$

where the symbol $[\ ]_0$ is used to denote that the enclosed expression is to be evaluated at the stationary phase points.

Inasmuch as the method of stationary phase rests on the supposition that the principal contributions to the value of the integral arise from regions in the complex plane in the immediate vicinity of the stationary phase points, Equation (2.12) may be approximated by the relation

$$\phi_t(x,y_0,z) = \frac{i}{2\pi\ k_{1y}} [T]_0\ e^{i[\psi]_0} \iint\limits_{-\infty}^{\infty} \exp[\frac{i}{2}\left\{[\frac{\partial^2 \psi}{\partial k_{1x}^2}]_0 (k_{1x} - k_{1x}')^2\right.$$

$$+ [\frac{\partial^2 \psi}{\partial k_{1z}^2}]_0 (k_{1z} - k_{1z}')^2 + 2[\frac{\partial^2 \psi}{\partial k_{1x}\partial k_{1z}}]_0 (k_{ix} - k_{ix}')$$

$$\left. \cdot (k_{1z} - k_{1z}') + \ldots\right\}\ ]\ dk_{1x} dk_{1z}\ . \qquad (2.19)$$

For the geometrical optics approximation, there is no need to retain terms in Equation (2.19) above the second order. It is shown in Appendix A that, under these conditions, Equation (2.19) may be directly integrated with the result that:

$$\phi_t(x,y_0,z) \simeq [\frac{T}{k_{1y}}]_0 \, e^{i[\psi]_0} \left\{ [\frac{\partial^2 \psi}{\partial k_{1x}^2}]_0 \, [\frac{\partial^2 \psi}{\partial k_{1z}^2}]_0 - [\frac{\partial^2 \psi}{\partial k_{1x}\partial k_{1z}}]_0^2 \right\}^{-1/2} .$$

(2.20)

Using Equations (2.15) and (2.17), it follows immediately that

$$[\psi]_0 = k_1 R_0 \quad,$$

$$[\frac{\partial^2 \psi}{\partial k_{1x}^2}]_0 = - \frac{R_0(R_0^2 - z^2)}{k_1 (y_0 - h)^2} \quad,$$

$$[\frac{\partial^2 \psi}{\partial k_{1z}^2}]_0 = - \frac{R_0 (R_0^2 - x^2)}{k_1 (y_0 - h)^2} \quad,$$

(2.21)

and

$$[\frac{\partial^2 \psi}{\partial k_{1x}\partial k_{1z}}]_0 = - \frac{R_0 xz}{k_1 (y_0-h)^2} \quad,$$

with which Equation (2.20) may be evaluated, obtaining:

$$\phi_t(x,y_0,z) \simeq [T]_0 \, \frac{e^{ik_1 R_0}}{R_0} \quad .$$

(2.22)

In an exactly analogous manner, the scattered potential at the portion of the interface adjacent to medium 1 can be found to be given as

$$\phi_r(x,y_0,z) \simeq [S]_0 \, \frac{e^{ik_1 R_0}}{R_0} \quad,$$

(2.23)

where

$$S = \frac{\rho_2 c_2 \cos \theta_1 - \rho_1 c_1 \cos \theta_2}{\rho_2 c_2 \cos \theta_1 + \rho_1 c_1 \cos \theta_2}$$

(2.24)

is the reflection coefficient in which θ_2 is again related to θ_1 by means of Snell's law.

Geometrical Optics Result for the Normal Derivative

To compute an expression for the normal derivative of the potential at the surface suitable for the geometrical optics approximation, we proceed in a somewhat heuristic manner. We suppose that the potential at a point on the transmitted ray, only slightly removed from the interface, is of the form

$$\phi_t^+(x,y_0,z) = \frac{i}{2\pi} \iint\limits_{-\infty}^{\infty} T \, \exp \, i(k_1 R_0 + k_2 R_2) \, \frac{dk_{1x} dk_{1z}}{k_{1y}} \quad , \qquad (2.25)$$

where the symbol ϕ_t^+ denotes the transmitted potential evaluated very close to the point x, y_0, z. Now, for surfaces of comparatively gentle slope, the space rate of change of the transmission coefficient may be expected to be small compared to that of the exponential and

$$\nabla\phi_t^+(x,y_0,z) = \frac{i}{2\pi} \iint\limits_{-\infty}^{\infty} T \, \nabla\exp \, i(k_1 R_0 + k_2 R_2) \, \frac{dk_{1x} dk_{1z}}{k_{1y}} \quad . \qquad (2.26)$$

Moreover, since the maximum space rate of change of the phase must occur along the rays,

$$\nabla \, \exp \, i(k_1 R_0 + k_2 R_2) = i \, \vec{k}_t \, \exp \, i(k_1 R_0 + k_2 R_2) \, , \qquad (2.27)$$

where $\vec{k}_t$ is the transmitted ray which is related to the incident ray by Snell's law. Thus, the gradient of the potential evaluated at the surface becomes:

$$\nabla\phi_t(x,y_0,z) \underset{\sim}{\sim} \frac{i}{2\pi} \iint\limits_{-\infty}^{\infty} T \frac{i\vec{k}_t}{k_{1y}} \exp(ik_1R_0)dk_{1x}dk_{1z} \quad . \tag{2.28}$$

Noting the similarity of Equation (2.28) with Equation (2.12), the geometrical optics solution to Equation (2.28) follows immediately as:

$$\nabla\phi_t(x,y_0,z) = i[\vec{k}_tT]_0 \frac{e^{ik_1R_0}}{R_0} \quad . \tag{2.29}$$

Using a coordinate system centered at the point P, and new unit vectors $\vec{a}_n$ and $\vec{a}_t$ aligned with the normal and tangent to the surface, it is not difficult to show that

$$\frac{\partial}{\partial n}\phi_t(x,y_0,z) = i\,k_2\,[T]_0\,(\frac{e^{ik_1R_0}}{R_0^2})\,\frac{h-y_0-x\omega_S H\,\sin(\omega_S x-\gamma)}{[1+\omega_S^2 H^2\sin^2(\omega_S x-\gamma)]^{1/2}} \, , \tag{2.30}$$

where the positive sense of the normal derivative is that directed from medium 2 into medium 1.

Integral Equations for Reflection and Transmission

Substituting the expressions previously obtained for the potential and its normal derivative into the Kirchoff integral, we obtain:

$$\phi_t(x_2,y_2,z_2) = \frac{ik_2}{4\pi} \oint\limits_S \frac{e^{i(k_1R_0 + k_2R_2)}}{R_0R_2}\,[T]_0$$

$$[\frac{h-H\cos(\omega_S x-\gamma)-x\omega_S H\,\sin(\omega_S x-\gamma)}{R_0[1+\omega_S^2 H^2\sin^2(\omega_S x-\gamma)]^{1/2}} + 1]\,ds \quad , \tag{2.31}$$

where

$$[T]_0 = \frac{2\rho_1 c_2 \cos \theta_1}{\rho_2 c_2 \cos \theta_1 + \rho_1 c_1 \cos \theta_2} \quad ,$$

$$\cos \theta_2 = [1 - (\frac{c_2}{c_1})^2 + (\frac{c_2}{c_1})^2 \cos^2 \theta_1]^{1/2} \quad ,$$

$$\cos \theta_1 = \frac{h - H\cos(\omega_S x - \gamma) - x\omega_S H \sin(\omega_S x - \gamma)}{R_0 [1 + \omega_S^2 H^2 \sin^2(\omega_S x - \gamma)]^{1/2}} \quad ,$$

$$R_0 = [x^2 + z^2 + (y_0 - h)^2]^{1/2} \quad ,$$

and

$$R_2 = [(x_2 - x)^2 + (z_2 - z)^2 + (y_2 - y_0)^2]^{1/2} \quad . \tag{2.32}$$

In an exactly analogous manner, the reflected potential turns out to be:

$$\phi_r(x_1, y_1, z_1) = \frac{ik_1}{4\pi} \oint_S \frac{e^{i(k_1 R_0 + k_1 R_1)}}{R_0 R_1} [s]_0$$

$$[\frac{H\cos(\omega_S x - \gamma) - h + x\omega_S H \sin(\omega_S x - \gamma)}{R_0 [1 + \omega_S^2 H^2 \sin^2(\omega_S x - \gamma)]^{1/2}} + 1] \, ds \quad ,$$

$$\tag{2.33}$$

where

$$[s]_0 = \frac{\rho_2 c_2 \cos \theta_1 - \rho_1 c_1 \cos \theta_2}{\rho_2 c_2 \cos \theta_1 + \rho_1 c_1 \cos \theta_2}$$

and

$$R_1 = [(x_1 - x)^2 + (z_1 - z)^2 + (y_1 - y_0)^2]^{1/2} \quad . \tag{2.34}$$

An expression which will be useful in subsequent sections is that expressing the ratio of the transmitted pressure at $(x_2 y_2 z_2)$ to the source pressure at unit reference distance and is given by:

$$\left|\frac{P_t}{P_i}\right| = \frac{\rho_2}{\rho_1} \phi_t(x_2, y_2, z_2) \qquad . \tag{2.35}$$

Equation (2.35) may be readily evaluated numerically, and the FORTRAN IV listing of a digital program written to carry out the computations is included as Appendix B. The only nonzero contributions from the integral arise from the region of the corrugations and the surface integral becomes a definite double integral with

$$ds = \left[1 + \omega_S^2 H^2 \sin^2 (\omega_S x - \gamma)\right]^{1/2} dxdz \qquad . \tag{2.36}$$

Special-Case Solutions for the Transmission Integral

A closed-form solution for Equation (2.31) is extremely difficult, if not impossible, to obtain in the general case. Even for an extended interface, the determination of the stationary phase points, which enables one to calculate a solution valid in the geometrical optics sense, leads to transcendental equations which can only be solved numerically. Nevertheless, it is worthwhile to outline the development of such a solution in general terms and to evaluate it for special cases in which application of suitable parametric constraints renders the mathematics tractable.

To compute the stationary phase points, we first define the phase function from Equation (2.31) as:

$$\psi = k_1 R_0 + k_2 R_2 \quad , \tag{2.37}$$

then the stationary phase points, x_m and z_m, follow as the real solutions to the relation

$$\frac{\partial \psi}{\partial x} = \frac{\partial \psi}{\partial z} = 0 \qquad . \tag{2.38}$$

Using Equation (2.37) in Equation (2.38), the equations for the stationary phase points may be written as

$$x_m(1 + n \frac{R_{2m}}{R_{om}}) + y'_{om}[y_2 - y_{om} + n \frac{R_{2m}}{R_{om}}(h - y_{om})] - x_2 = 0 \quad . \tag{2.39}$$

and

$$z_m(1 - n \frac{R_{2m}}{R_{om}}) - z_2 = 0 \quad , \tag{2.40}$$

where:

$$R_{om} = [x_m^2 + z_m^2 + (y_{om} - h)^2]^{1/2} \quad ,$$

$$R_{2m} = [(x_2 - x_m)^2 + (z_2 - z_m)^2 + (y_2 - y_{om})^2]^{1/2} \quad ,$$

$$y_{om} = H \cos (\omega_S x_m - \gamma) \quad ,$$

$$y'_{om} = - \frac{\partial y_{om}}{\partial x} = \omega_S H \sin(\omega_S x_m - \gamma) \quad ,$$

and

$$n = c_2/c_1 \quad .$$

Using the stationary phase points obtained as the solutions to the above equations, the evaluation of the transmitted potential corresponding to each stationary phase point can be carried out in the limit of geometrical optics in a manner completely analogous to that developed in previous sections of this chapter, with the result that

$$
\phi_{tm}(x_2,y_2,z_2) = \frac{\rho_1 \omega e^{i[\psi]_m}}{R_{om}R_{2m}} \frac{k_m}{(\rho_2 c_2 + \rho_1 c_1 B_m)} \left\{ \left| [\frac{\partial^2 \psi}{\partial x^2}]_m \, [\frac{\partial^2 \psi}{\partial z^2}]_m \right. \right.
$$
$$
\left. \left. - [\frac{\partial^2 \psi}{\partial x \partial z}]_m \right| \right\}^{-1/2} \quad . \tag{2.41}
$$

where, in addition to the special variables defined previously, we have:

$$
[\psi]_m = k_1 R_{om} + k_2 R_{2m}
$$

$$
k_m = \left\{ [1 + (y'_{om})^2]^{1/2} + \frac{h_m - x_m y'_{om}}{R_{om}} \right\}
$$

$$
B_m = (1-n^2) \frac{R_{om}^2 [1+(y'_{om})^2]}{[h_m - x_m y'_{om}]^2} + n^2
$$

$$
h_m = h - y_{om}
$$

and

$$
\frac{c_2}{\omega} [\frac{\partial^2 \psi}{\partial x^2}]_m = \frac{n}{R_{om}} [1 + h_m \omega_S^2 y_{om} + (y'_{om})^2 - \frac{(x_m + h_m y'_{om})^2}{R_{om}^2}]
$$
$$
+ \frac{1}{R_{2m}} [1 + y_{2m} \omega_S^2 y_{om} + (y'_{om})^2 - \frac{(x_m - x_2 + y_{2m} y'_{om})^2}{R_{2m}^2}]
$$

$$\frac{c_2}{\omega} \left[\frac{\partial^2 \psi}{\partial z^2}\right]_m = \frac{n}{R_{om}} \left(1 - \frac{z_m^2}{R_{om}^2}\right) + \frac{1}{R_{2m}} \left[1 - \frac{(z_2 - z_m)^2}{R_{2m}^2}\right]$$

$$\frac{c_2}{\omega} \left[\frac{\partial^2 \psi}{\partial x \partial z}\right]_m = -\frac{n z_m}{R_{om}^3} (x_m + h_m y'_{om}) + \frac{(z_2 - z_m)}{R_{2m}^3} (x_m - x_2 + y_{2m} y'_{om}) \quad ,$$

with

$$y_{2m} = y_2 - y_{om} = -(d + y_{om}) \quad .$$

As an example of the use of Equation (2.41), we proceed to solve the comparatively simple problem of sound transmission from a monopole source to a receiver directly below it when the boundary separating the source medium from the receiver medium is that of an extended plane (H=0). This problem provides a valuable end-point check on the theory since a solution to this problem using other techniques has already been reported by Weinstein (1965) and Hudimac (1957). For a receiver at depth, d, the solution to Equation (2.39) and (2.40) is:

$$x_m = z_m = 0 \quad , \tag{2.42}$$

so that Equation (2.41) becomes:

$$\phi_t(0,d,0) = \frac{2\rho_1 c_2 e^{i(k_1 h + k_2 d)}}{(\rho_2 c_2 + \rho_1 c_1)(h + nd)} \tag{2.43}$$

for the case of a plane boundary and, of course, a unit amplitude source. The expression for the potential can be readily transformed to an expression for the pressure amplitude at depth, d, in a water medium

due to the operation of a one erg per second point source in the air medium above it and the result is

$$\left| P_t \ (0,d,0) \right| = \left(\frac{2\rho_1 c_1}{\pi} \right)^{1/2} \frac{1}{(h + nd)} \qquad . \qquad (2.44)$$

This last expression is precisely that obtained by Weinstein (1965) and Hudimac (1957) using other methods.

It is interesting to note that the expression describing the ratio transmitted pressure to the source pressure (at unit distance), i.e.,

$$\left| \frac{P_t}{P_i} \right| = \frac{2\rho_2 c_2}{(\rho_2 c_2 + \rho_1 c_1) \ (h+nd)} \qquad (2.45)$$

indicates that the transmitted pressure level is directly proportional to the ratio formed by the characteristic impedances of the two media. This proportionality constant is analogous to the transfer function of a resistive voltage divider in elementary electric network theory.

Another feature of Equation (2.45) which is noteworthy is the effect of the velocity contrast factor, n, as a multiplier on the water depth parameter. The presence of this term indicates that changes in the pressure ratio brought about by changes in receiver depth are n times more effective than changes in this ratio brought about by adjusting the source height. In fact, at sufficiently high depth-to-height ratios for the air to water transmission case, only very small changes in the received pressure level will be observed for comparatively large changes in source height. It must be kept in mind, however, that Weinstein (1965) showed that the velocity contrast

multiplier is correct only for the geometrical optics case for which it applies; it does not appear in the limiting case of low frequencies.

To illustrate how the simplified geometrical optics solution may be evaluated for the more complex case of a corrugated boundary, a digital program was written to carry out the analysis required to locate the stationary phase points and to subsequently compute the transmitted pressure ratio by means of the relation (2.35) applied to the potential given by Equation (2.41). The FORTRAN IV listing for this program is included in Appendix C and some examples of its use will be presented in Chapter IV. Note that when more than one stationary phase point is involved, the total solution is the complex sum of the potentials obtained for each stationary point.

To simplify the process of finding the stationary phase points, the particular embodiment of the solution (2.41) just described assumes that $z_2=0$, so that $z_m=0$ from Equation (2.40). The roots, x_m, are then computed using Equation (2.39) under the constraint that the receiver lies in the x-y plane containing the source. Note that solution (2.41) is particularly useful when the characteristics of sound transmitted through a corrugated interface of large extent are to be found. In such a case, the numerical evaluation of the transmission integral can consume considerable computer time, whereas substantially identical results can be obtained using the simpler solution. On the other hand, numerical solution of the integral equation is preferred over that of the simpler solution represented by Equation (2.41) when the corrugated

section of the interface is of only limited extent. In these cases,
one often finds that only a very few, perhaps only one, stationary
phase point may exist. When this happens, the approximate solution
tends to produce results that average out the interference effects
arising from the combination of various rays at the receiver and thus,
some of the finer sound field pattern detail contained in the integral
solution may be lost. Examples of this effect will be illustrated in
Chapter IV.

CHAPTER III

EXPERIMENTAL PROCEDURE

Description of Laboratory Apparatus

To provide experimental corroboration of the theory developed in
Chapter II, a complementary experimental program was carried out using
the anechoic tank facility at the Ordnance Research Laboratory of The
Pennsylvania State University. To simulate the monopole source, a
high quality enclosed back loudspeaker (tweeter) was used in an
unbaffled configuration. To implement the finite, corrugated boundary,
several model corrugated surface sections were constructed of one-
eighth-inch ABS (acrylonitrile-butadiene-styrene) sheet material
manufactured by Marbon Chemical Division of Borg-Warner Corp. Before
corrugated models were constructed, however, the suitability of ABS
for acoustically simulating an uneven water boundary was examined by
comparing data obtained on sound transmitted through a flat water
boundary to that obtained when ABS sheet was used on the water surface.
Although these preliminary tests did show some minor discrepancies,
the general conclusion was that ABS could be used to faithfully
simulate the acoustic properties of the water surface when insonified
from the air medium, providing intimate contact is maintained between
the lower portion of the sheet and the main body of water.

For the purposes of this study, four model corrugated surfaces were constructed and photographs of these are included as Figure 2 through 5, inclusive. The principal characteristics of these surface models are summarized in Table I.

While in use, each surface model is stabilized by lead ballast connected to each of the four corners. The ballast permits each corrugated surface to float at a level attitude and with the corrugations completely submerged. Before placing the surface model on the water, the corrugated ABS sheet is treated with a wetting agent to exclude air bubbles and ensure intimate contact between the water and the underside of the corrugated material. From the air medium, this section of the surface constitutes a stationary, corrugated air/water boundary. As an additional precaution against reflections, all inside vertical surfaces of the model-surface frames are covered with about an inch of acoustic damping material. Finally, before tests were made, all other portions of the tank surface were covered with acoustic damping material to substantially attenuate the stray acoustic paths between the air and water.

To facilitate collection of the laboratory data, an automatic hydrophone positioning and recording system was designed, constructed and installed in the anechoic tank. By means of this system, the hydrophone used to record the underwater sound field could be automatically swept over the entire length of the acoustic tank and at any predetermined depth. An electrical output derived from the drive system was used to accurately position the pen of an X-Y recorder in

TABLE I

PHYSICAL CHARACTERISTICS OF MODEL CORRUGATIONS

Surface Model No.	Overall Dimensions (in.)	No. of Periods	λ_s (in.)	Wave Height, 2H (in.)	r_{cm} (in.)	$2H/\lambda_s$	Frequency (kHz) at Which	
							$\lambda_a = \lambda_s$	$\lambda_w = \lambda_s$
1	45 x 35	2	22.0	3.0	8.2	0.14	0.6	2.7
2	30 x 30	1	30.0	6.0	7.6	0.20	0.45	2.0
3	26 x 26	4	6.0	0.25	7.2	0.042	2.2	10.0
4	26 x 26	4	6.0	0.50	3.6	0.083	2.2	10.0

accordance with the horizontal position of the hydrophone.

Since acoustic damping material was used over all of the tank
surface except that portion covered by the model interface section,
direct observation of the hydrophone could not be maintained during
the tests. Consequently, an electro-optical system was provided to
automatically shut down the sweep and produce a spatial calibration
marker to the recorder upon reaching a fixed position at either end of
the tank.

Figure 6 shows the major mechanical portion of the sweep system.
The large drumlike assembly behind the tank was used to adjust the
sweep to a given depth. The small probe hydrophone was mounted to the
center of a horizontal L frame constructed of ABS sheet. (The acoustic
impedance of ABS material is very close to that of the water in which
it is immersed.) Also visible in the photograph are the lights used
for the optical position sensors. These sensors, located on the
traverse, fore and aft of the wheel assembly, provide the sense signal
required for automatic shut down of the sweep when the leading light
aligns itself with a photocell mounted on the end of the frame.

In Figure 7, a block diagram of the experimental apparatus, the
configuration depicted is one that utilizes narrow-band random-noise
(NBRN) excitation of the loudspeaker source. It was found during the
course of these tests that NBRN is the most satisfactory means for
obtaining laboratory data, particularly when the complex patterns
produced by corrugated interfaces are to be studied. The CW or

warble-tone (FM) signals usually fail to provide satisfactory pattern definition because of the existence of residual reflections in air (such as those that exist between the speaker and the surface) and underwater (as between the bottom and the surface). Supplying wide-band noise to the loudspeaker (and filtering the received signal only) is also unsatisfactory because of the power limitations of the source.

Calibration

The form of the transmission equations which relate received pressure to incident pressure (or source level) is particularly convenient for making comparisons with experimental data. Using these equations, the theoretical data was computed as sound pressure in decibels relative to the source level. It could then be readily related to received sound pressure level by adjusting the relative level by the figure obtained for the loudspeaker source level (LSL) given by:

$$LSL = G_{Sp} + 20 \log E_{in} - 29.4 \quad , \tag{3.1}$$

where

    LSL = Loudspeaker Source Level

        (dB re 1 μbar at 1 ft.)   ,

    G_{Sp} = Loudspeaker (EIA) Rating

        (dB re 0.0002 μbar and $1m_\omega$ at 30 ft.)   ,

and

E_{in} = Loudspeaker Input Level

(rms volts)   .

In all the experimental work to be reported herein, the loudspeaker input level was maintained at +8dBv(rms). This figure represented the maximum input voltage which could safely be accommodated by the loudspeaker without leading to excessive distortion or mechanical failure of the voice-coil.

Calibration of the receiving system was accomplished simply by recording the deflections produced at the recorder for known input signals and adjusting these figures to account for the receiving sensitivity of the hydrophone. Pertinent calibration data obtained for the loudspeaker and hydrophone are summarized in Table II.

Practical Considerations in the Design of the Experiment

The choice of the various parameters of the corrugated surface models, as well as the selection of the excitation frequencies used in the tests, were heavily influenced by the performance characteristics of the acustic source and the anechoic tank. In order to develop sufficiently high source levels when using NBRN, it was necessary to restrict the source center frequency to values not in excess of about 20 kHz. However, even if this limitation did not exist, it would be difficult to employ source frequencies much higher than this due to the accuracy requirements which the use of such short acoustic

Table II

SOURCE AND RECEIVER CALIBRATION DATA

Frequency (kHz)	Gsp[a] (dB re 0.002 μbar and 1 m$_\omega$ at 30 ft.)	Sensitivity[b] (dB re 1 volt and 1 μbar)
8	50.0	108.2
9	47.8	106.5
10	46.5	105.0
11	46.5	104.5
12	46.5	103.5
14	47.5	102.9
16	53.0	105.5
18	51.5	105.5
20	46.0	105.1

[a] University Sphericon Tweeter

[b] Atlantic Research LC10 hydrophone

wavelengths would impose on the fabrication of the surface model. Instead of the comparatively simple heat forming process used in the construction of the models used here, it would be necessary to utilize much more precise construction techniques, as well as to provide much more sophisticated apparatus to measure and maintain the various physical parameters used in describing the experiment.

The lower frequency limitation of the experimental procedure arose as a result of two considerations. First, the acoustic absorption of the tank liner was highest in the frequency range near 20 kHz and diminished drastically for frequencies below 10 kHz. Consequently, any data obtained for frequencies below 10 kHz was questionable due to the reduction in received signal-to-noise ratio caused by the increased reverberation in the tank. Secondly, for the longer wave lengths, it became increasingly more difficult to acoustically mask the unused surface of the tank, and the existence of stray acoustic paths which bypassed the region of the corrugated model began to seriously degrade the quality of the data. Thus, it was concluded that meaningful data could not be obtained for frequencies less than about 10 kHz.

With excitation center frequencies limited to the 10 to 20 kHz range, the design of the corrugated models was undertaken as a compromise between requirements which tend to favor the use of models of large physical size and those which favor the use of smaller ones. Whereas larger overall size permits a greater amount of the incident energy to be transmitted into the water and also allows a larger number

of undulations to be used, larger models suffer from the disadvantage that the receiver must be located at a greater distance from the interface in order to be in the far field of the extended radiator at the surface (the corrugated model). With the depth of the receiving hydrophone limited to nine feet with the sweep system installed, it appears that the use of surface models larger than about one foot on a side could lead to difficulty, especially at the lower frequencies. In practice however, it was found that somewhat larger corrugated models could be used and useful results obtained even in the near-field of the corrugated model.

CHAPTER IV

DISCUSSION OF RESULTS

Comparison of Theory with Experiment

In this section, the theoretical data obtained by numerical evaluation of the Transmission Equation [Eq. (2.31)] are compared to experimental data obtained for the case of air-to-water sound transmission using the experimental program described in the previous chapter. Of particular interest is the examination of the accuracy of the theoretical predictions for sound transmission through a number of surface model corrugations designed with various waveheights, slopes, corrugation wavelengths and radii of curvature.

The results of the data comparison are presented below for each surface model in turn beginning with model No. 1. For each model, test results are presented for various excitation frequencies beginning with the lowest one. This order of presentation is then continued for each successively larger loudspeaker tilt angle used for that particular surface model. For loudspeaker inclinations different from zero, the actual location of the loudspeaker is to the left of an imaginary vertical line passing through the center of the surface model. With respect to the curves given, these positions then correspond to positions to the left (negative side) of zero.

Figure 8 is a comparison of theory and experiment for surface model No. 1, the largest of the models. The data was taken at a test frequency of 10 kHz with the axis of the loudspeaker aligned with the vertical line passing through the center of the surface.

Figures 9 through 11, inclusive, also represent data taken with zero loudspeaker tilt angle, although at higher frequencies. For this model surface, normal loudspeaker incidence (zero tilt angle) produced the least accurate match between theory and experiment. Even so, the data can be seen to agree well with respect to average transmitted pressure level, and the differences which do exist tend to be confined to the finer details of the pattern shapes. However, for the highest frequency used, 20 kHz, Figure 11 shows that even the finer details of the pattern are in close agreement with theory.

The somewhat irregular appearance of the experimental data is attributed to two factors: the fluctuation in the excitation signal which arises out of the requirement to use very narrow bandwidths at the loudspeaker input to produce adequate radiated power levels with NBRN excitation; and the spatial irregularities caused by partially coherent reflections. In fact, some rather pronounced excursions are often associated with the edge of the plots (the ends of the acoustic tank) and particularly for cases in which a null should appear in the data. This is due to the fact that equipment installed at the corners of the tank to support the hydrophone positioning apparatus leads to a higher incidence of reflections as the receiving hydrophone approaches

the limits of its sweep. For example, irregularities in the data which appear to arise in this way are seen in Figure 8 in the region to the left of the figure and in Figure 11 at horizontal sweep positions between 25 and 45 inches on the right side of the figure.

Figures 12 through 16, inclusive, are for a loudspeaker tilt angle of three degrees and frequencies in the 10 kHz to 20 kHz range. In all cases, agreement between average transmitted levels and fine pattern detail is well within expected experimental limits for a large region containing the principal lobes of the transmitted sound field. Again, the agreement between theory and experiment tends to improve with an increase in frequency and for the highest frequency 20 kHz (Fig. 16), it is exceptionally good throughout the entire sweep range. Figures 17 through 22, inclusive, represent data for a speaker tilt angle of six degrees. Agreement between theory and experiment is again very good for all frequencies in the 10 kHz to 20 kHz range.

Figures 23, 24 and 25 show data taken for the model 1 surface at eight degree speaker tilt angle. These curves, and especially that of Figure 23, indicate a tendency for stronger lobes to concentrate in the region beneath the actual location of the source which, in this case, is located in the air medium at about the 13-inch horizontal position. This is obviously not a general property of the transmitted sound field patterns, however. At least for small changes in the loudspeaker angle, some tendency for the sound field pattern to retain its shape but shift its relative position in response to changes in louspeaker

angle (position) was also noted. Usually, the amount of the pattern shift can be estimated using Snell's law. This is to be expected since the portion of the loudspeaker pattern which insonifies the surface model is essentially omnidirectional. Hence, if the surface section was very large, one could expect the basic underwater sound patterns to be spacially repetitive or periodic (with respect to a vertical reference line through the source) as the source is moved in a given horizontal direction.

Figures 26 through 31, inclusive, are examples of underwater sound field data compiled for surface model No. 2. This corrugated section actually consists of just a single large wave, but has the highest value for the waveheight (H) and wave steepness figure ($2H/\lambda_S$) of any of the model corrugations used. The slope of a tangent drawn at the point of inflection of this wave has an inclination of about 32 degrees. Even so, it is seen that satisfactory agreement between theory and experiment is again obtained for all frequencies an angles of loudspeaker inclinations used. The tendency for the pattern details to agree more closely as the frequency is increased is again noted in the data.

The satisfactory agreement between theory and experiment for the transmitted sound fields of models No. 1 and No. 2 at frequencies between 10 and 20 kHz indicates that the theory is probably acceptable when used for frequencies somewhat below 10 kHz. Unfortunately, this could not be substantiated with the acoustic tank used because data

below 10 kHz was not considered valid for the reasons previously discussed.

Figure 32 is an example of a comparison between theory and experiment for surface model No. 3 at zero degree loudspeaker inclination and at a moderately high (16 kHz) value of excitation frequency. The agreement between the two curves is satisfactory although sufficient definition of the three center lobes which should be present on the experimental curve is lacking.

Generally, it was found to be difficult to obtain experimental transmission patterns that were well defined and symmetrical for this surface model and for the vertical loudspeaker position. Although all the tests carried out at 12 kHz and above compared very well with respect to the transmitted pressure levels, Figure 32 represents the best pattern shape agreement obtained during the zero degree loud-speaker tests. It is felt that mechanical inaccuracies in the construction of the model surface were largely responsible for the lack of pattern symmetry observed.

Figures 33 through 36, inclusive, were obtained for a loudspeaker tilt angle of three degrees. Comparison of the data obtained at 10 kHz (Fig. 33) with that obtained at 12 kHz (Fig. 34) illustrates that satisfactory agreement between theory and experiment is lost in the vicinity of 10 kHz (and probably for frequencies below this value). At these low frequencies, the experimental data is at variance with the theory, particularly with regard to the existence of a broad null just

to the right of positions directly below the center of the surface model. Although an experimental null in the region of about +17 inches is almost non-existent at 10 kHz, a broad null at abouʟ ·30 inches does appear at a frequency of 12 kHz and is illustrated by Figure 34. Thus, it is at frequencies of 12 kHz and above that the experimental data begin to display increasingly better agreement with theory. For example at 16 kHz (Fig. 35) and at 20 kHz (Fig. 36), both pattern shapes and overall levels are in good agreement.

Figures 37 through 41, inclusive, represent model No. 3 transmitted pres؟ure data at a loudspeaker inclination of six degrees. As in the case of three degree inclination described previously, the data taken at 10 kHz disagree with respect to the existence of a dip in transmitted pressure in the region to the right of zero inches. However, in this case, the discrepancy is rather small because the pressure dip is not pronounced. For the data at 12 kHz (Fig. 38), there is a broad null in the region of +50 to +70 inches and, again, the experimental data also displays a null in this region at this higher frequency. At still higher frequencies, such as 16 kHz (Fig. 39), 18 kHz (Fig. 40) and 20 kHz (Fig. 41), agreement between theory and experiment once again is very good.

The final collection of experimental data to be examined is that which illustrates the transmitted sound field data for surface model No. 4. Referring to Table 1, it can be seen that this surface model is designed with a value of slope factor $(2H/\lambda_S)$ smaller than that of either models No. 1 or No. 2, but twice that of model No. 3. However,

the wavelength of model No. 4 is identical to that of model No. 3, so
that the effects of increased slope and curvature on the accuracy of
the theory may be examined.

As had been expected, the pronounced curvature of model No. 4 is
sufficient to produce a situation in which the geometrical optics
solution proves to be deficient for predicting the experimental data.
In fact, for this surface, agreement between the data is generally poor
throughout the 10 to 20 kHz frequency range and for small speaker tilt
angles. For example, Figure 42 illustrates such a comparison of data
at 12 kHz and 3 degree tilt angle. Although the average predicted
pressure levels in this case tend to agree within a few decibels, the
pattern shapes display little similarity. The same conclusion is
reached for data taken at higher frequencies such as that for 14 kHz
(Fig. 43), 16 kHz (Fig. 44), 18 kHz (Fig. 45) and 20 kHz (Fig. 46).
Furthermore, from these data, it does not appear that any trend yet
exists toward increased agreement between the curves for higher
frequencies although such a trend is to be expected. In fact, the data
at 20 kHz is in particularly poor agreement. It is likely that
frequencies much higher than those available for these tests would need
to be used before such a trend becomes discernible.

Model No. 4 transmitted sound field data for six degree loudspeaker
tilt angle is included as Figures 47 through 51. Although the curves
still do not agree as closely as they do under similar circumstances
using the other model surfaces, the agreement is much improved over

that obtained at three degrees. For the frequency range 12 to 18 kHz,
average predicted pressure levels are very close to experimental data
and the pattern shape details are generally acceptable. However, the
data at 20 kHz (Fig. 51) once again must be considered one of the
poorest cases.

In addition to demonstrating the accuracy of a mathematical model
for the transmission problem based on a solution of the geometrical
optics type, the above comparisons between theory and experiment
provide useful insight into the limitations imposed by the use of such
a theory. One of the limiting conditions on the theory which is
illustrated by the above work is that imposed by the use of acoustic
wavelengths which are approximately equal to or greater than the
corrugation wavelength. At such frequencies, it appears that detailed
transmitted pattern information cannot be predicted accurately by the
theory. Although the actual conditions under which the theory begins
to break down are rather vague due to the subjective nature of the
processes involved in matching pattern shapes, it appears that gradual
loss of the ability to predict pattern shape provides the first
indication of theory deficiency. Substantial discrepancies in
predicting average pressure levels tend to occur only when the acoustic
wavelengths are increased still more. This is an expected result,
since it is the phase relationships between the transmitted rays
reaching the receiver which largely establish the characteristics of
the transmitted sound field pattern. Thus, substantial variations in

the pattern shape details arise from only relatively small discrepancies in predicting these phase relationships.

As an example of this limit on the theory, consider the data obtained for model No. 3 at 10 kHz (Fig. 33 and Fig. 37). For either loudspeaker angle, noticeable differences in pattern shape are observed between theory and experiment at 10 kHz, but these disappear when the frequency is raised to 12 kHz (Fig. 34, three degree speaker angle) or to 11 kHz (Fig. 38, six degree speaker angle). There also appears to be some tendency for the data to agree somewhat more closely at a given frequency as the speaker inclination is increased, but inasmuch as the loudspeaker pattern in the region of the interface is essentially omnidirectional, the improvement noted is probably due to the spatial relationship of the loudspeaker to the undulations below it rather than on its inclination, per se.

It is important to note that these apparent deficiencies in the theory occur for this model surface (No. 3) at the frequency for which the acoustic wavelength in one of the media equals the corrugation wavelength. Specifically, Table 1 shows that the wavelength in water (the high velocity medium) is equal to the corrugation wavelength at 10 kHz. Finally, we remark that the tendency for the geometrical optics solution to be deficient when the acoustic wavelength in either medium is comparable to or greater than the corrugation wavelength also appears to be indicated by the work of Asano (1966) which was cited previously. His theoretical data for plane wave incidence on an

extended corrugated surface shows that the low-order coefficients of his series solution for the transmitted potential tend to vary very rapidly with frequency in the type of situation described above, and that the range over which these coefficients vary increases with the velocity contrast between the two media. Evidently, the observed "instability" of the series coefficients relates to the convergence of the series solution and to the tendency of the geometrical optics solution to be deficient at lower frequencies. The limitation on the theory described above may be referred to as a lower bound on the applicability of the geometrical optics-type solution to the transmission problem. The method can also fail at frequencies above those dictated by corrugation wavelength considerations alone, however, and these attendant limitations arise as a consequence of other assumptions made in the development of the theory.

Comparing the data obtained for model No. 4 with the results obtained with the other model surfaces provides an appreciation of the effects of other parameters on the applicability of the theory. For this model corrugation, the predictability of pattern details, in particular, was generally poor even up to 20 kHz, with the exception of data taken at six degree loudspeaker angle and frequencies of 14 and 16 kHz. Obviously, corrugation wavelength considerations alone do not explain these observations since the wavelength of model No. 4 is identical to that of model No. 3 for which accurate results were obtained above 10 kHz. Neither does the influence of large waveheight

nor large slope account for the difference since both model surfaces
No. 1 and No. 2 have substantially higher waveheights and steeper slope
figures than model No. 4. One feature which does stand out, however,
is the fact that model No. 4 has a minimum radius of curvature
($r_{cm} = 1/\omega_S^2 H$) of about one-half of that of the other models. Thus, it
is likely that the poor agreement between theory and experiment for
this model can be attributed to the inapplicability of the tangent
plane approximation for the frequencies used.

To test this supposition, we note that Park and Erteza (1969) give
Brekhovskikh's criterion for the validity of the tangent plane
approximation as:

$$4\pi r_c \cos \alpha \gg \lambda \quad , \tag{4.1}$$

where r_c is the radius of curvature and α is the local angle of
incidence. Evidently, the wavelength (λ) refers to that in the high
velocity medium.

The influence of the local angle of incidence is difficult to
consider in the present case, since it takes on many different values
along the surface (as does r_c). However, if we assume that this term
is equal to unity, we may still obtain estimates on the limits of the
tangent plane approximation as follows. Rewriting Equation (4.1) in
terms of the excitation frequency, f, we obtain the inequality

$$f \gg \frac{c_2}{4\pi r_c} \quad . \tag{4.2}$$

Using the fact that the transmitted sound field pattern of surface model No. 3 can be accurately predicted by the theory at frequencies as low as 10 kHz, inequality (4.2) indicates that the limiting frequency for the tangent plane approximation for this surface is at least of the order of 15 times the characteristic frequency factors, $c_2/4\pi r_c$. Note that, for model No. 3, the tangent plane approximation is valid for frequencies down to the region where $\lambda_\omega = \lambda_S$, but at these frequencies, the tangent plane approximation must surely fail unless the waveheight is only a small fraction of the acoustic wavelength. Extrapolating our results for model No. 3 to the case of model No. 4, then, inequality (4.2) indicates that the tangent plane approximation is invalid unless the frequency used with model No. 4 exceeds 20 kHz and this conclusion substantiates our previous observations.

Discussion of Experimental Discrepancies

During this investigation, supplementary work was carried out in an attempt to estimate expected discrepancies between theory and experiment and thus provide a reasonable basis for evaluating the accuracy of the solution techniques. As already indicated, comparisons of computed results with experiment indicated that generally good agreement in both pattern shape and acoustic levels was obtained for those cases in which very low frequencies or very severe corrugation properties (small r_c) were not encountered. It was also discovered, however, that there were cases for which optimum agreement between

theoretical and experimental curves required some minor adjustment of
the X-axis spatial-reference position between the two curves. Proper
adjustment of the zero reference then resulted in coincidence of the
two patterns. Since there was strong correlation between the amount
of adjustment required and the date on which various experiments were
carried out, it was clear that these adjustments were required due to
the presence of various mechanical errors in the experimental setup.

Some of the possible errors that were considered to be contrib-
uting to the existence of this pattern dislocation effect include, in
order of importance:

1. Errors in the measurement of and uncertainty in the
position, orientation, and alignment of the loudspeaker
source, the model surface section, and the underwater
receiver.

2. Physical errors in the slope, size, and construction
of the model corrugations.

3. Flexing and bending of the model due to stresses
applied by ballast weight and hydrostatic pressure.

The type of laboratory or theoretical checks that were made to
assess the independent effects of position, orientation, and alignment
errors included:

1. Rotation of the surface model by turning it end-for-end
to check for pattern variation when the direction of
corrugations are reversed; this evaluates the physical

symmetry of the corrugated model and provides a check
on how accurately the surface level can be established.

2. Rotation of the speaker about its axis to check for
   alignment of the mechanical and acoustic axes.

3. Movement of the surface model to different locations
   in the tank to establish repeatability of established
   test conditions and check uniformity of the underwater
   acoustic environment.

4. Introduction of small angular errors into speaker and
   surface model orientation to observe the effect on the
   pattern.

5. Introduction of a small positioning error into the
   location of the speaker relative to the surface model.

As a result of tests of the type described above, the following
conclusions were reached regarding the relative importance of various
parameters on the horizontal positioning accuracy of the experimental
underwater sound field:

1. Rotation of the surface model affects the structure
   of the main lobes somewhat and can result in uncertainty
   in the positioning of the nulls in the data by as much
   as 12 inches. This effect is complicated by its
   dependence on speaker angle, hydrophone depth, frequency,
   and corrugation characteristics. This, of course, is
   true of most of the errors that were examined.

2. No misalignment of mechanical and acoustic axes could be discerned for the loudspeaker.

3. Reestablishing experimental conditions demonstrated that repeatability of patterns is uncertain wit. regard to null positions by distances of the order of 2 inches.

4. Errors in measuring the speaker and surface model inclinations are very important. A surface inclination uncertainty of about 2 degrees was observed to affect the resulting underwater sound pattern by about 10 to 15 inches (horizontally) at a 9 ft. depth. Changes in speaker tilt angle of about 1 degree, for nominal inclinations near normal, can result in pattern shifts of the order of 10 to 12 inches at a 9 ft. depth.

5. Small variations (of the order of 1 inch) in the loudspeaker height have no appreciable effect on the pattern. However, inaccuracies in the horizontal displacement of the speaker relative to the center of the interface are significant. Here, measurement errors of as little as 1 inch can cause pattern position errors of the order of 5 to 10 inches.

There are other sources of error but these were considered to be insignificant and no evaluation of these were therefore attempted. These include discrepancies introduced by:

1. Approximation errors arising from the use of a piecewise planar approximation to the surface geometry.

2. Neglecting multiple scattering of sound at the interface (in air and in water).

3. Truncation and round-off noise produced by the computer program during the execution of the arithmetic operations.

As a result of the above work, it was concluded that the uncertainties experienced in the substantiation of the computational procedure were within reasonable tolerances, and that experimental results were generally in good agreement with theory except in those cases for which the geometrical optics solution does not apply.

Examples of the Use of the Approximate Closed-Form Solution

In this section, several examples are provided to illustrate the use of the approximate closed-form solution derived previously and to establish the usefulness of this method as an alternative to direct numerical integration of Equation (2.31).

A comparison of the results of the approximate solution with a representative set of experimental data is presented as Figure 52. Here, the experimental data, previously presented in Figure 36 (model No. 3 at 3 degree loudspeaker angle and 20 kHz), is compared with the results of the approximate solution. It can be seen that very good agreement between theory and experiment has been obtained. Further, comparison of the approximate theoretical solution of Figure 52 with

the theoretical data presented in Figure 36 shows that the two methods lead to very similar results.

For the theoretical data of Figure 52, the number of stationary phase points found within the interface boundaries averaged about eight and was evidently sufficient to produce adequate definition of the shape of the transmitted sound field pattern. There are cases, however, when the location of the source and receiver, as well as the interface size and geometry, lead to only a very few stationary phase points. For example, Figure 53 is a comparison of theoretical data obtained for a corrugated surface with a waveheight equal to that of model No. 4, but with a larger wavelength specification. Note that these data are computed for zero source angle and a symmetrical interface; thus, the patterns are symmetrical about the zero-inch reference point.

For eight foot source height and nine foot receiver depth specifications used in Figure 53, only one stationary phase point was found with the receiver in the regions of zero to 47 inches and 77 to 110 inches. For this reason, the approximate solution tends to predict values closer to the average pressure levels in these regions and fails to account for the large variations in the received pressure level caused by interference effects. For the region between 50 inches and 75 inches, three stationary phase points exist and it can be seen that this leads to much better prediction of the transmitted pattern shape.

Figure 54 is another comparison between the two theoretical methods, assuming the same corrugation properties previously used in Figure 53, but at 40 kHz excitation frequency. Only the region between 50 inches and 75 inches leads to more than one stationary phase point and one again notes the tendency for the approximate solution to predict average levels rather than the pattern detail when only one stationary phase point exists.

To illustrate the substantial improvement in the approximate solution in cases for which a larger number of stationary phase points exists, refer to Figure 55. Here, the transmitted sound field is again computed for an interface with the same corrugation properties used in Figures 53 and 54, but with the source height increased to 20 feet. In this case, a larger portion of the interface is insonified by the source and the stationary phase points become more numerous. The data is once again symmetrical about the zero-inch horizontal reference point and the generally good agreement between the two methods is clearly evident. Although the number of stationary phase points is about three, on the average, only one stationary phase point was found for data in the regions from zero to 10 inches and again for the region from 50 to 62 inches.

This particular case (Figure 55) provides an excellent example of the utility of the approximate closed-form solution for predicting the transmitted sound field for an extensive interface. It was possible to obtain data for this case with only about two percent of the expenditure of computer time required by the numerical integration of Equation (2.31).

CHAPTER V

SUMMARY AND CONCLUSIONS

Statemen of the Problem

With the development of increasingly more sophisticated equipment to measure, record and analyze underwater acoustic signals, it has become evident that the usefulness of underwater acoustic sensors can be enhanced by extending their range of application to the reception and detailed analysis of underwater acoustic signals produced by airborne sources. However, in order to fully exploit any capability of processing or otherwise utilizing acoustic energy transmitted between fluids in general, more detailed knowledge is required of the processes involved in the transmission of acoustic energy between fluid media separated by arbitrary boundary geometries. To advance our understanding of these processes, this investigation was undertaken with the intention of developing practical techniques for solving the important basic problem of sound transmission from a monopole source through a finite, corrugated boundary between fluid media and to corroborate these techniques by means of laboratory data obtained for the important case of air-to-water sound transmission.

Procedure of the Investigation

The subject matter of this investigation is divided into two major sections. The first of these deals with the theoretical aspects of the

study and includes:

1. The derivation of mathematical models, based on a
   particular form of the Kirchoff radiation integral,
   which may be used to compute the properties of the
   reflected and transmitted sound fields of a monopole
   source after its modification by a finite, uneven,
   fluid-fluid boundary composed of regular corrugations
   (sinusoidal undulations).

2. The development of approximate closed-form solutions
   to the transmission integral described in (1) above
   which are useful in the study of sound transmission
   through certain extended interfaces which are
   insonified by high frequency sources.

3. The reduction of the equations involved in both the
   integral solution and the approximate closed-form
   solution (for sound transmission) to digital computer
   programs in order to facilitate their numerical
   evaluation.

4. Examples of the practical application of the
   mathematical models by computing the transmitted
   sound field in numerous cases for which independent
   evaluation of the quality of the solutions can be
   carried out.

The second major section of this study concerns the experimental corroboration of the transmission integral, and the related computational model, by means of experimental data obtained for the case of air-to-water sound transmission through several finite, corrugated interface sections.

Discussion of Results

The most significant results obtained during this study were the development and experimental corroboration of practical techniques for predicting sound transmission through a finite, fluid-fluid interface of sinusoidal cross section. These tests of the theory were carried out by utilizing four laboratory models of corrugated surface sections. These model corrugations were designed to simulate different corrugation properties of the interface and were fabricated specifically for use in obtaining data on the problem of sound transmission from air to water. Thus, by varying both the orientation and frequency of the loudspeaker source used to insonify each model surface section, underwater sound field data for transmission through corrugated boundary surfaces was obtained over a comparatively wide range of test parameters and for two fluids of widely different acoustic impedance. For the first three of the four model surfaces, i.e., those designed with parameters within the presumed range of validity of the theory, very good comparison between theory and experiment was generally noted for all frequencies used, thereby corroborating the theory.

Model No. 4, which was designed with more severe corrugation properties, was employed to obtain information on the limitation of the theory when it is applied to a surface geometry containing regions with small radius of curvature. As expected, use of this corrugated model interface produced marginal results when the experimental data was compared to the predictions of the theory, particularly with regard to the lack of agreement which was displayed by the spacial details of the transmitted sound field patterns. From these data, it was shown that the principal limitation of the theory arose at low frequencies as a result of the inapplicability of the tangent plane approximation used in fitting the boundary conditions at the uneven interface. Using a form of Brekhovskikh's criterion (4.2) for the applicability of the tangent-plane approximation, an order-of-magnitude relation was proposed to predict the lower frequency limit for the theory in terms of the velocity of propogation in the water (the high velocity medium) and the minimum radius of curvature of the corrugated boundary. It was shown that the least lower bound on the theory occurred when the acoustic wavelength in one of the media was equal to the corrugation wavelength.

To demonstrate the use of the approximate closed-form solution to the transmission integral, several exemplary solutions obtained with this technique were compared with corresponding ones obtained by direct (numerical) evaluation of the integral. It was shown that, even when only a very few stationary phase points exist, the approximate

solution predicted the average transmitted pressure level reasonably well. However, the best results were obtained when the interface was large and moderately rough and the source and receiver were not too close to the interface. In such a case, the stationary phase points are sufficiently numerous to permit a good approximation to be made to the shape of the transmitted sound field pattern as well as to the average pressure level. Noteworthy is the fact that the approximate closed-form solution works well in situations involving comparatively large interfaces--situations in which numerical evaluation of the transmission integral requires a large amount of computational effort.

Conclusions and Specific Contributions of This Study

As a result of this investigation, theoretical solutions have been obtained for the problem of transmission of sound from a monopole source through a finite corrugated boundary separating two fluid media. These solutions have been shown to be valid in the limit of geometrical optics for interface geometries which do not contain undulations with a minimum radius of curvature of the order of a wavelength of sound (or less) in the high velocity medium.

The specific contributions of this study can be briefly outlined as follows:

1. Integral expressions were derived to predict the transmitted and reflected potentials due to the impingement of sound from a monopole source on a corrugated interface separating two fluid media.

2. For the case of sound transmission through a corrugated interface, the integral expression for the transmitted potential was reduced to an approximate closed-form solution valid in the limit of geometrical optics.

3. Empirical data was obtained on the transmission of sound through several finite corrugated air-water boundary sections for various excitation frequencies and source orientations. It is believed that this is the first time that experimental data has been reported on transmission of vibrational waves through a rough boundary between fluids.

4. Computational techniques were developed to evaluate the transmission integral described in (1) above and the approximate closed-form solution described in (2).

5. Extensive comparisons were made between the theoretical results obtained by evaluating the transmission integral and the experimental data described in (4) above. These comparisons were used to corroborate the theory and to illustrate the conditions under which the accuracy of the theoretical procedures will be maintained.

6. Practical examples were provided to demonstrate the use of the approximate closed-form solution and comparisons were made with other data to illustrate its suitability as an alternative to numerical integration of Equation (2.31).
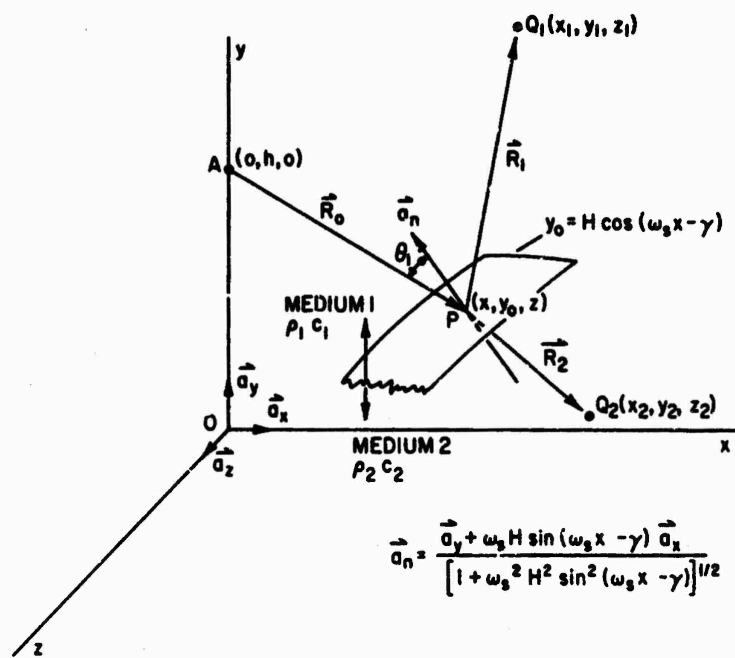
Figure 1. Geometry for Transmission and Reflection
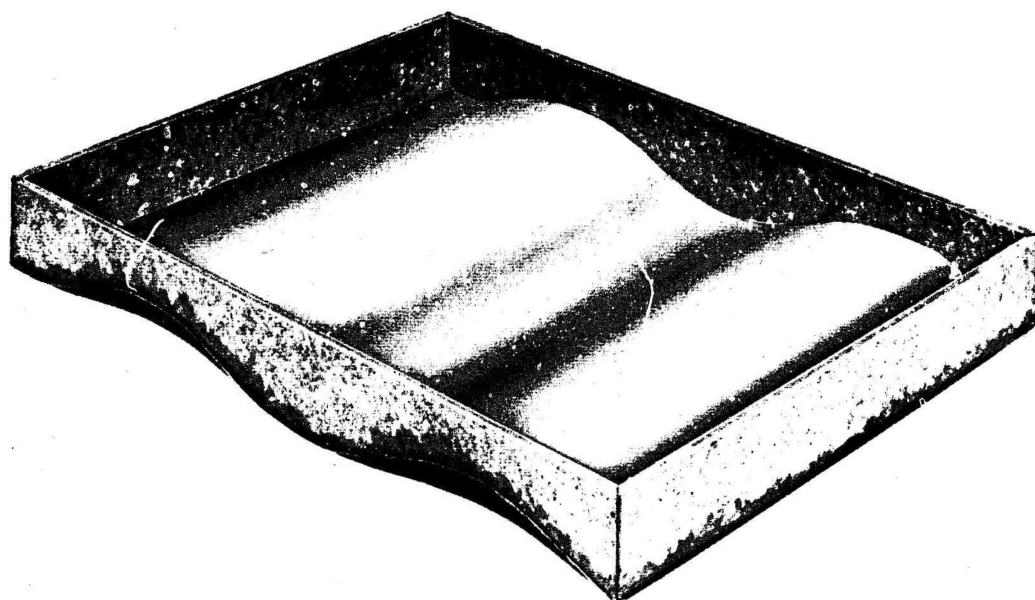
Figure 2. Surface Model No. 1
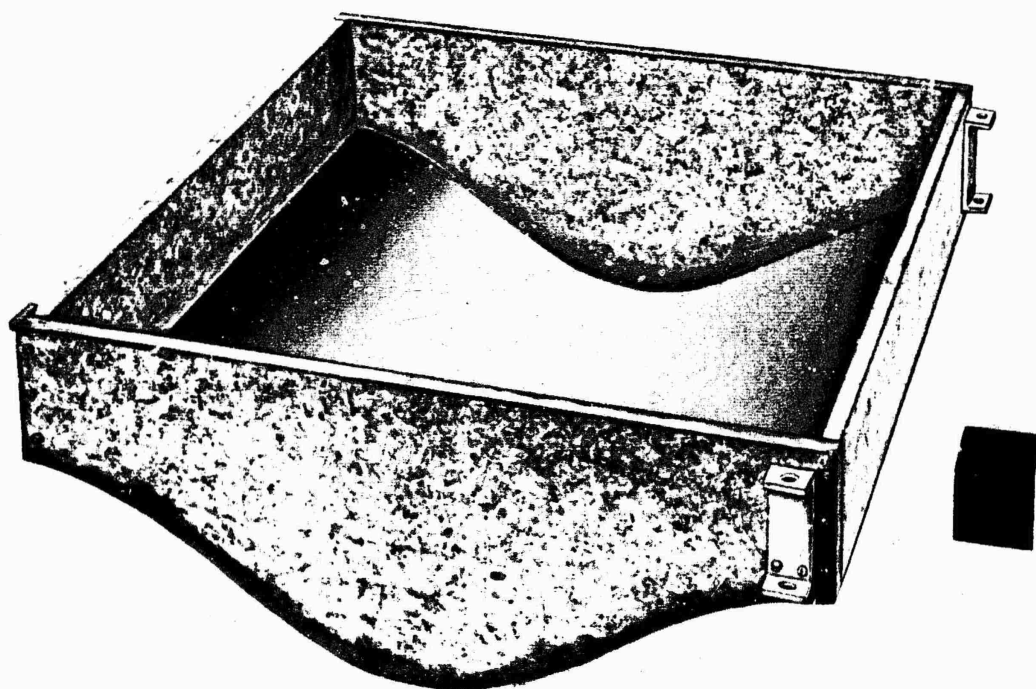
Figure 3. Surface Model No. 2
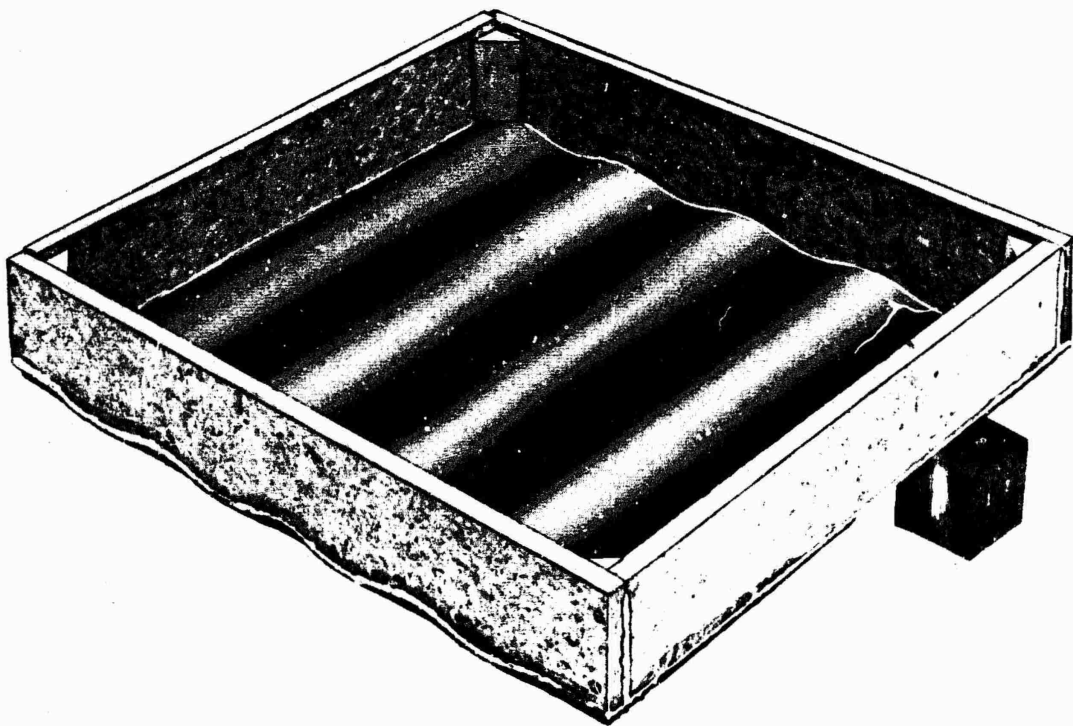
Figure 4. Surface Model No. 3

NOT REPRODUCIBLE
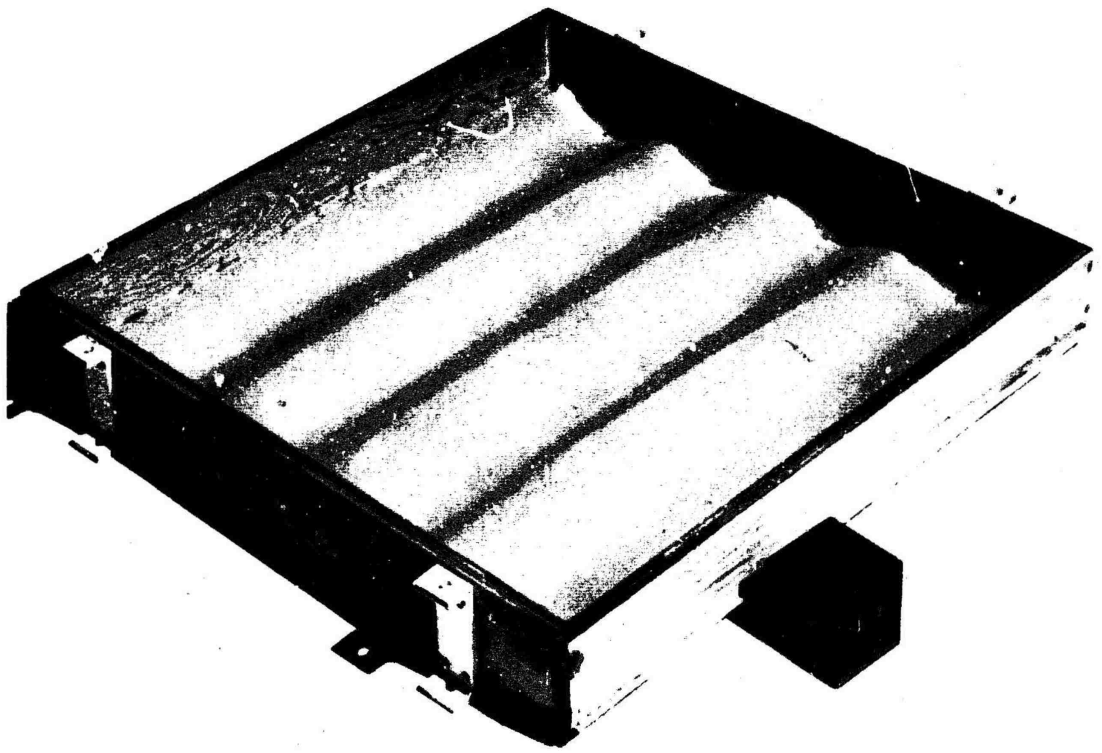
Figure 5.   Surface Model No. 4
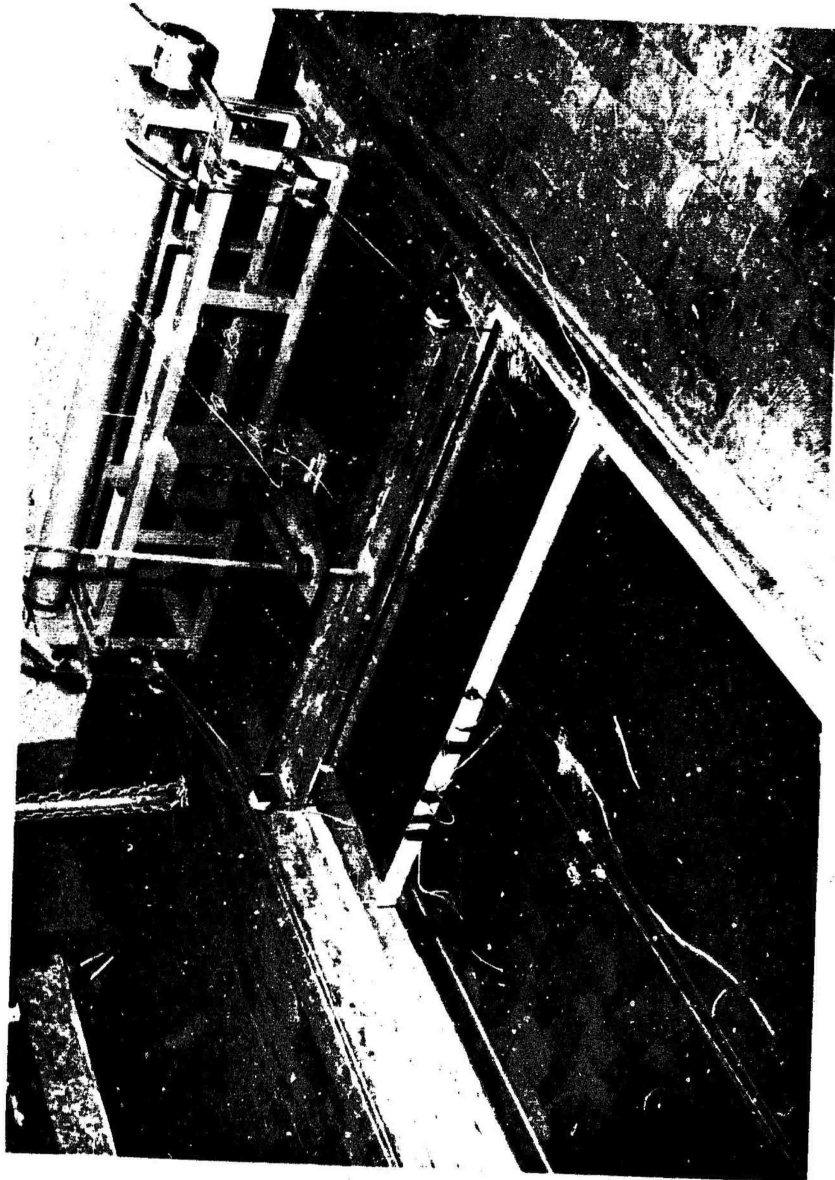
Figure 6. Hydrophone-Sweep System
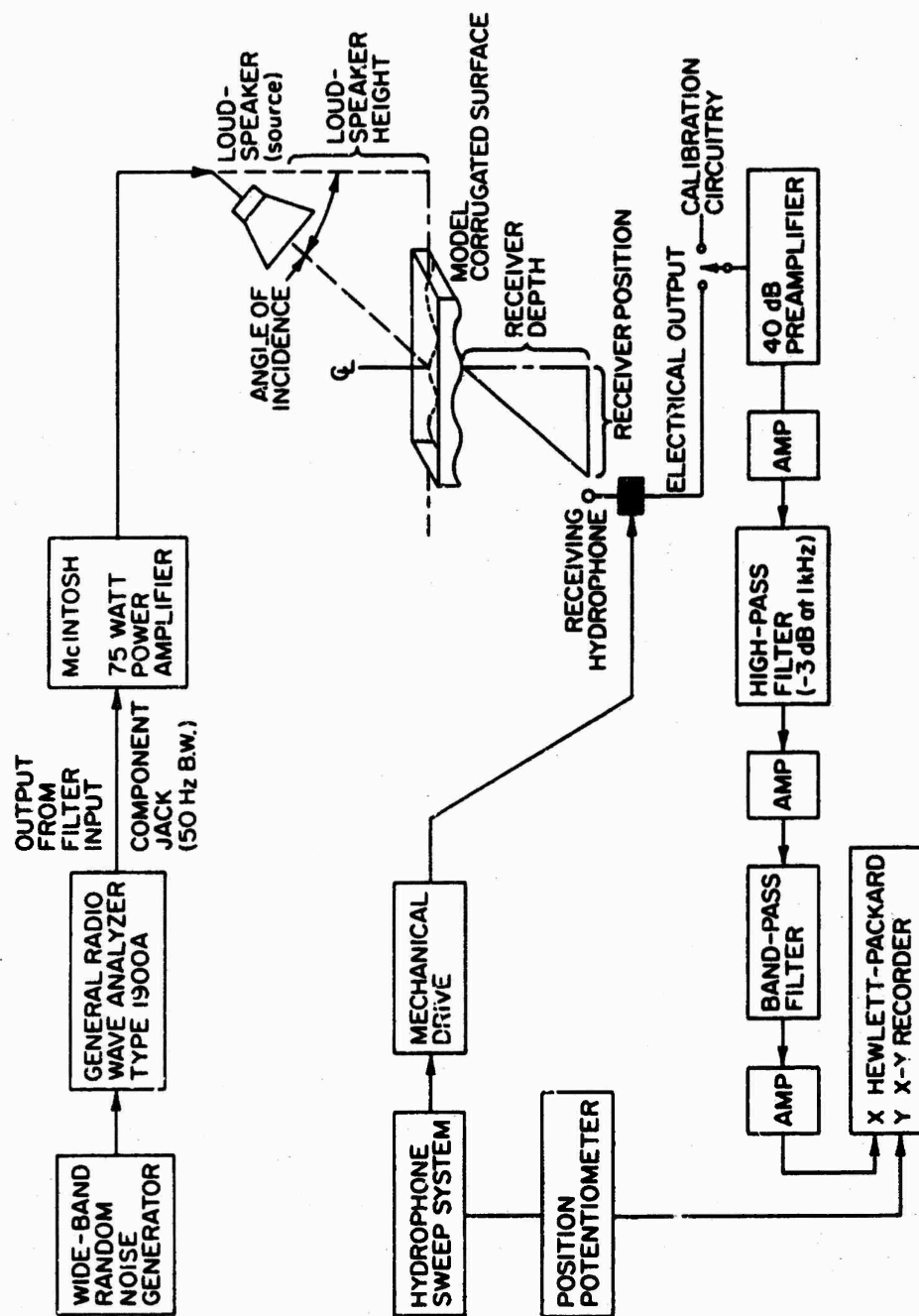
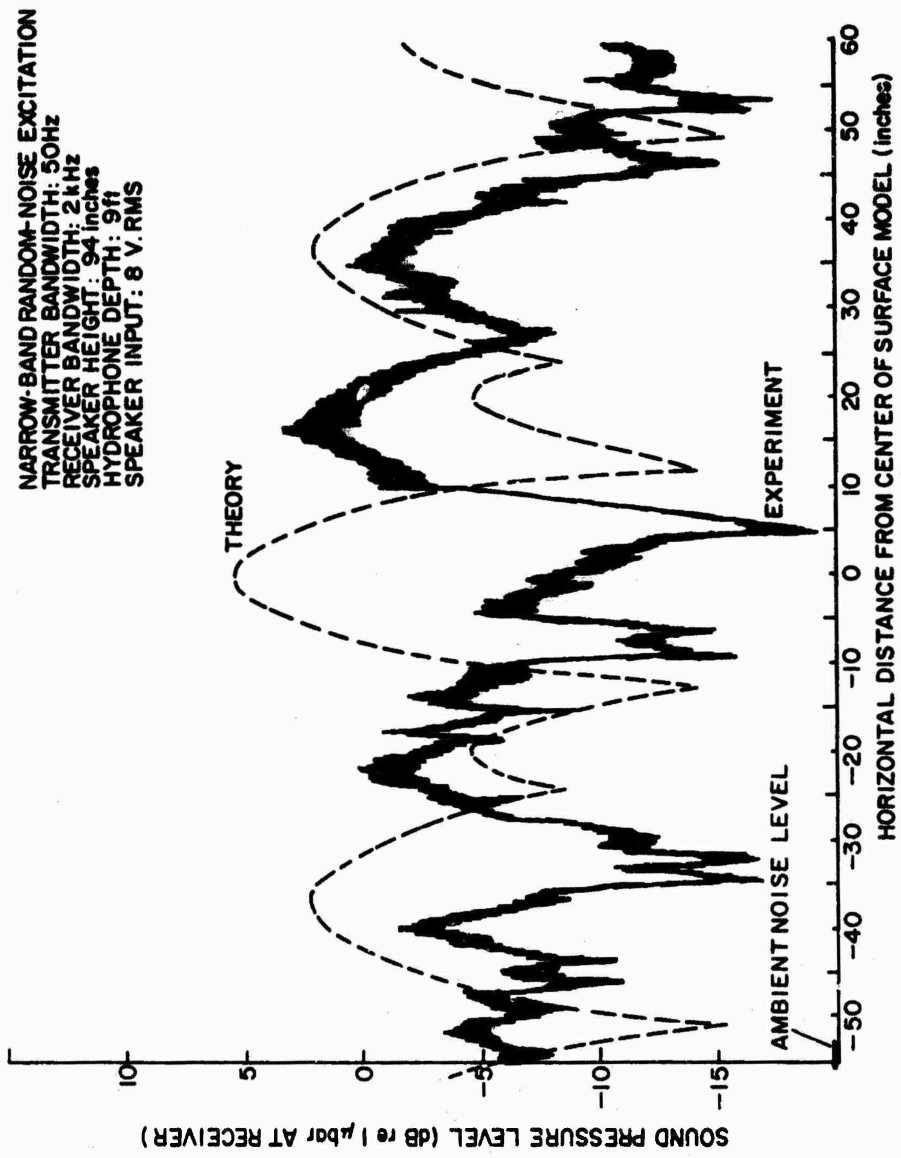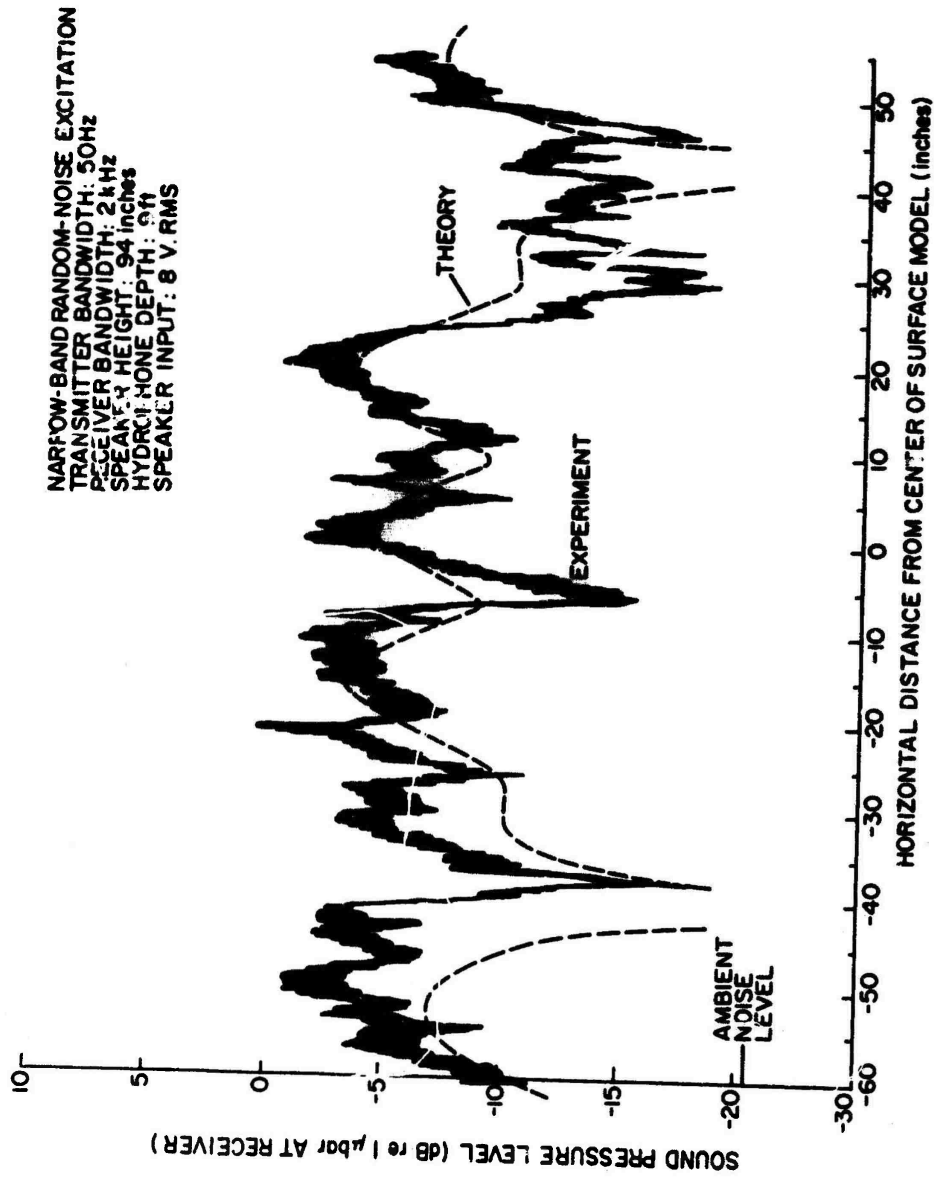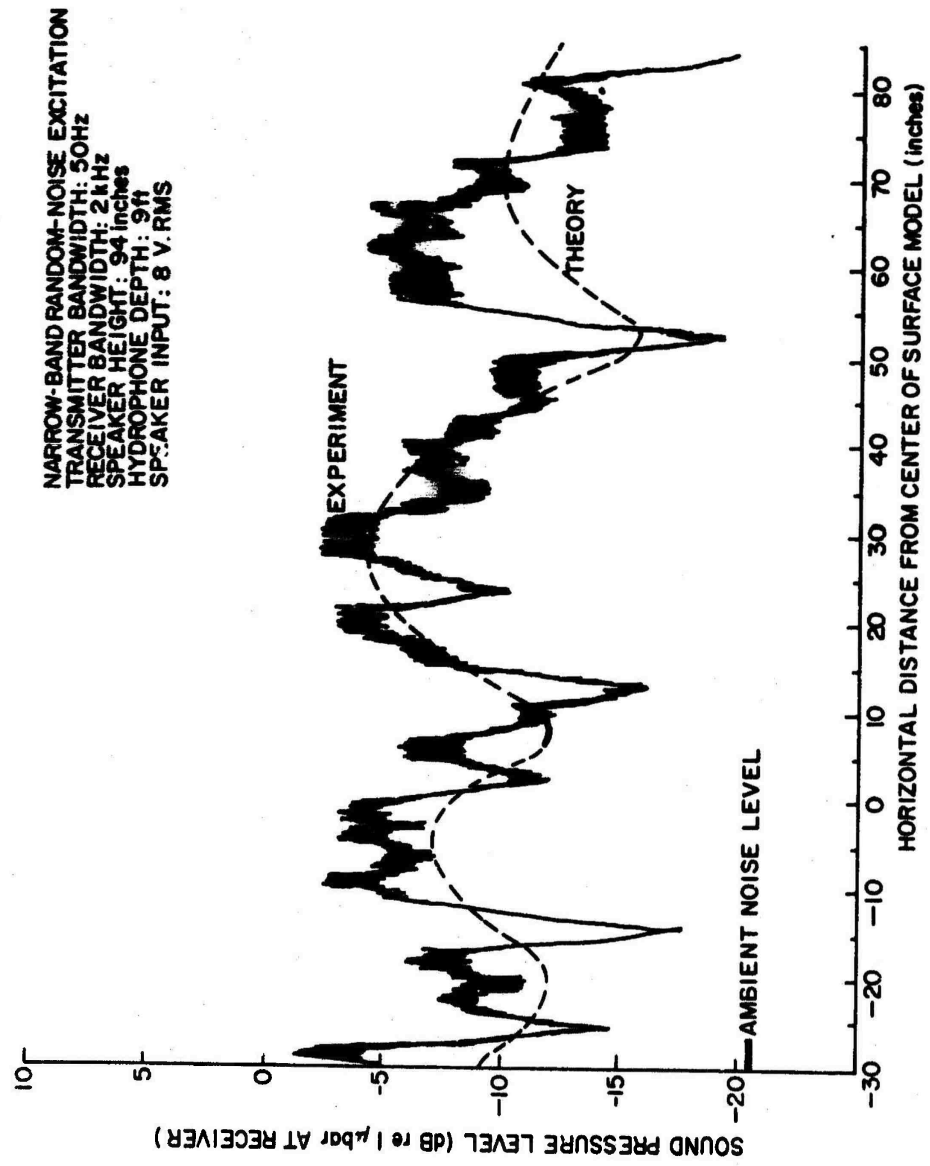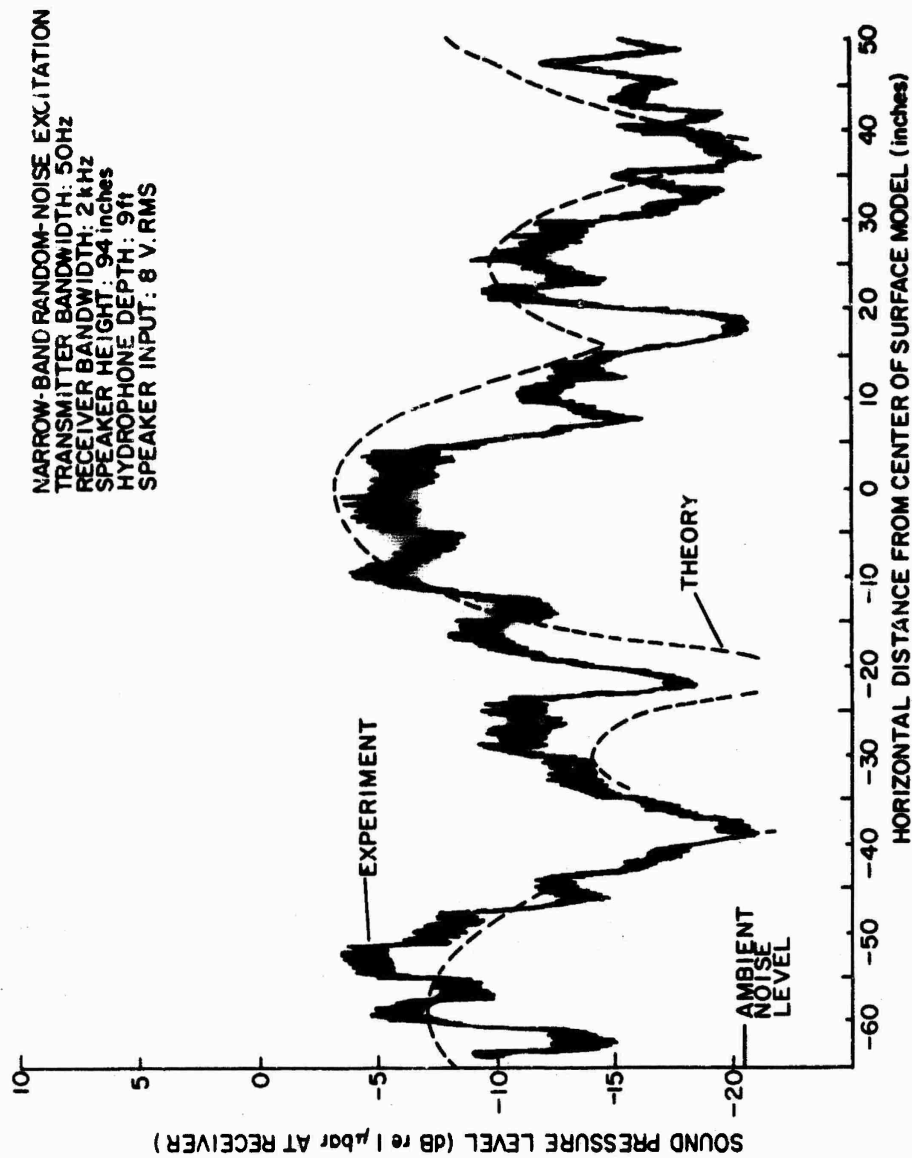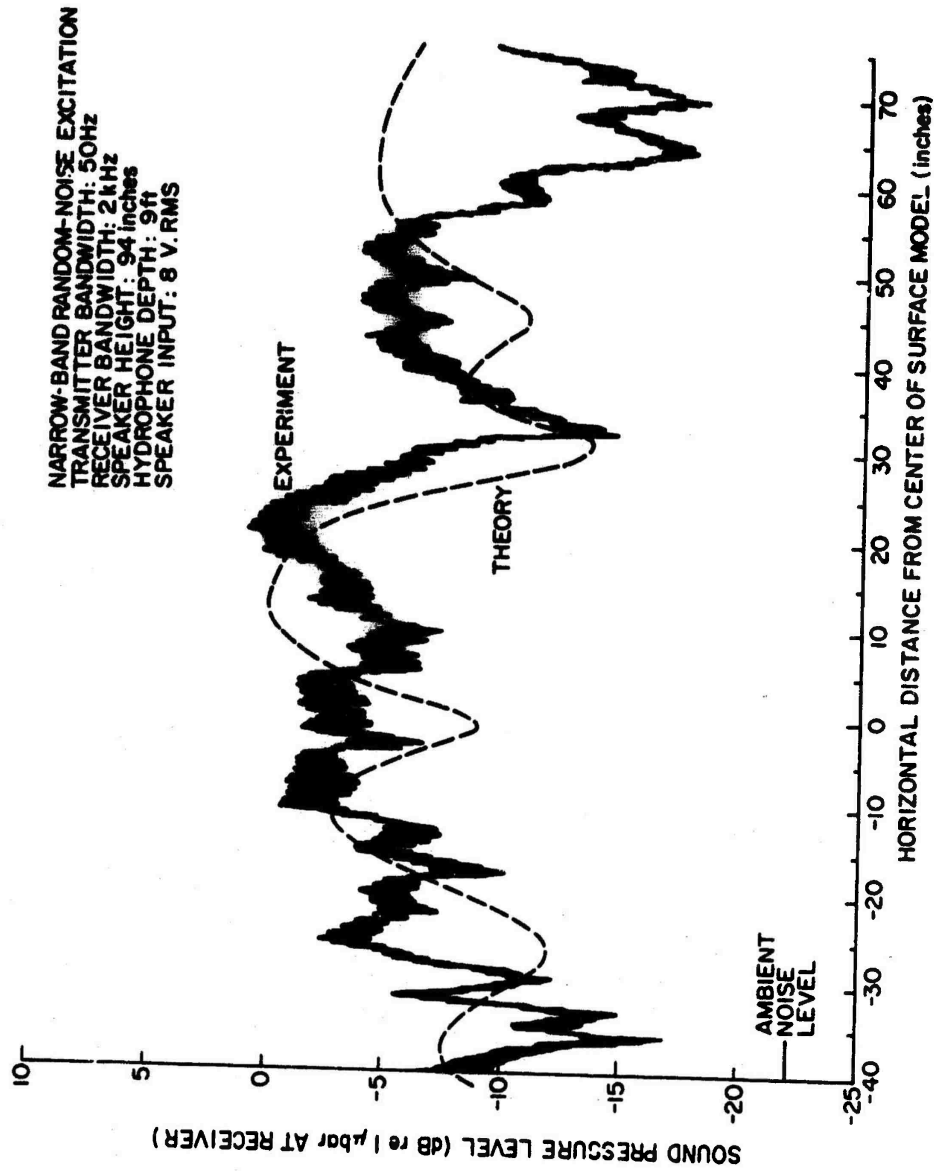Figure 7. Laboratory Apparatus for Measuring
Underwater Sound Field
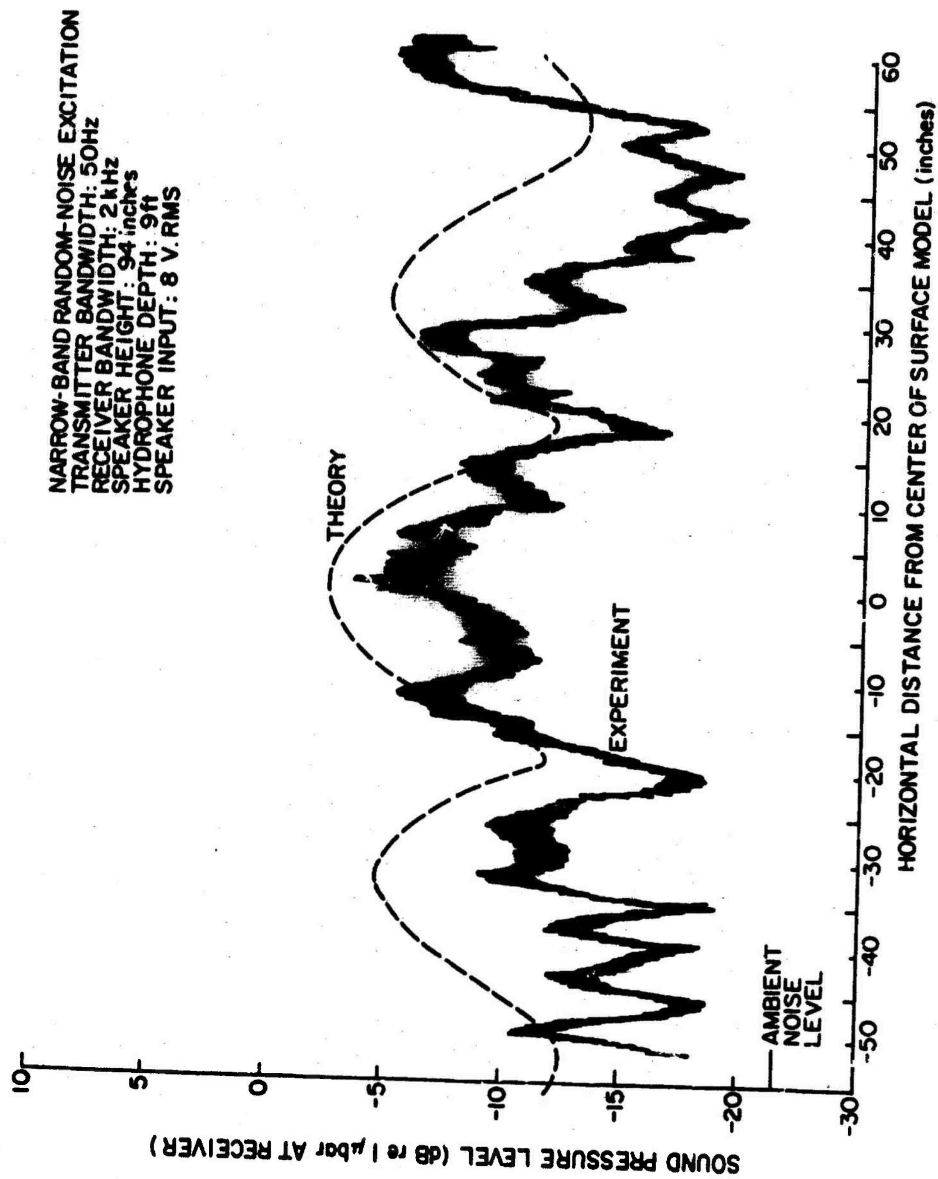
Figure 8.   Underwater Sound Field Beneath Surface Model
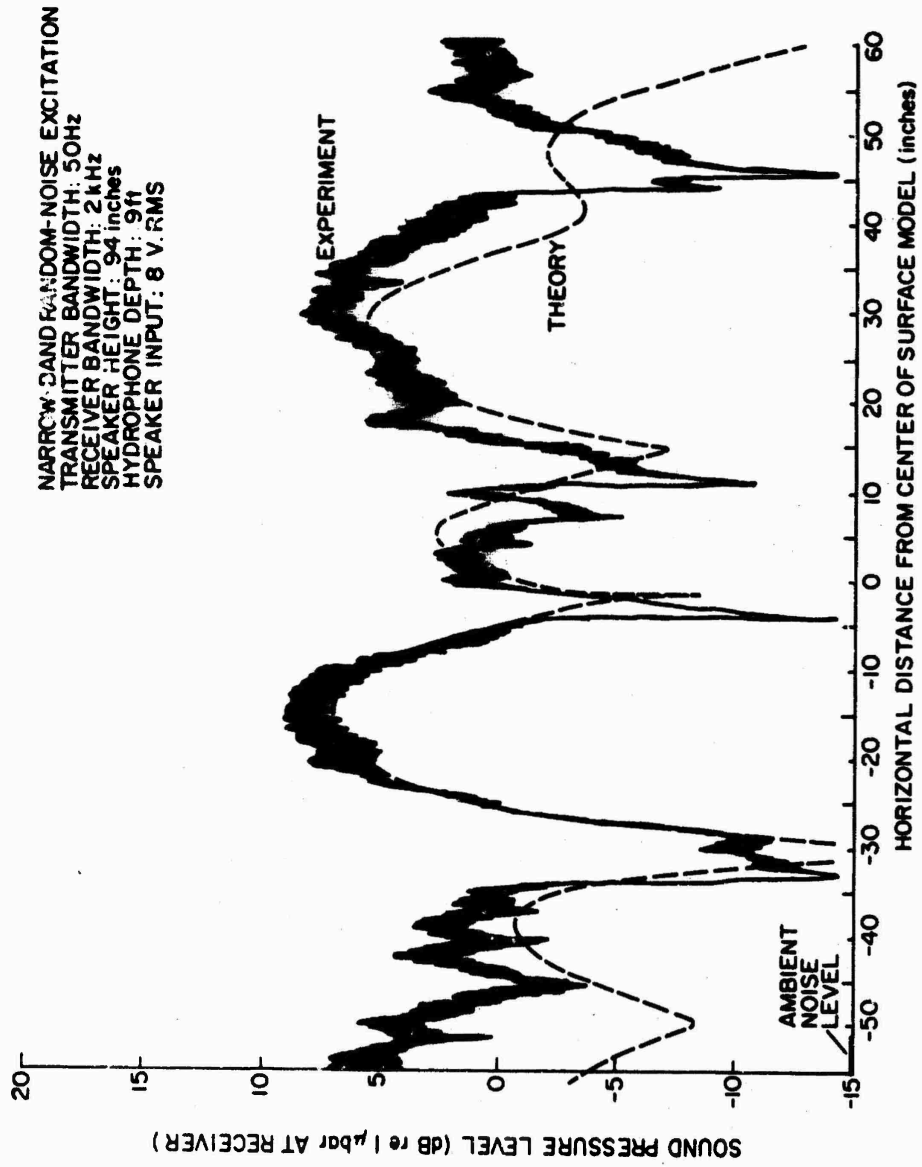No. 1 (Transmitter Frequency: 10 kHz, Speaker
Angle: 0 deg.)
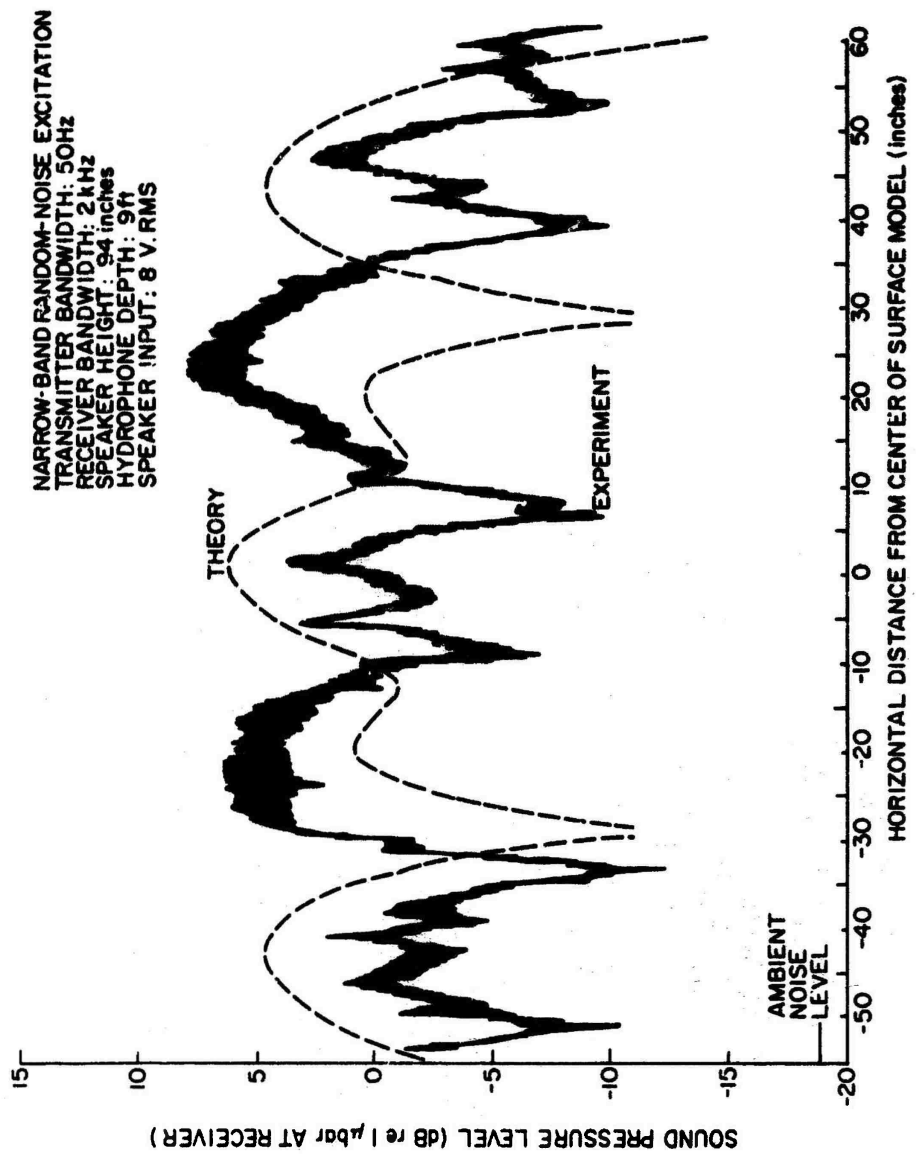
Figure 9. Underwater Sound Field Beneath Surface Model
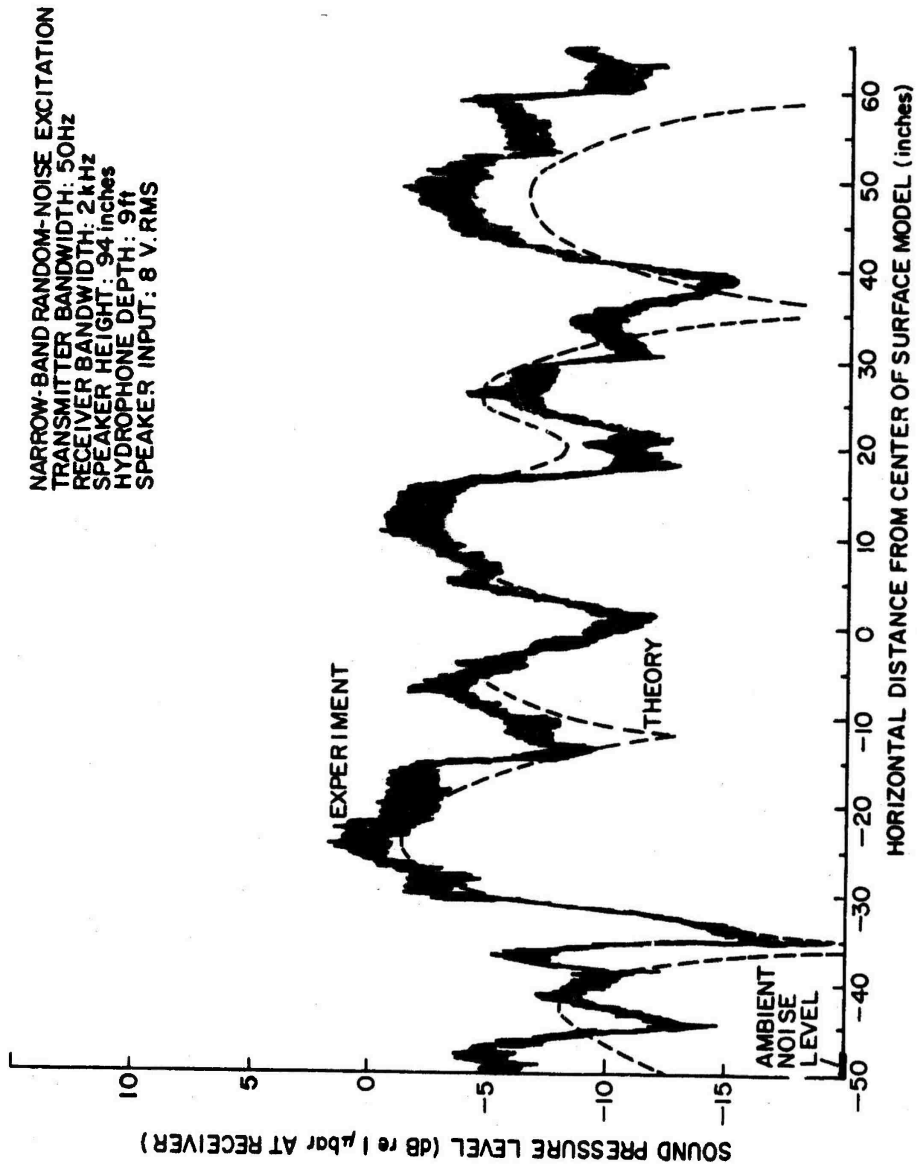No. 1 (Transmitter Frequency: 16 kHz, Speaker
Angle: 0 deg.)

Figure 10. Underwater Sound Field Beneath Surface Model
No. 1 (Transmitter Frequency: 18 kHz, Speaker
Angle: 0 deg.)

Figure 11. Underwater Sound Field Beneath Surface Model
No. 1 (Transmitter Frequency: 20 kHz, Speaker
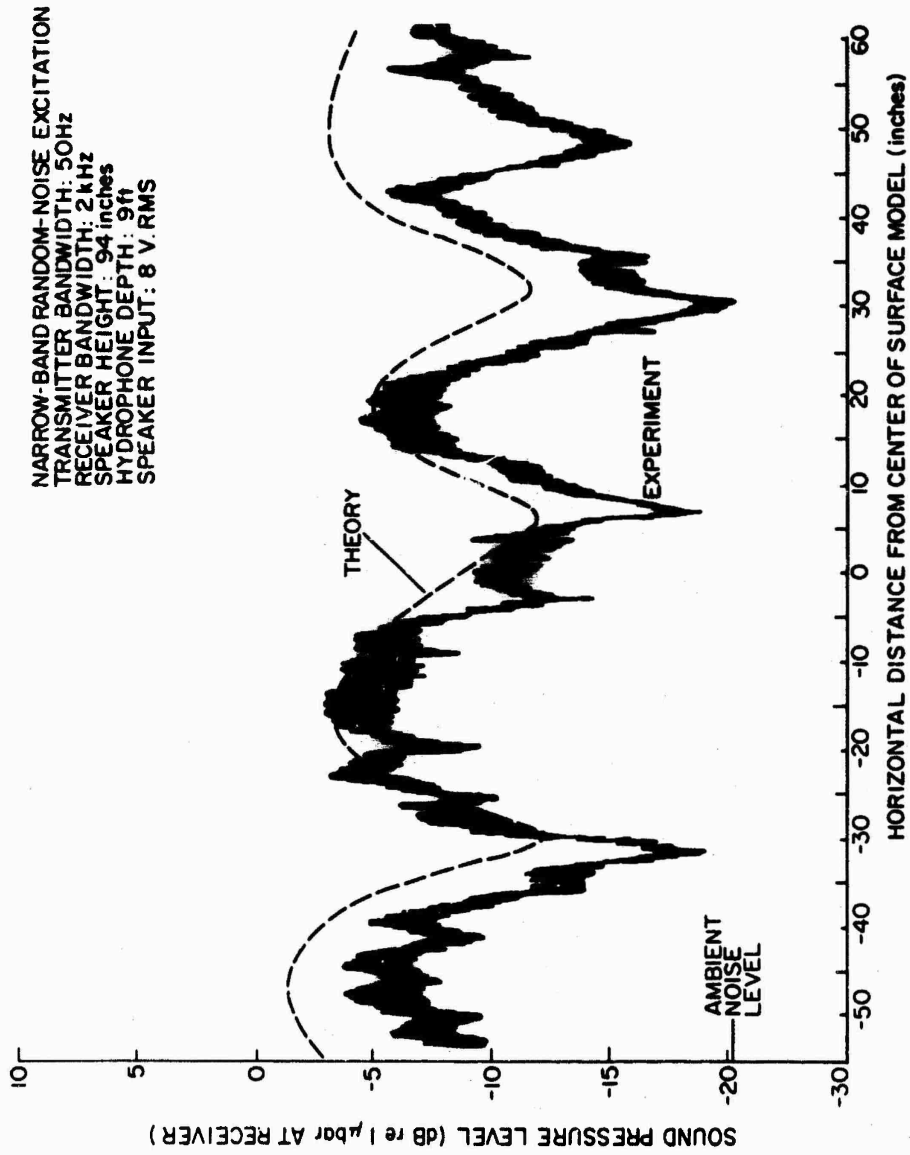Angle: 0 deg.)

Figure 12. Underwater Sound Field Beneath Surface Model
No. 1 (Transmitter Frequency: 10 kHz, Speaker
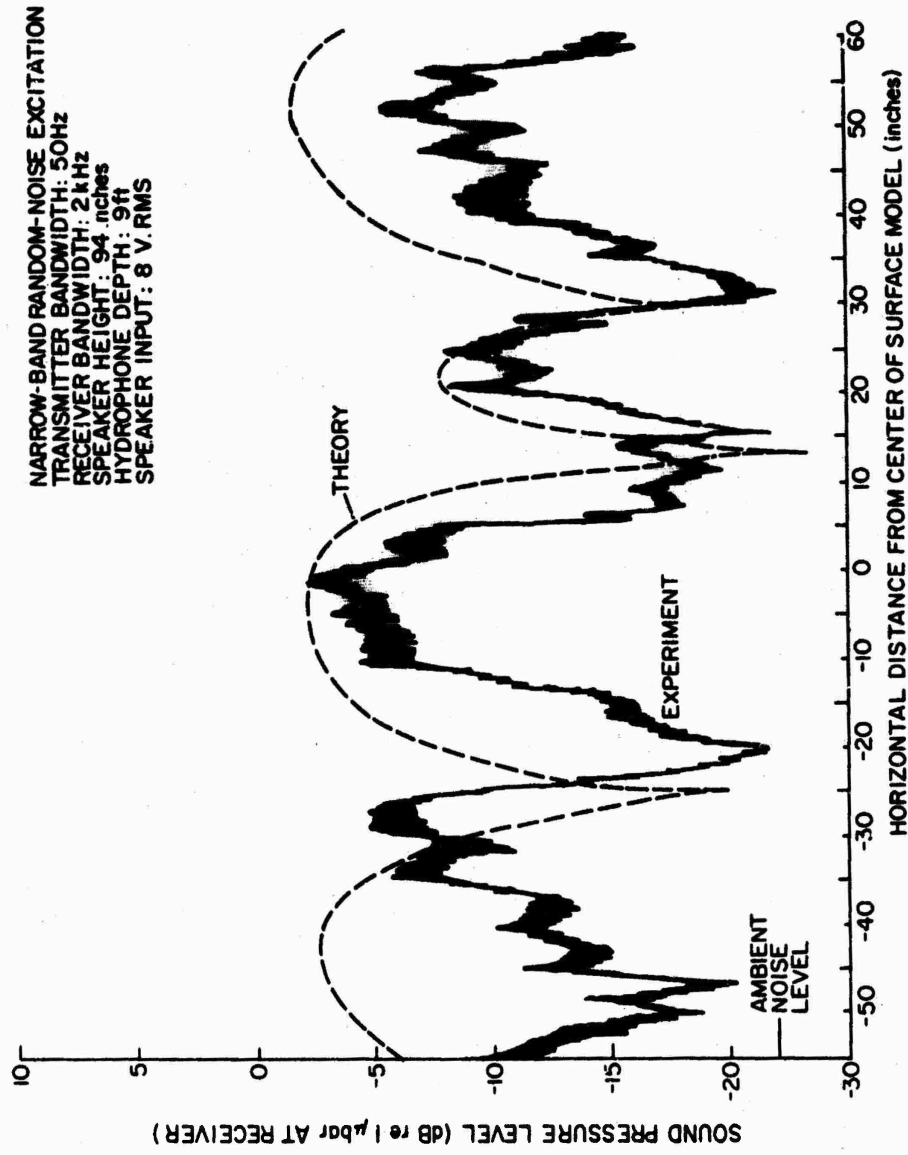Angle: 3 deg.)

Figure 13. Underwater Sound Field Beneath Surface Model
No. 1 (Transmitter Frequency: 12 kHz, Speaker
Angle: 3 deg.)

Figure 14. Underwater Sound Field Beneath Surface Model
No. 1 (Transmitter Frequency: 14 kHz, Speaker
Angle: 3 deg.)

Figure 15. Underwater Sound Field Beneath Surface Model
No. 1 (Transmitter Frequency: 16 kHz, Speaker
Angle: 3 deg.)

Figure 16. Underwater Sound Field Beneath Surface Model
No. 1 (Transmitter Frequency: 20 kHz, Speaker
Angle: 3 deg.)

Figure 17. Underwater Sound Field Beneath Surface Model
No. 1 (Transmitter Frequency: 10 kHz, Speaker
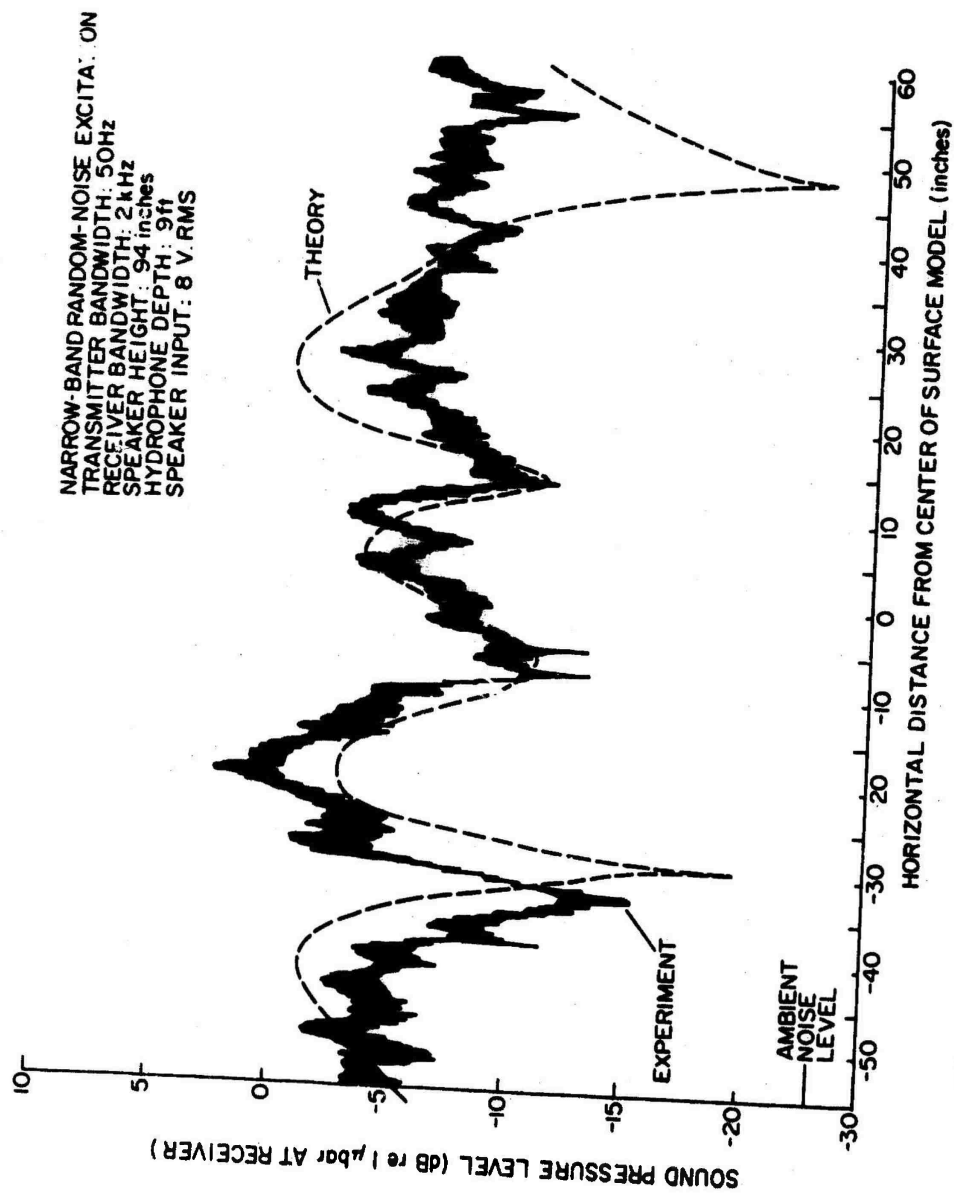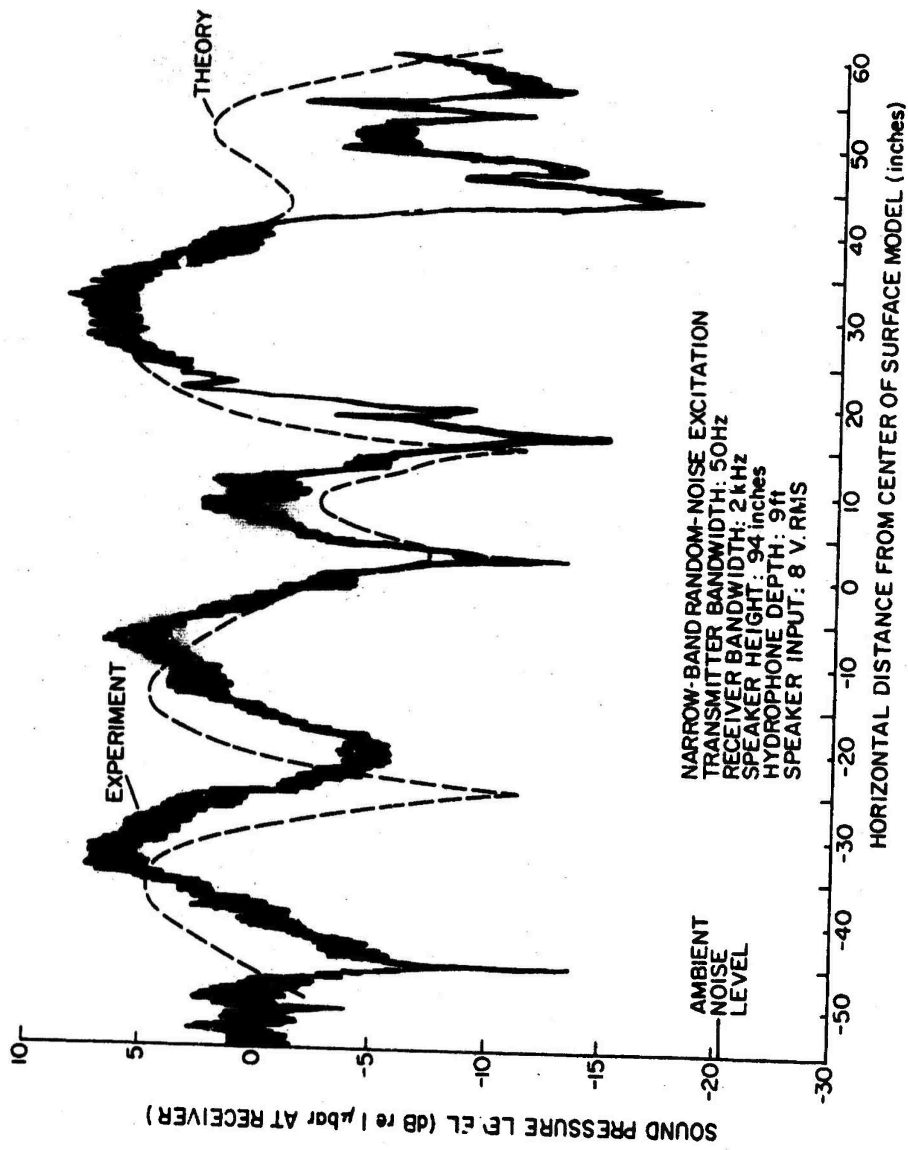Angle: 6 deg.)

NARROW-BAND RANDOM-NOISE EXCITATION
TRANSMITTER BANDWIDTH: 50Hz
RECEIVER BANDWIDTH: 2 kHz
SPEAKER HEIGHT: 94 inches
HYDROPHONE DEPTH: 9ft
SPEAKER INPUT: 8 V. RMS

THEORY

EXPERIMENT

AMBIENT
NOISE
LEVEL

HORIZONTAL DISTANCE FROM CENTER OF SURFACE MODEL (inches)

SOUND PRESSURE LEVEL (dB re 1 μbar AT RECEIVER)

Figure 18.   Underwater Sound Field Beneath Surface Model
No. 1 (Transmitter Frequency: 12 kHz,   Speaker
Angle: 6 deg.)

Figure 19. Underwater Sound Field Beneath Surface Model
No. 1 (Transmitter Frequency: 14 kHz, Speaker
Angle: 6 deg.)

Figure 20. Underwater Sound Field Beneath Surface Model No. 1 (Transmitter Frequency: 16 kHz, Speaker Angle: 6 deg.)
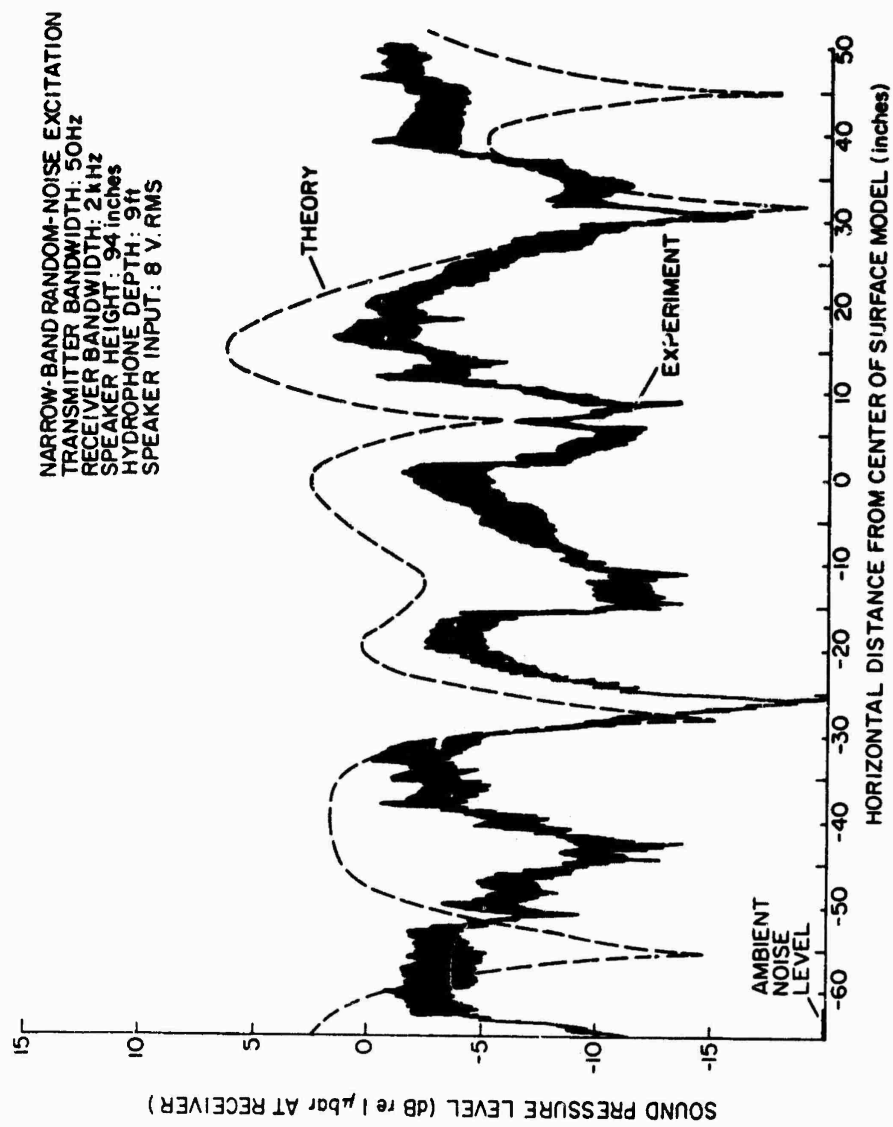
Figure 21. Underwater Sound Field Beneath Surface Model
No. 1 (Transmitter Frequency: 18 kHz, Speaker
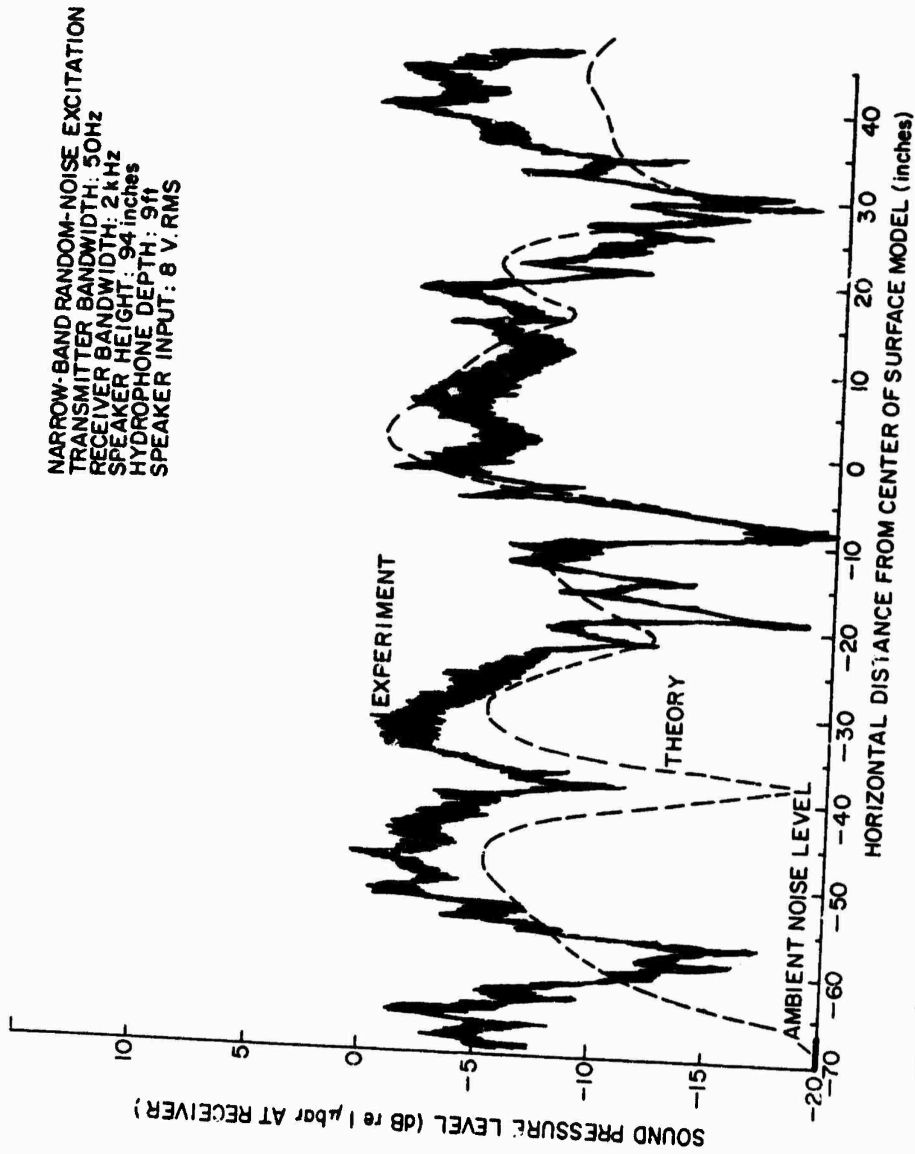Angle: 6 deg.)

Figure 22. Underwater Sound Field Beneath Surface Model No. 1 (Transmitter Frequency: 20 kHz, Speaker Angle: 6 deg.)
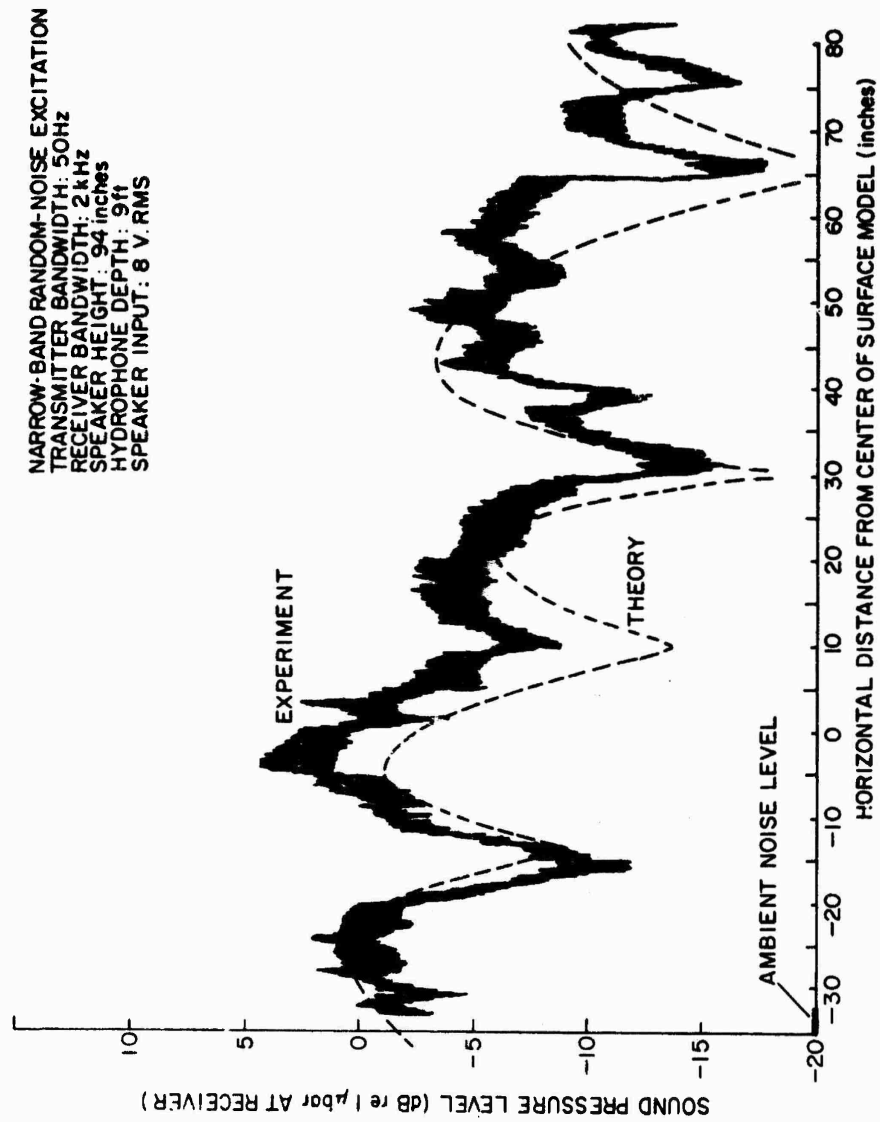
Figure 23. Underwater Sound Field Beneath Surface Model
No. 1 (Transmitter Frequency: 14 kHz, Speaker
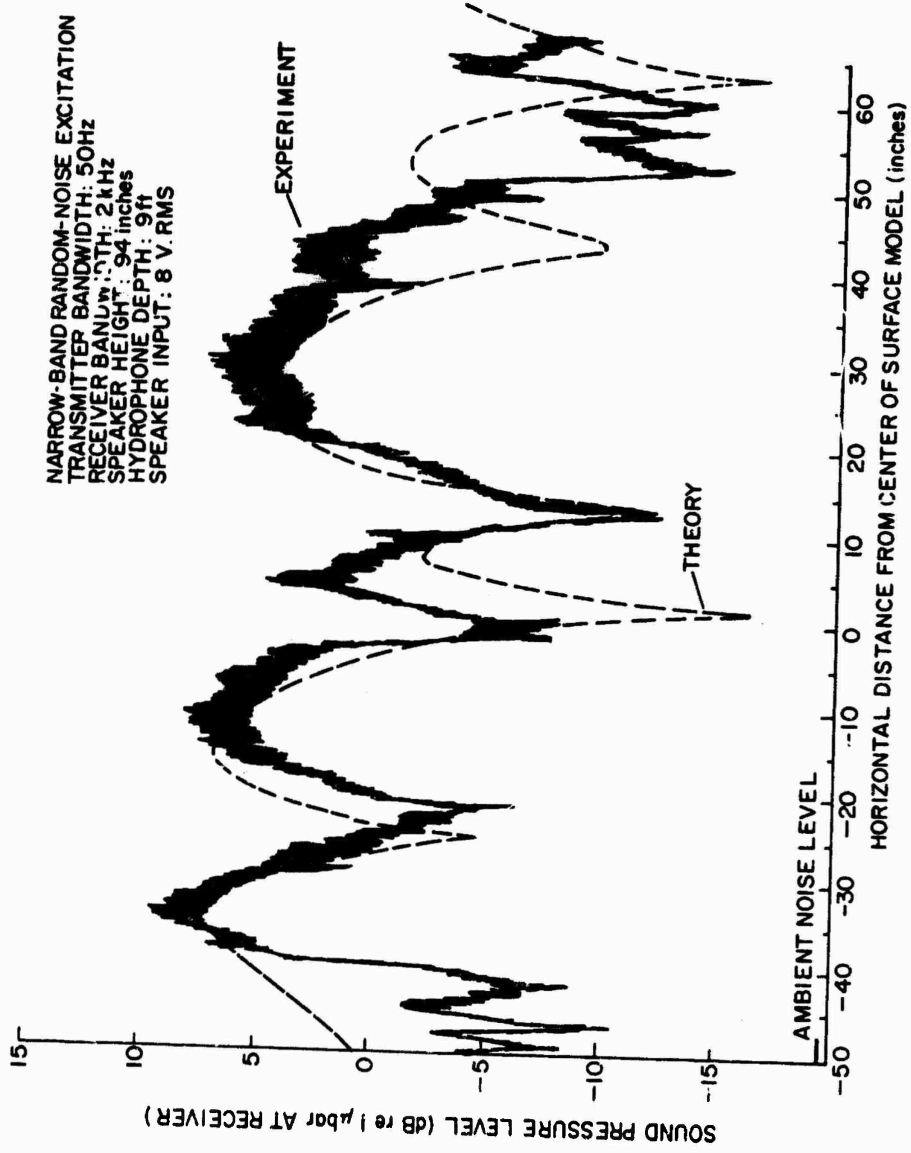Angle: 8 deg.)

Figure 24. Underwater Sound Field Beneath Surface Model
No. 1 (Transmitter Frequency: 16 kHz, Speaker
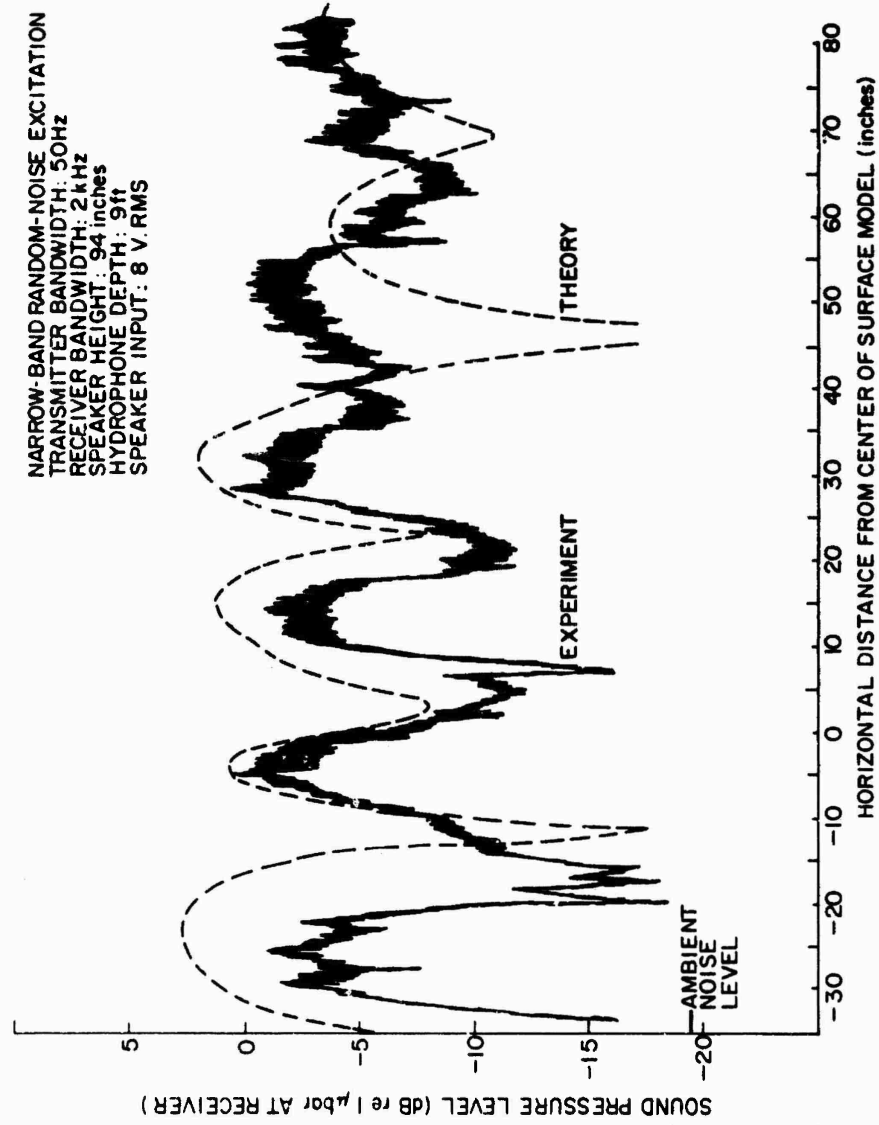Angle: 8 deg.)

Figure 25. Underwater Sound Field Beneath Surface Model
No. 1 (Transmitter Frequency: 18 kHz, Speaker
Angle: 8 deg.)

Figure 26. Underwater Sound Field Beneath Surface Model
No. 2 (Transmitter Frequency: 10 kHz, Speaker
Angle: 3 deg.)

Figure 27. Underwater Sound Field Beneath Surface Model
No. 2 (Transmitter Frequency: 14 kHz, Speaker
Angle: 3 deg.)

NARROW-BAND RANDOM-NOISE EXCITATION
TRANSMITTER BANDWIDTH: 50Hz
RECEIVER BANDWIDTH: 2kHz
SPEAKER HEIGHT: 94 inches
HYDROPHONE DEPTH: 9ft
SPEAKER INPUT: 8 V.RMS

THEORY

EXPERIMENT

AMBIENT
NOISE
LEVEL

HORIZONTAL DISTANCE FROM CENTER OF SURFACE MODEL (inches)

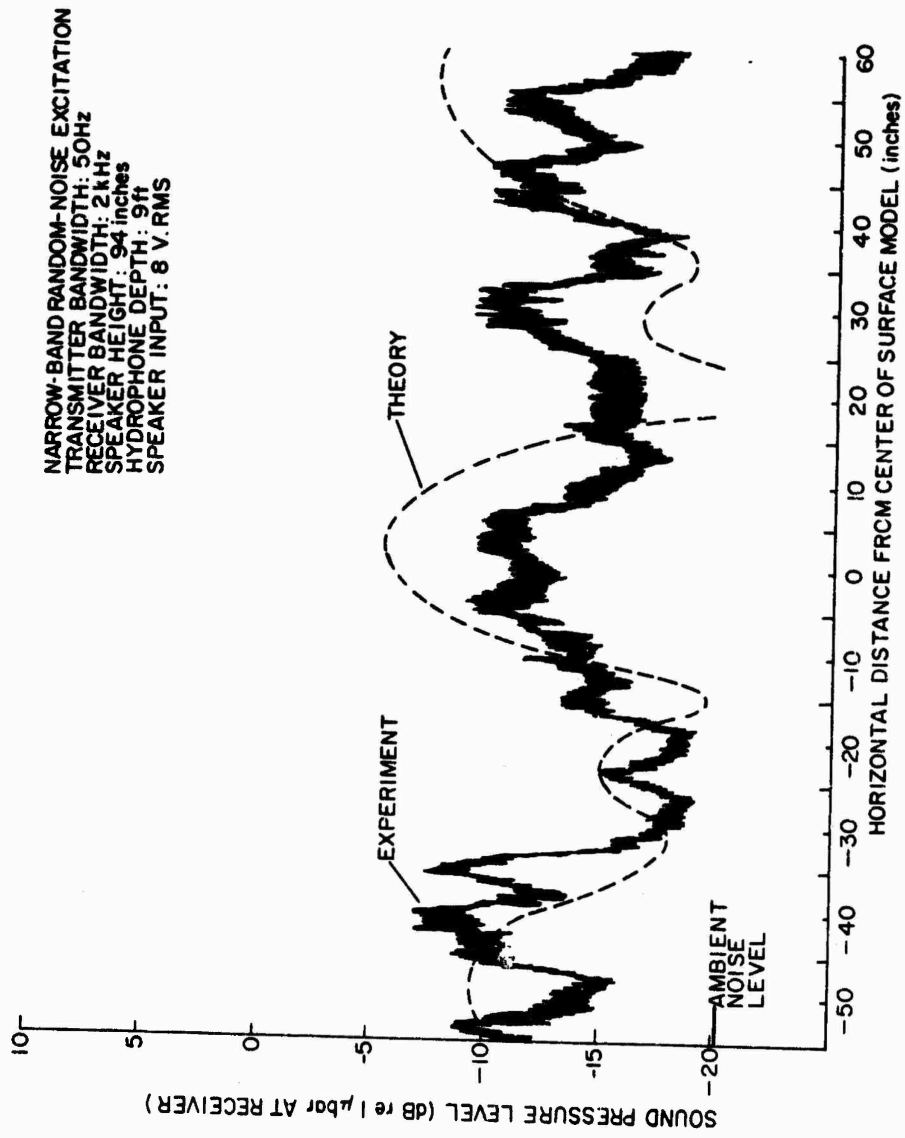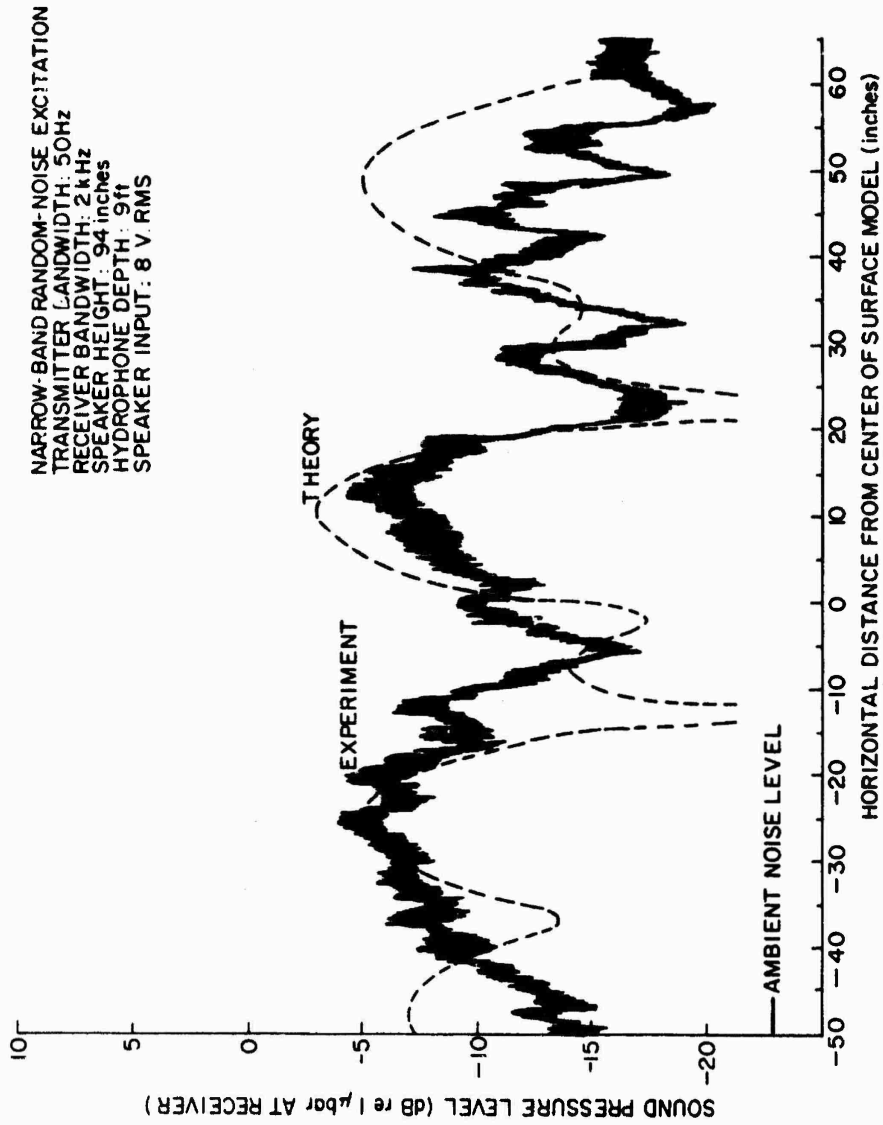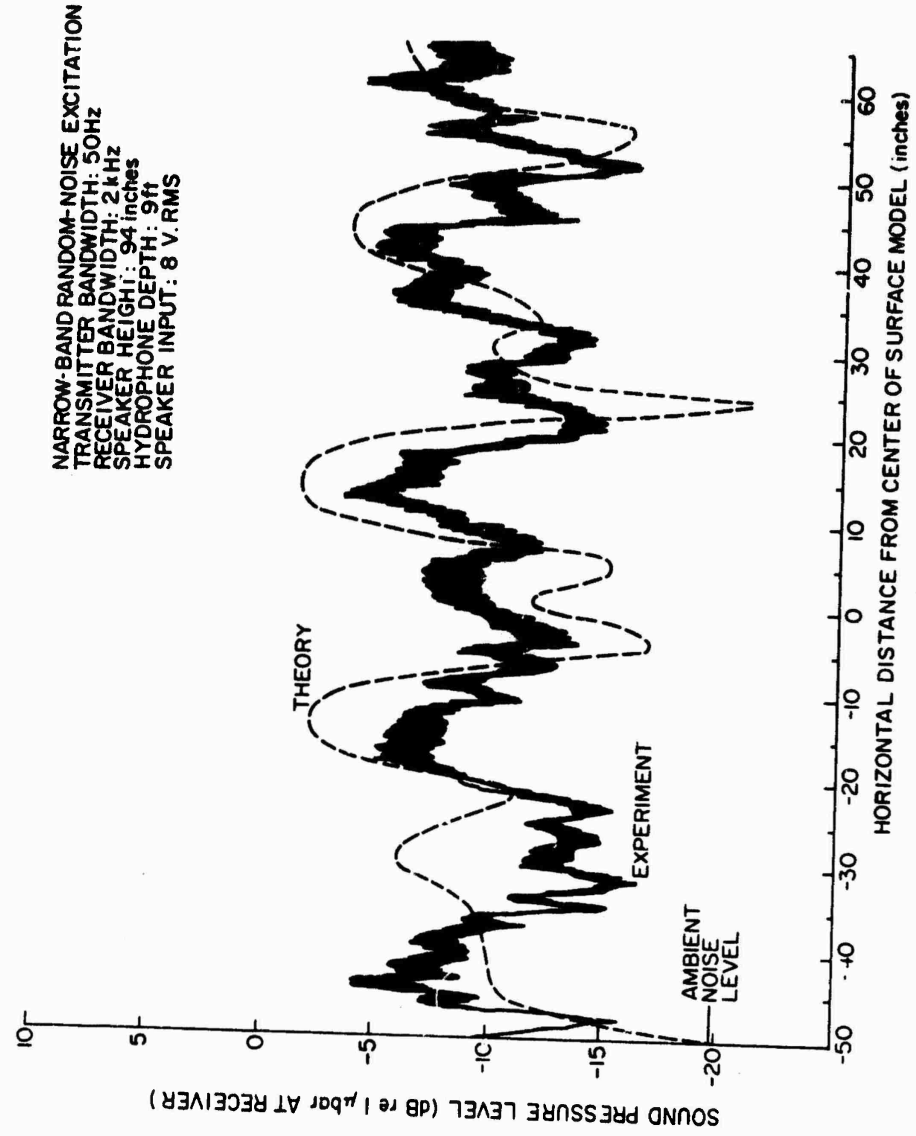SOUND PRESSURE LEVEL (dB re I μbar AT RECEIVER)

Figure 28.   Underwater Sound Field Beneath Surface Model
No. 2 (Transmitter Frequency: 18 kHz, Speaker
Angle: 3 deg.)

Figure 29. Underwater Sound Field Beneath Surface Model
No. 2 (Transmitter Frequency: 10 kHz, Speaker
Angle: 6 deg.)

Figure 30. Underwater Sound Field Beneath Surface Model
No. 2 (Transmitter Frequency: 14 kHz, Speaker
Angle: 6 deg.)

NARROW-BAND RANDOM-NOISE EXCITATION
TRANSMITTER BANDWIDTH: 50Hz
RECEIVER BANDWIDTH: 2kHz
SPEAKER HEIGHT: 94 inches
HYDROPHONE DEPTH: 9ft
SPEAKER INPUT: 8 V.RMS

THEORY

EXPERIMENT

AMBIENT
NOISE
LEVEL

HORIZONTAL DISTANCE FROM CENTER OF SURFACE MODEL (inches)

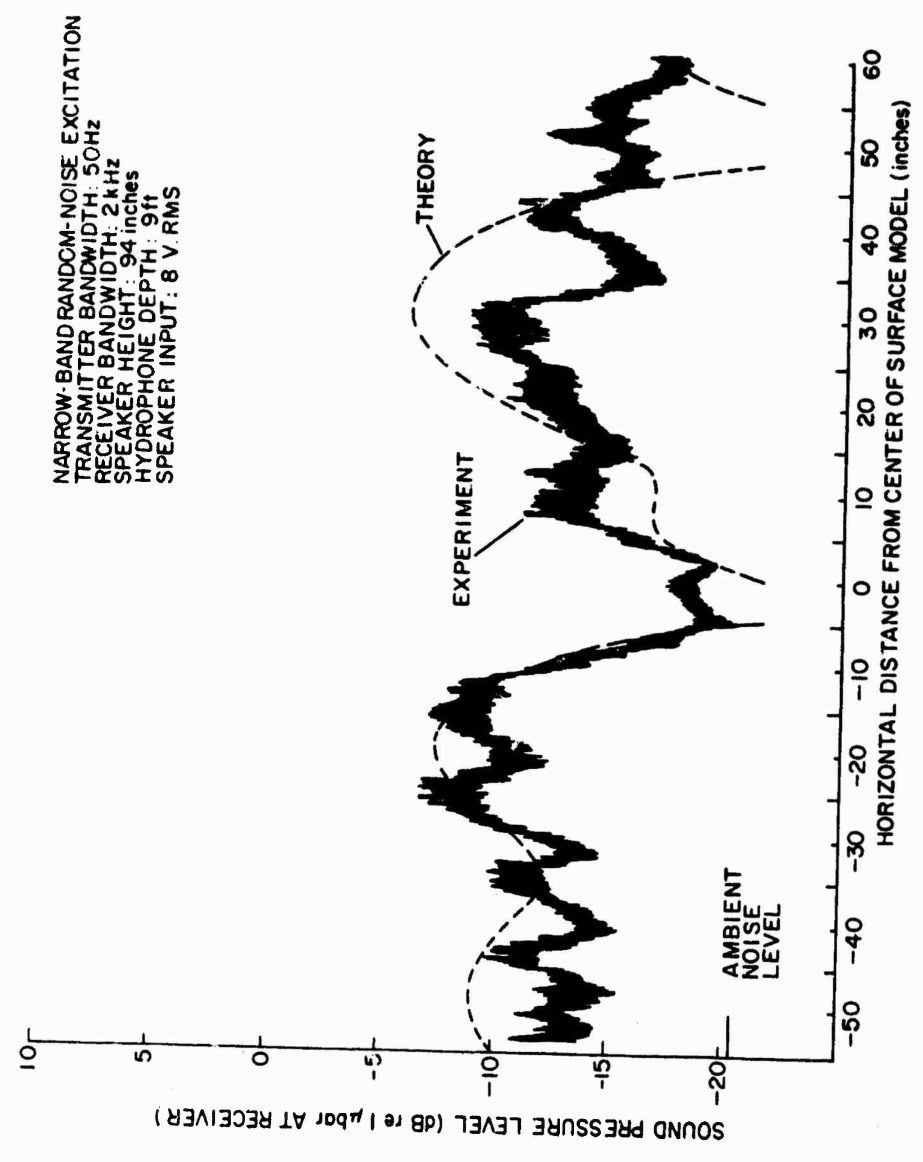SOUND PRESSURE LEVEL (dB re I µbar AT RECEIVER)

Figure 31. Underwater Sound Field Beneath Surface Model
No. 2 (Transmitter Frequency: 18 kHz, Speaker
Angle: 6 deg.)

Figure 32. Underwater Sound Field Beneath Surface Model
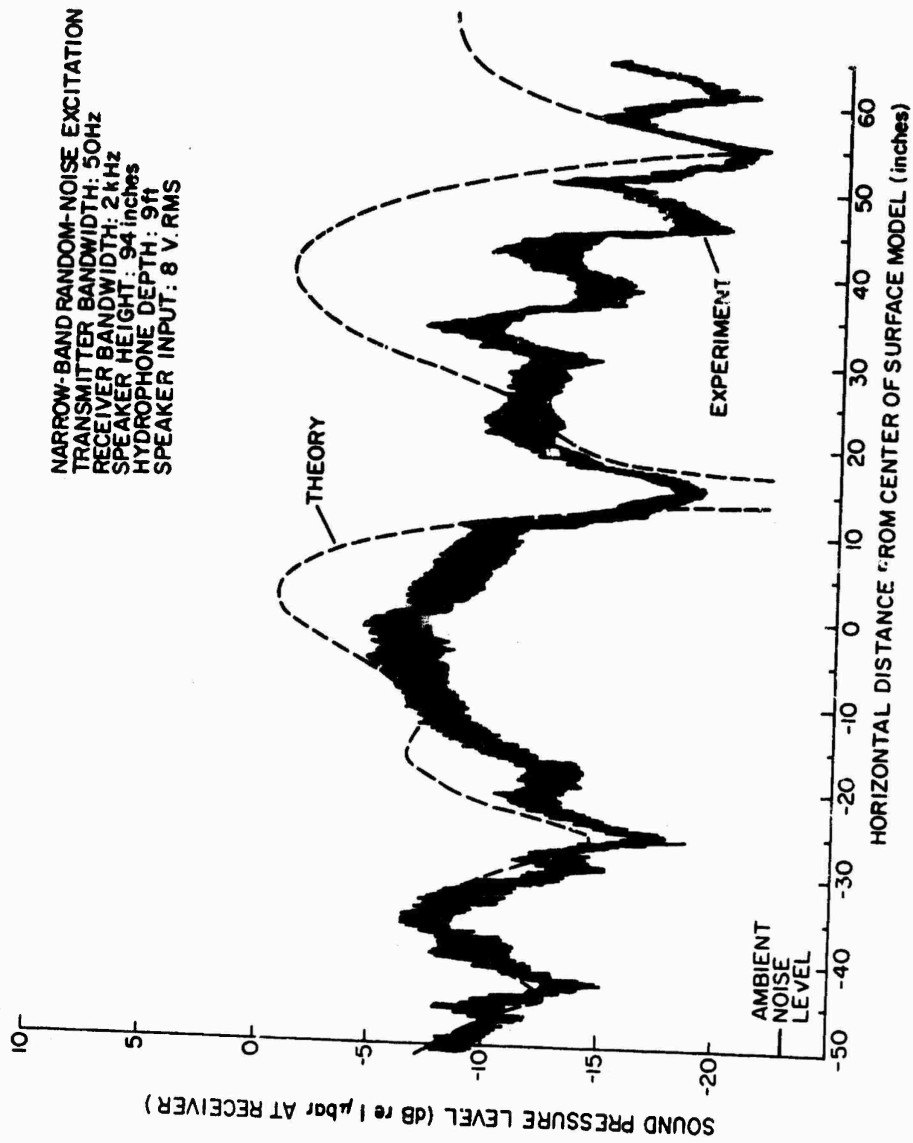No. 3 (Transmitter Frequency: 16 kHz, Speaker
Angle: 0 deg.)

Figure 33. Underwater Sound Field Beneath Surface Model No. 3 (Transmitter Frequency: 10 kHz, Speaker Angle: 3 deg.)

Figure 34. Underwater Sound Field Beneath Surface Model
No. 3 (Transmitter Frequency: 12 kHz, Speaker
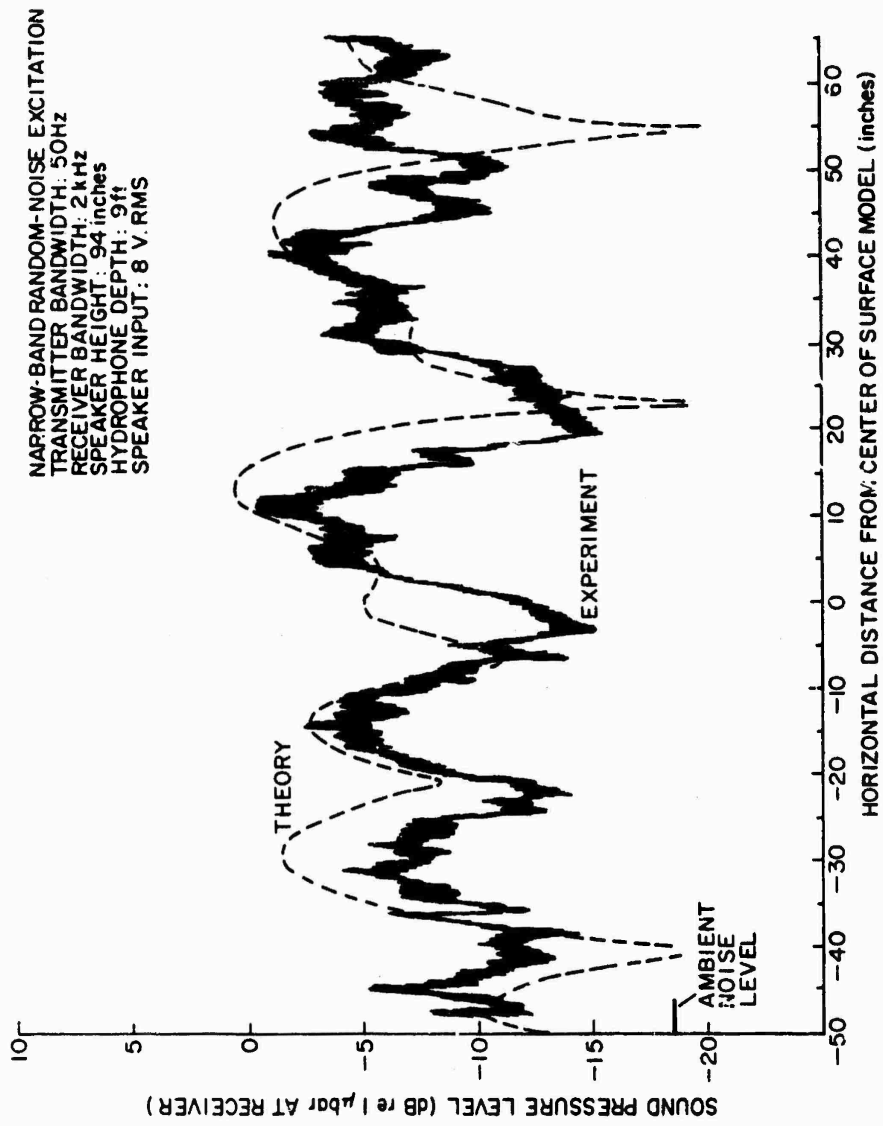Angle: 3 deg.)

Figure 35. Underwater Sound Field Beneath Surface Model No. 3 (Transmitter Frequency: 16 kHz, Speaker Angle: 3 deg.)

Figure 36. Underwater Sound Field Beneath Surface Model
No. 3 (Transmitter Frequency: 20 kHz, Speaker
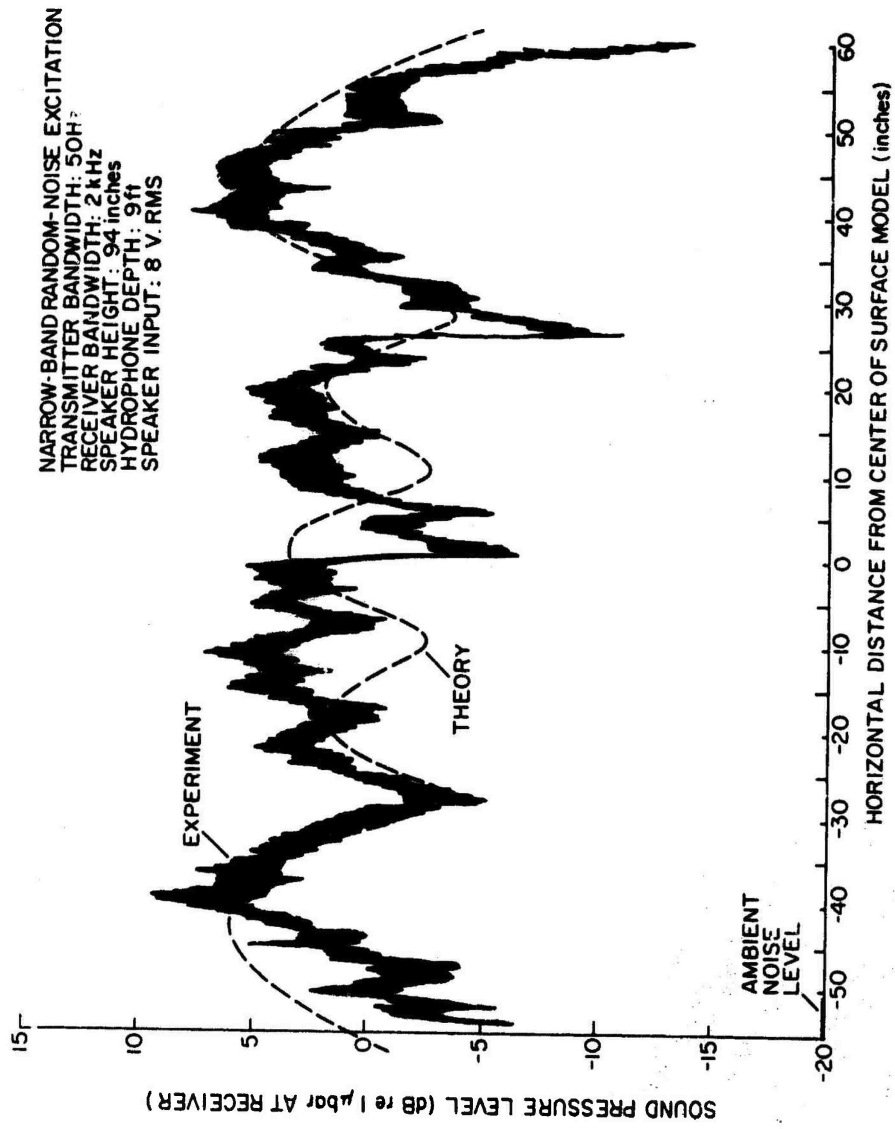Angle: 3 deg.)

Figure 37. Underwater Sound Field Beneath Surface Model
No. 3 (Transmitter Frequency: 10 kHz, Speaker
Angle: 6 deg.)

Figure 38. Underwater Sound Field Beneath Surface Model
No. 3 (Transmitter Frequency: 11 kHz, Speaker
Angle: 6 deg.)

Figure 39. Underwater Sound Field Beneath Surface Model
No. 3 (Transmitter Frequency: 16 kHz, Speaker
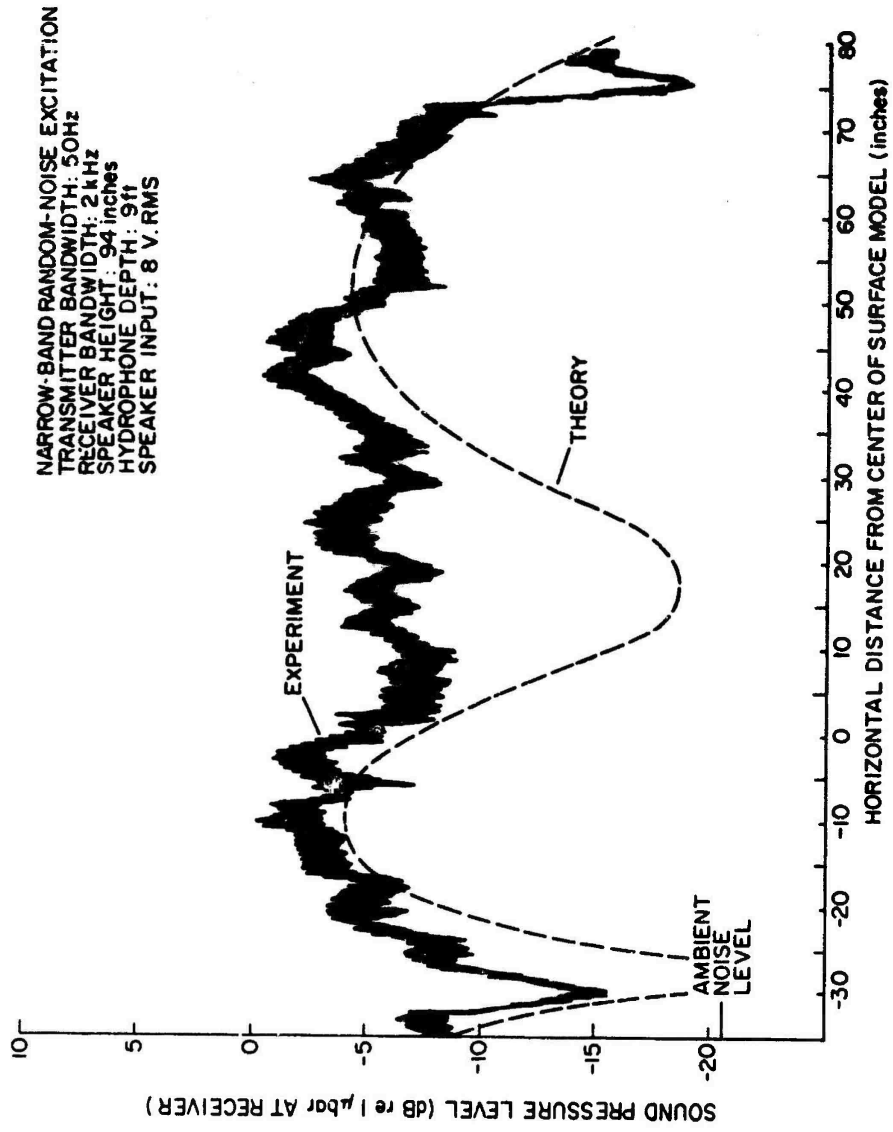Angle: 6 deg.)

Figure 40. Underwater Sound Field Beneath Surface Model
No. 3 (Transmitter Frequency: 18 kHz, Speaker
Angle: 6 deg.)

Figure 41. Underwater Sound Field Beneath Surface Model
No. 3 (Transmitter Frequency: 20 kHz, Speaker
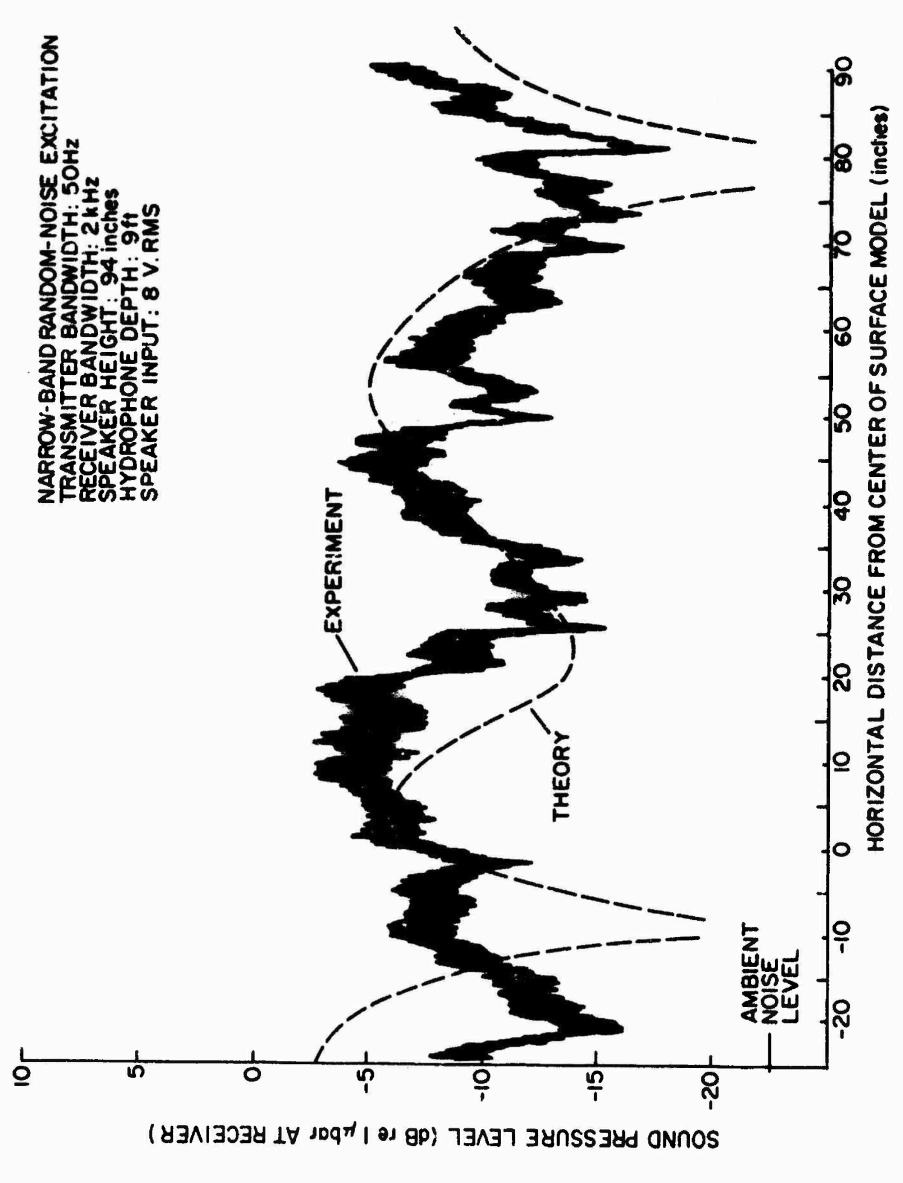Angle: 6 deg.)

Figure 42. Underwater Sound Field Beneath Surface Model
No. 4 (Transmitter Frequency: 12 kHz, Speaker
Angle: 3 deg.)

Figure 43. Underwater Sound Field Beneath Surface Model
No. 4 (Transmitter Frequency: 14 kHz, Speaker
Angle: 3 deg.)

Figure 44. Underwater Sound Field Beneath Surface Model
No. 4 (Transmitter Frequency: 16 kHz, Speaker
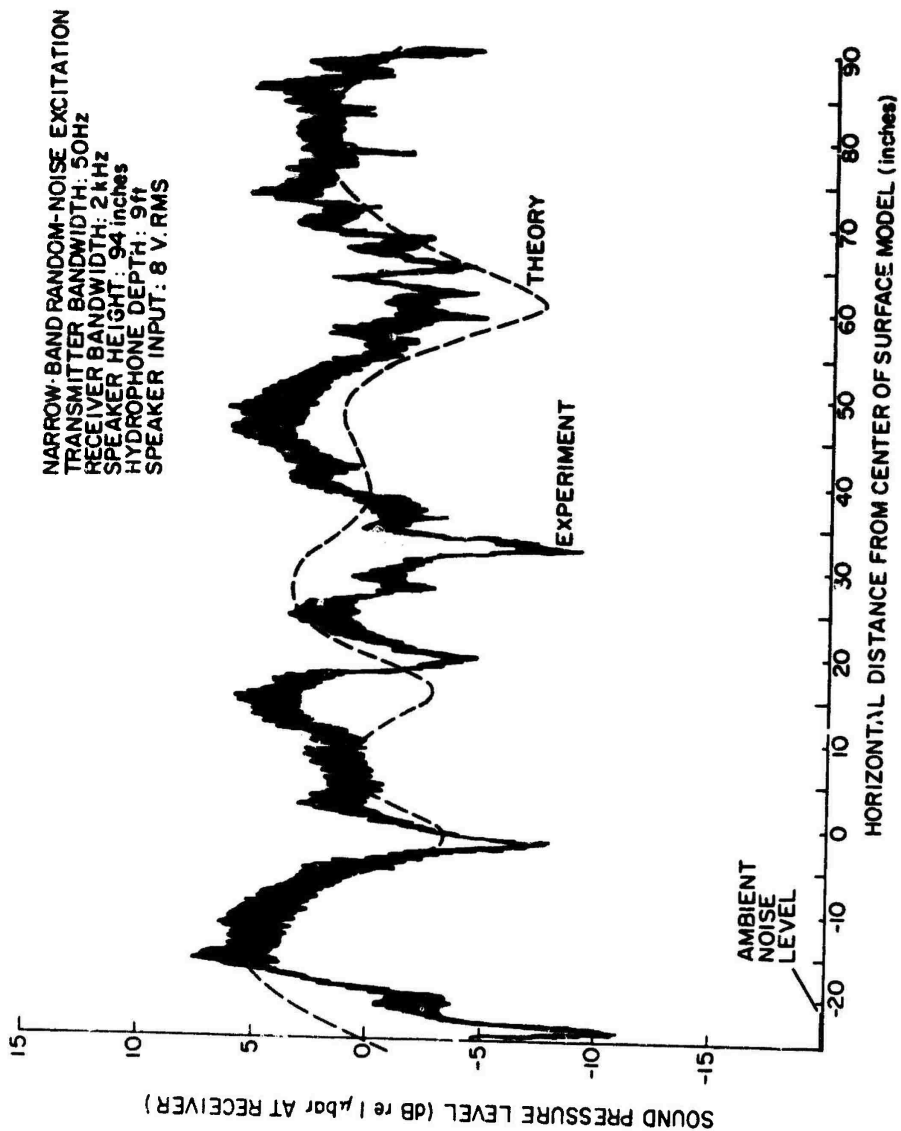Angle: 3 deg.)

Figure 45. Underwater Sound Field Beneath Surface Model
No. 4 (Transmitter Frequency: 18 kHz, Speaker
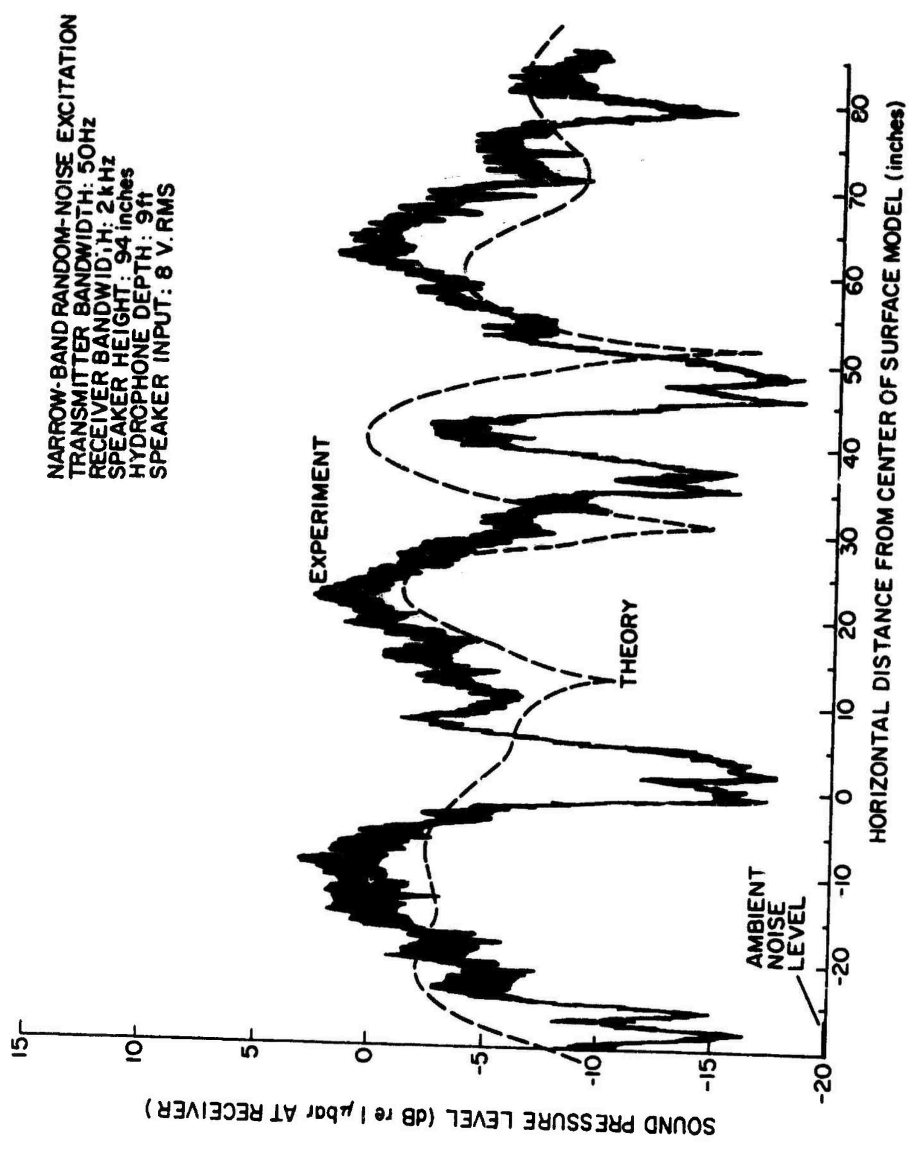Angle: 3 deg.)

Figure 46. Underwater Sound Field Beneath Surface Model
No. 4 (Transmitter Frequency: 20 kHz, Speaker
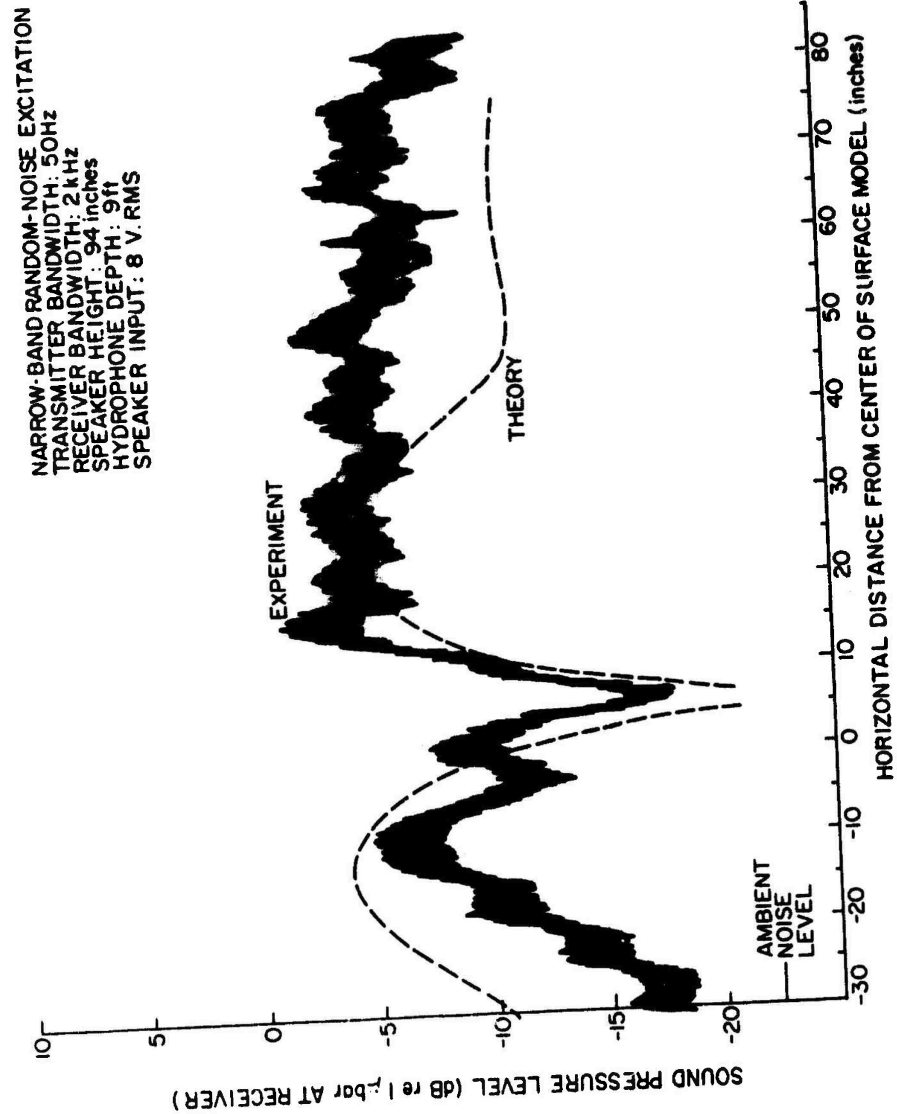Angle: 3 deg.)
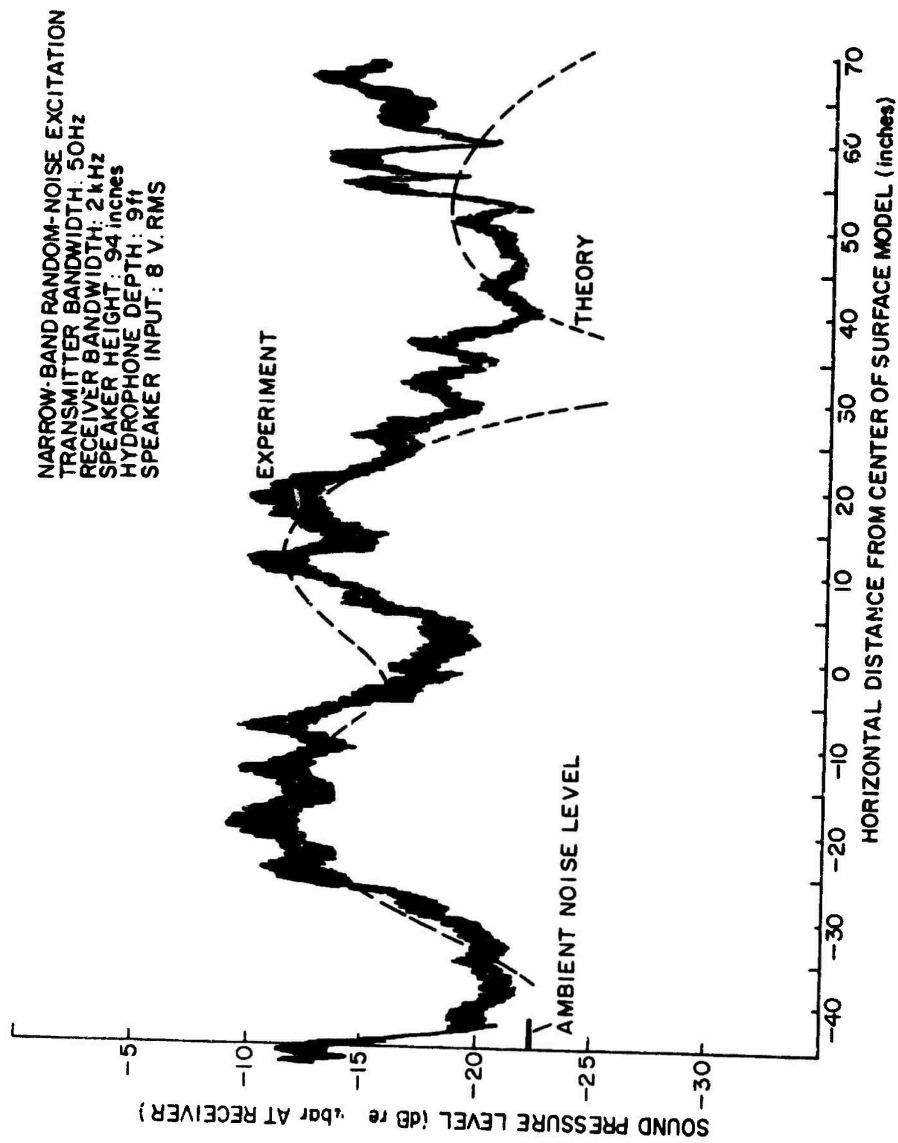
Figure 47. Underwater Sound Field Beneath Surface Model No. 4 (Transmitter Frequency: 12 kHz, Speaker Angle: 6 deg.)
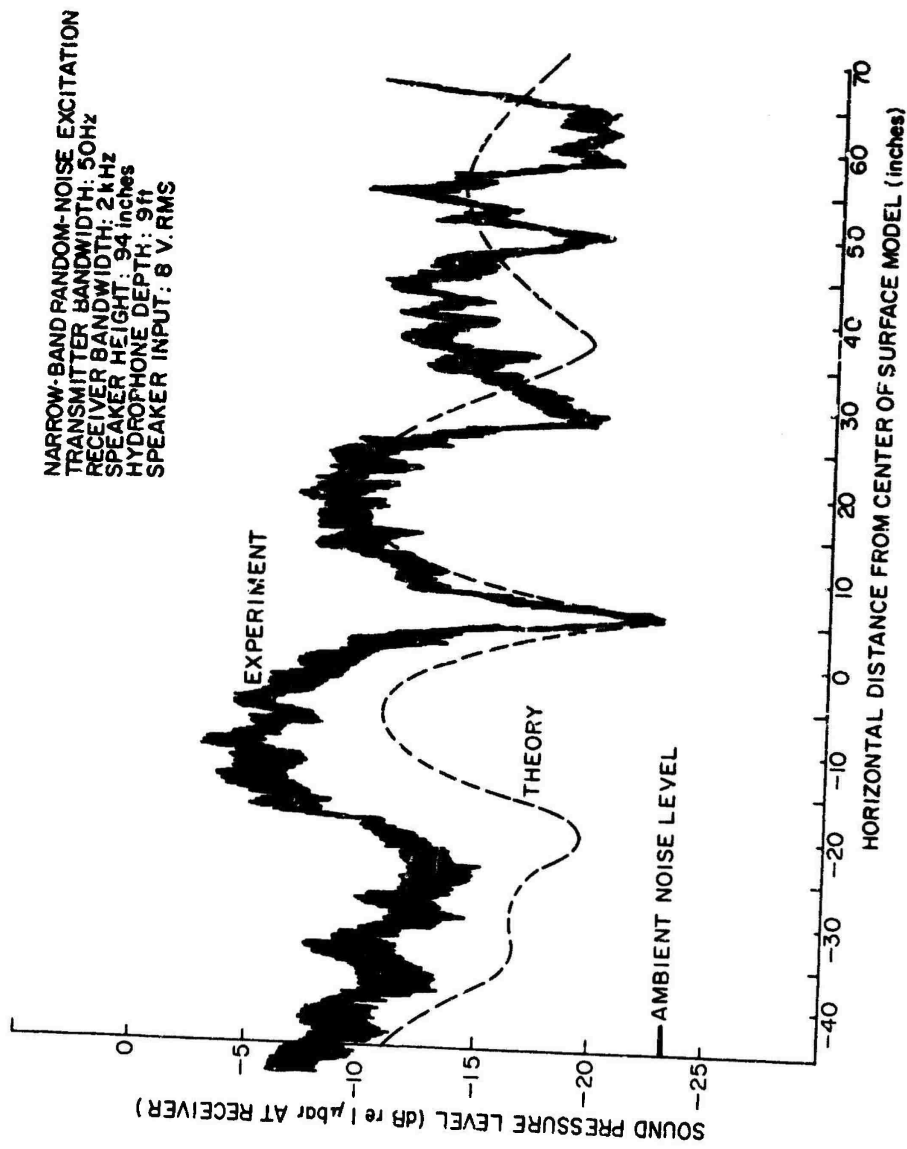
Figure 48. Underwater Sound Field Beneath Surface Model
No. 4 (Transmitter Frequency: 14 kHz, Speaker
Angle: 6 deg.)
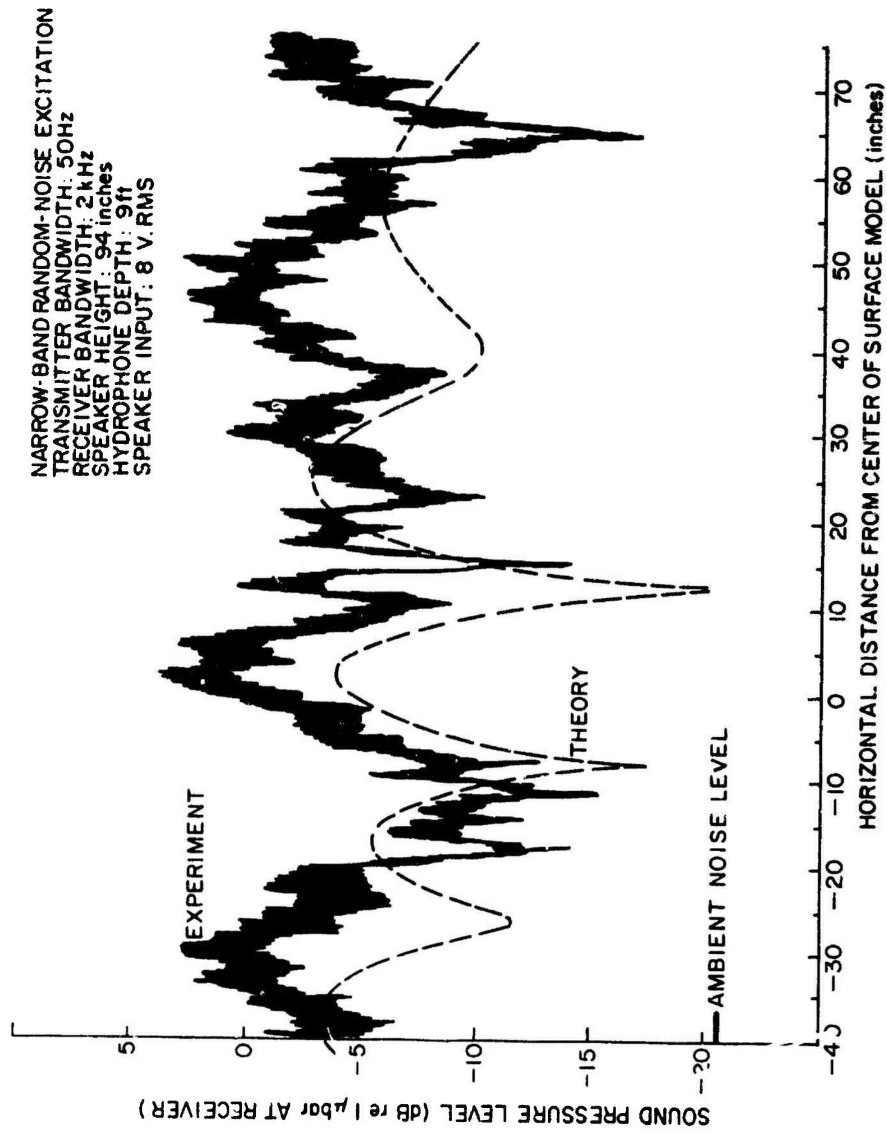
Figure 49. Underwater Sound Field Beneath Surface Model
No. 4 (Transmitter Frequency: 16 kHz, Speaker
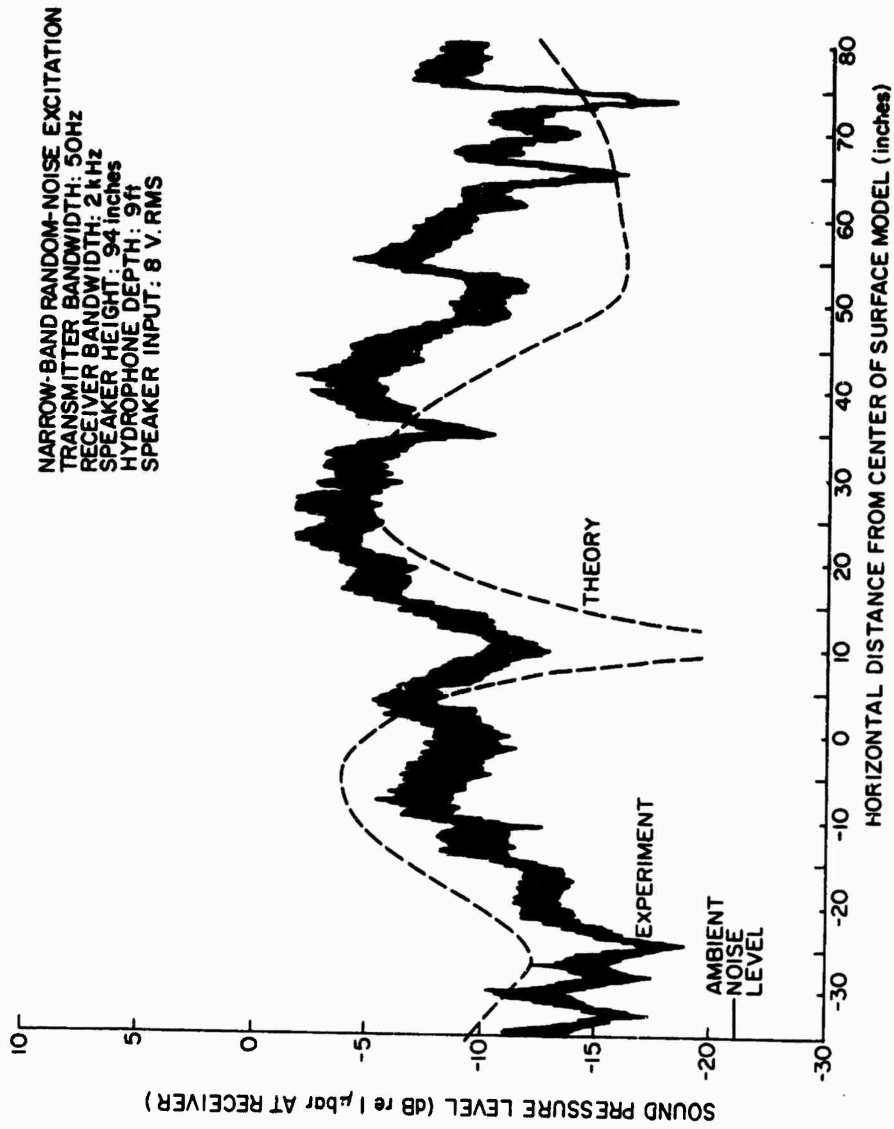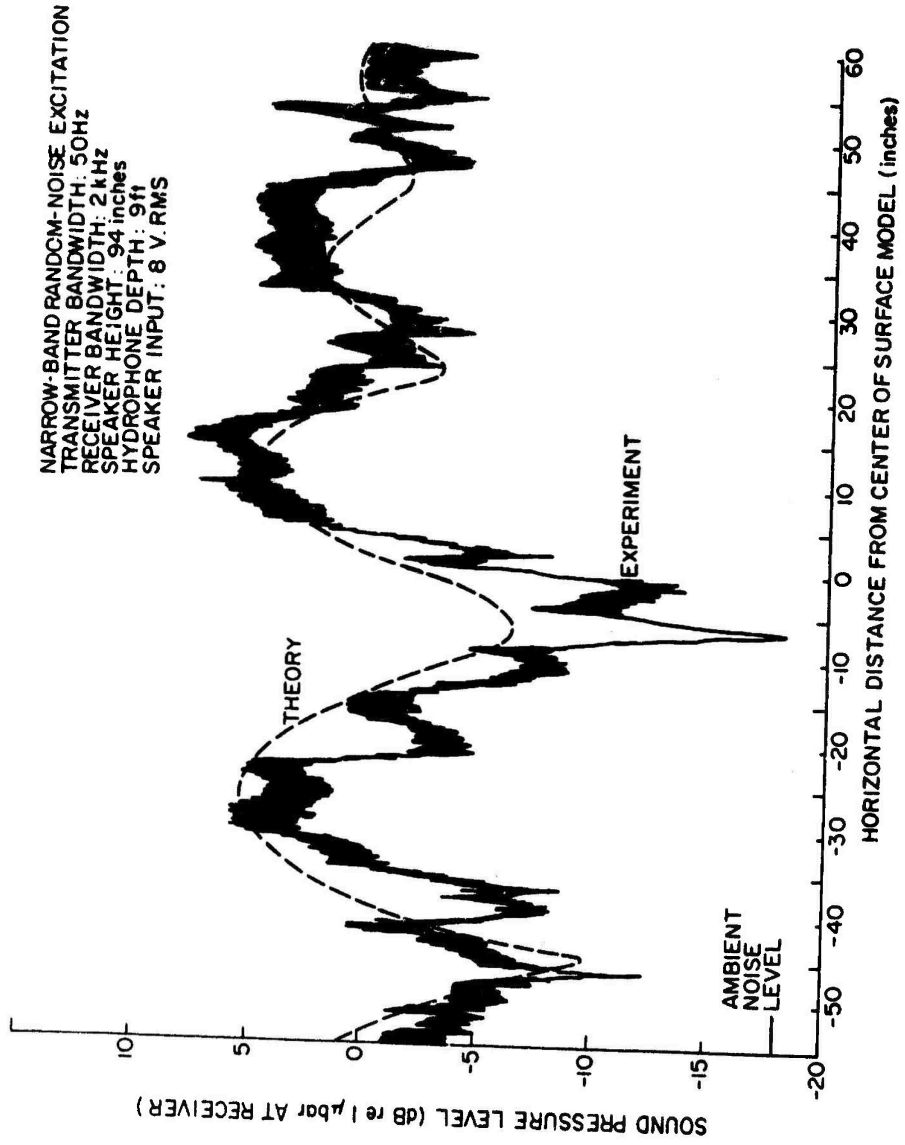Angle: 6 deg.)

108
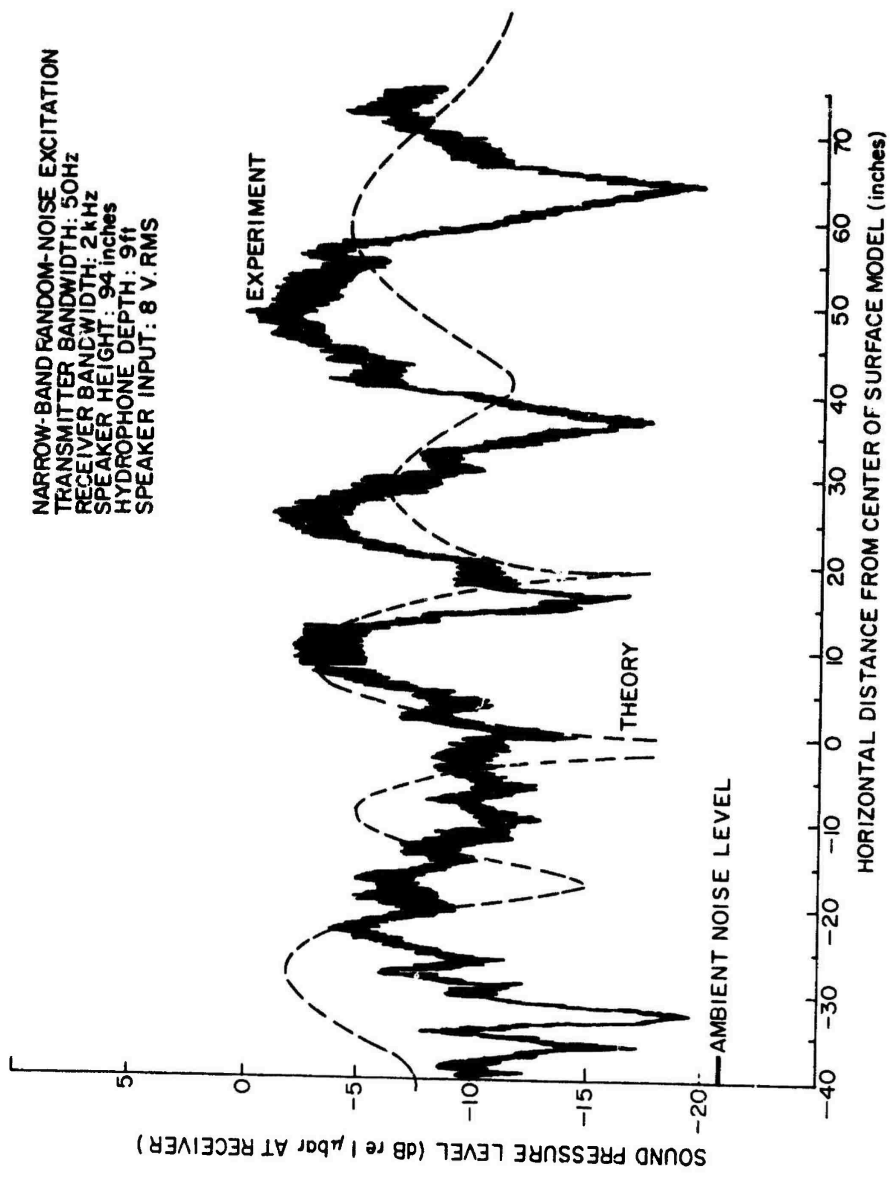
Figure 50. Underwater Sound Field Beneath Surface Model
No. 4 (Transmitter Frequency: 18 kHz, Speaker
Angle: 6 deg.)
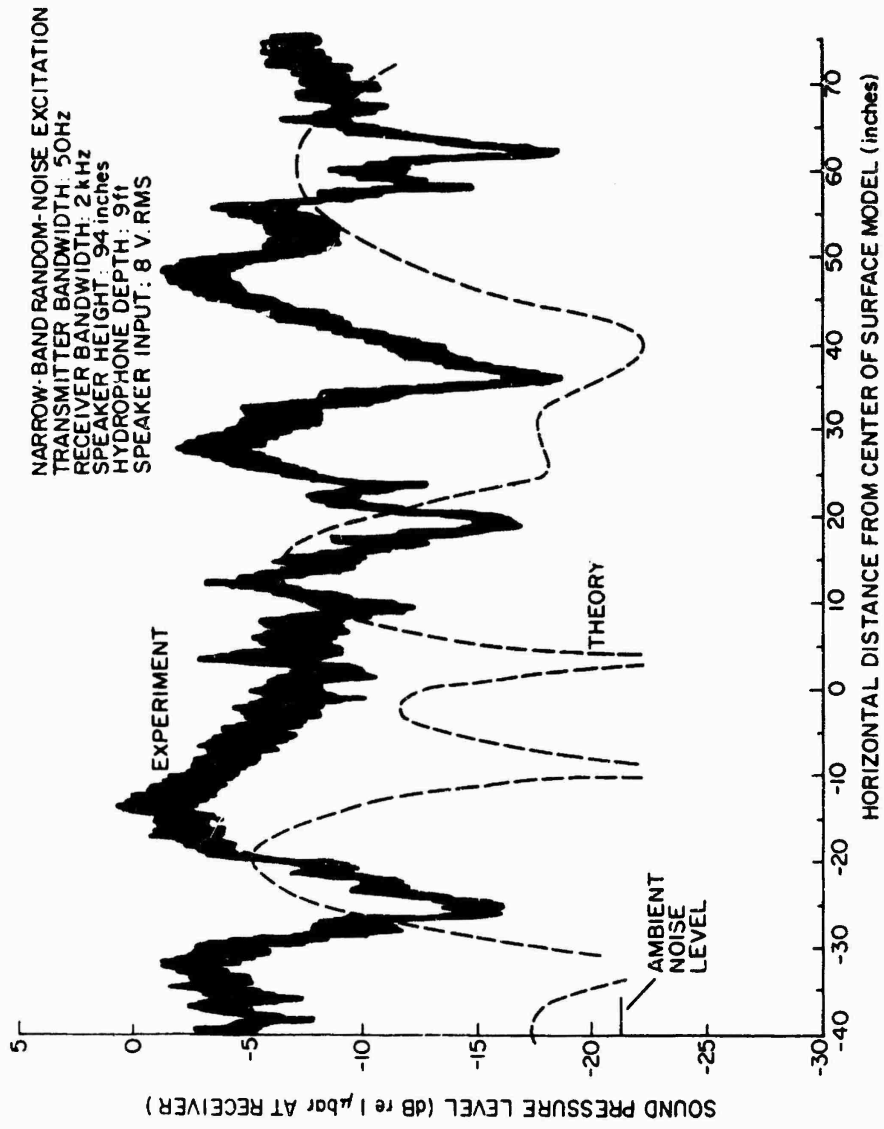
Figure 51. Underwater Sound Field Beneath Surface Model
No. 4 (Transmitter Frequency: 20 kHz, Speaker
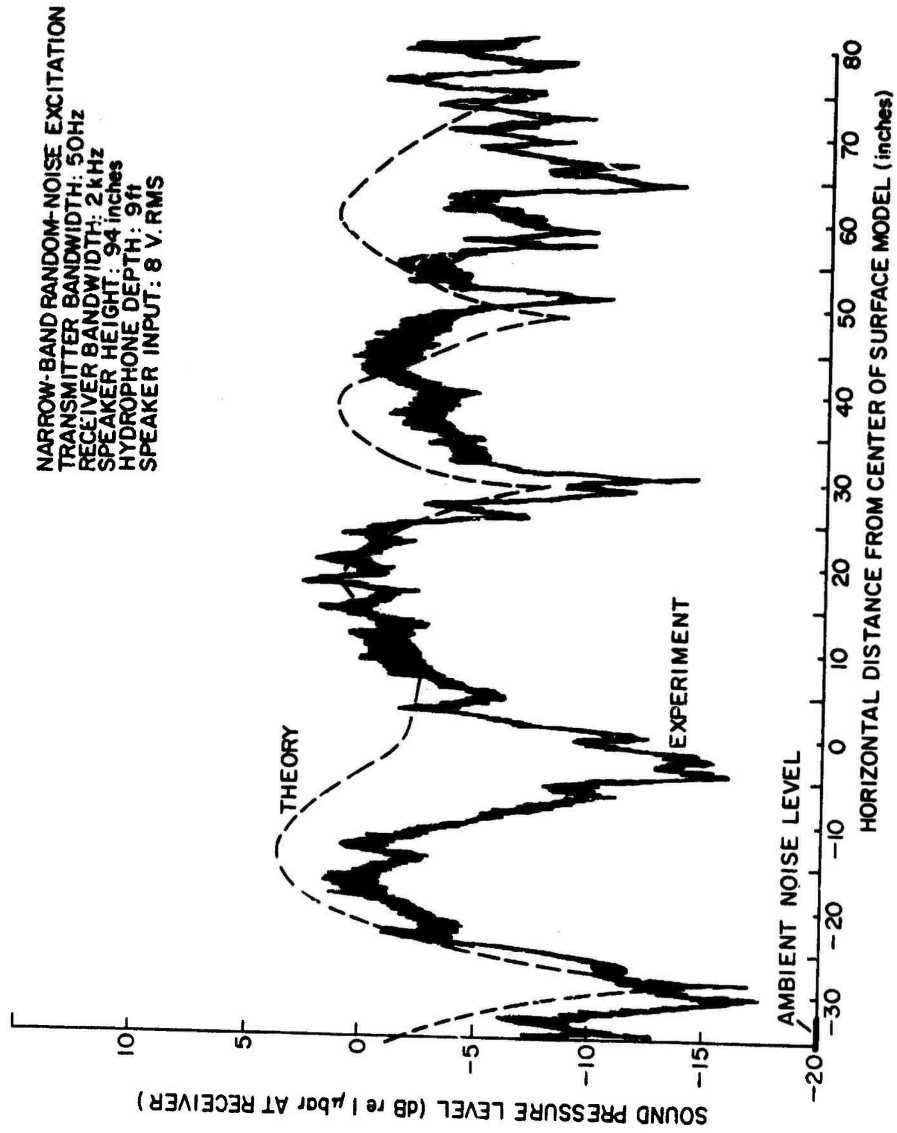Angle: 6 deg.)

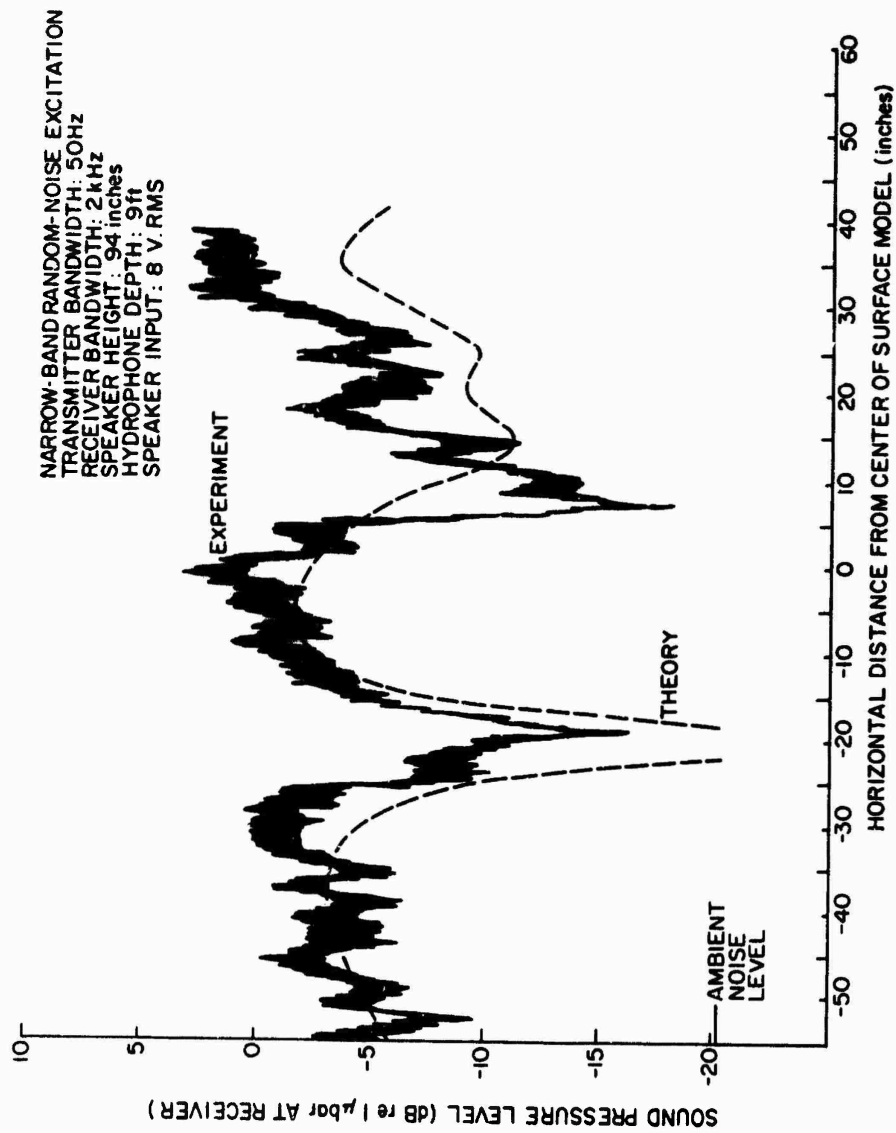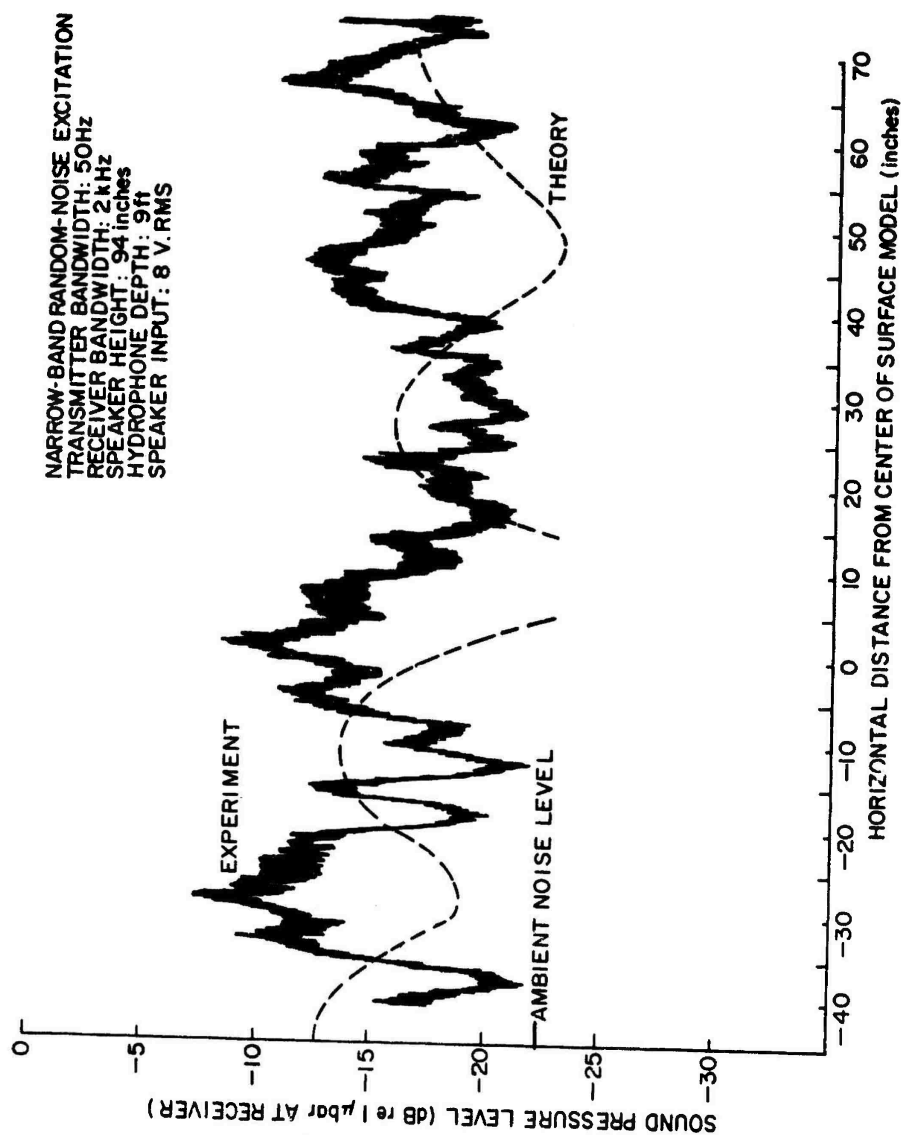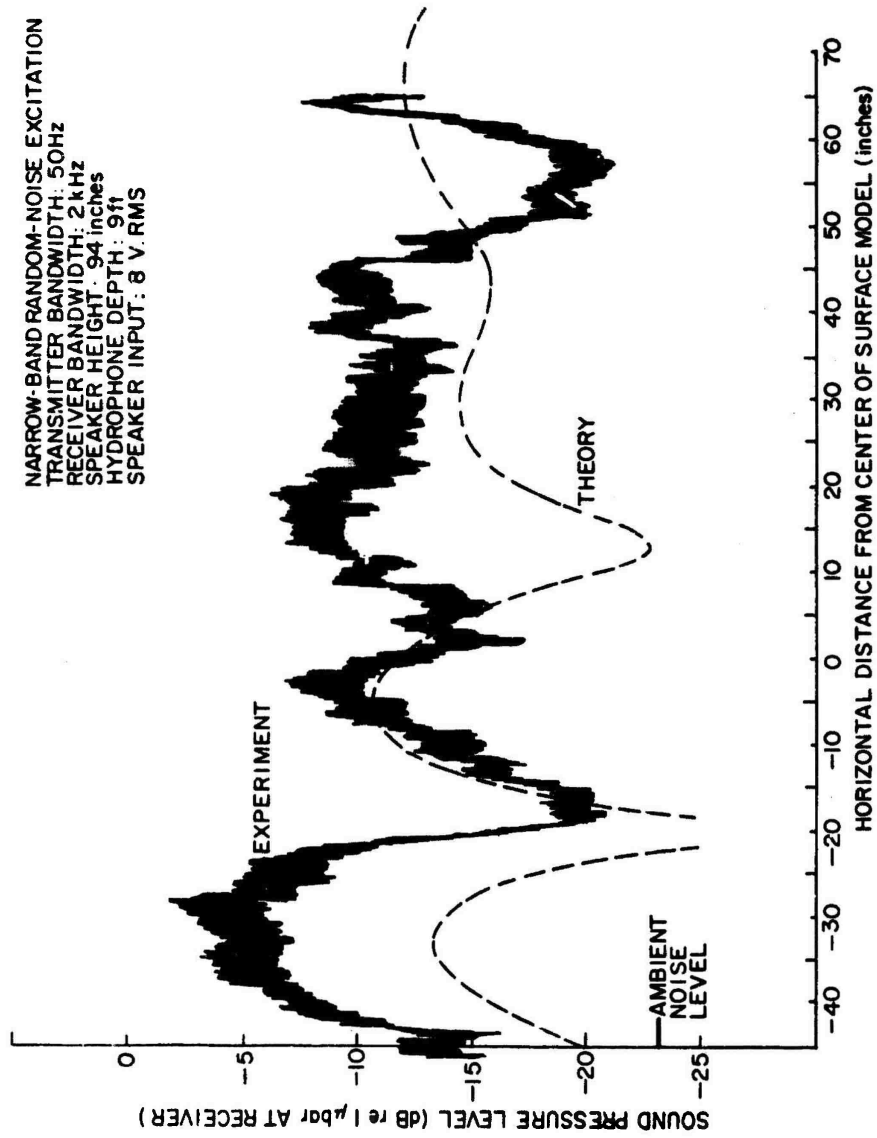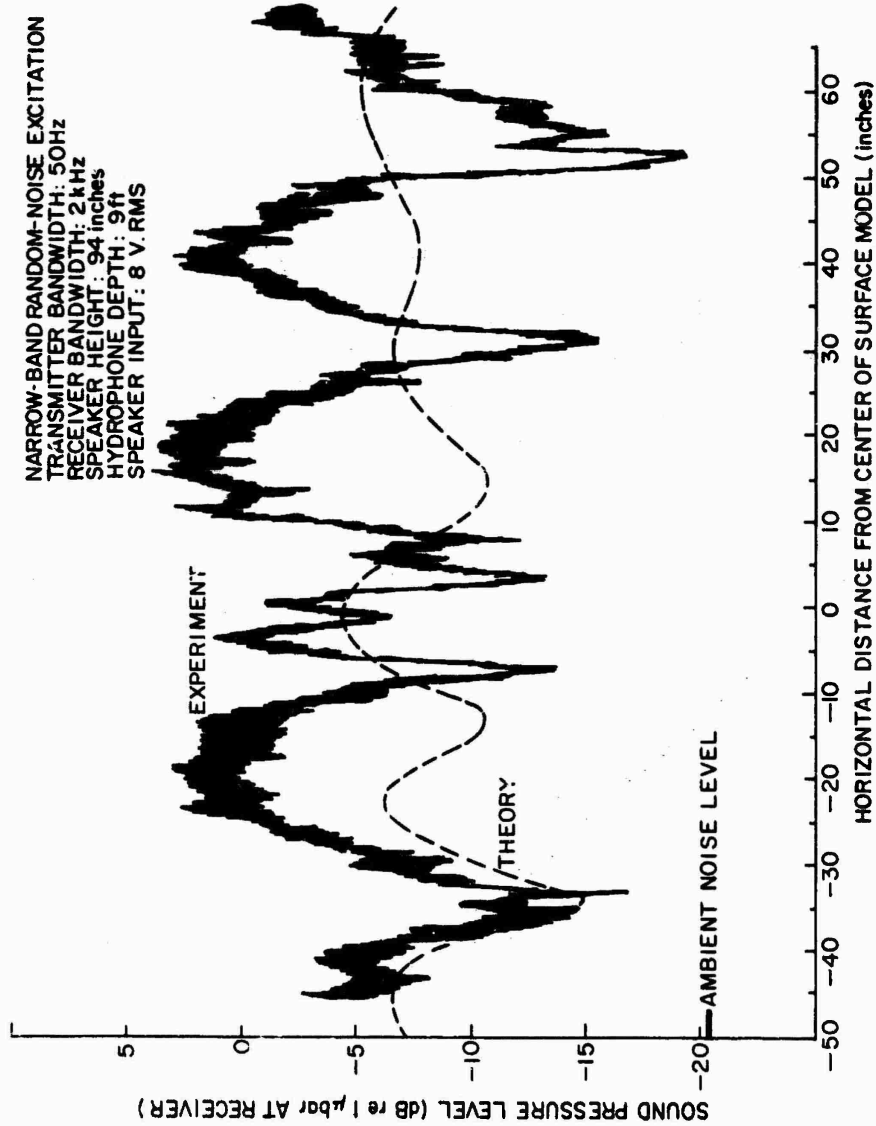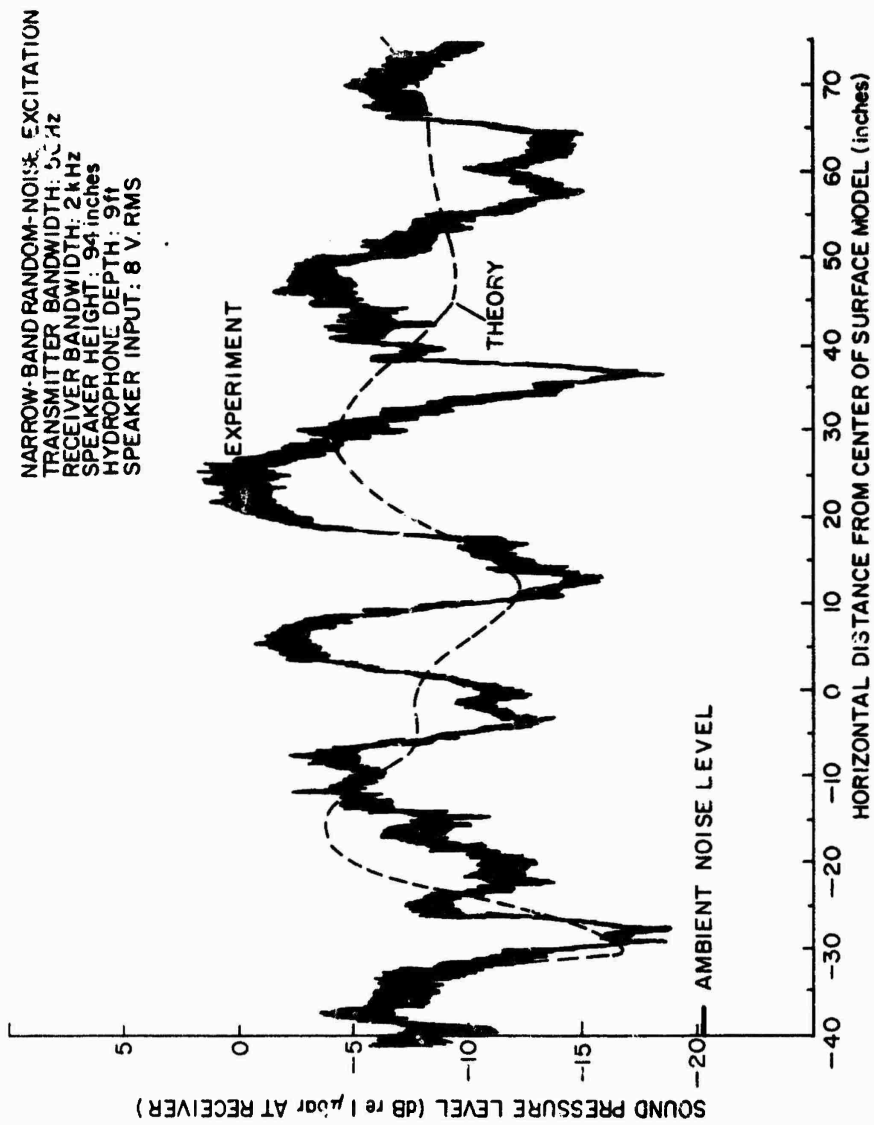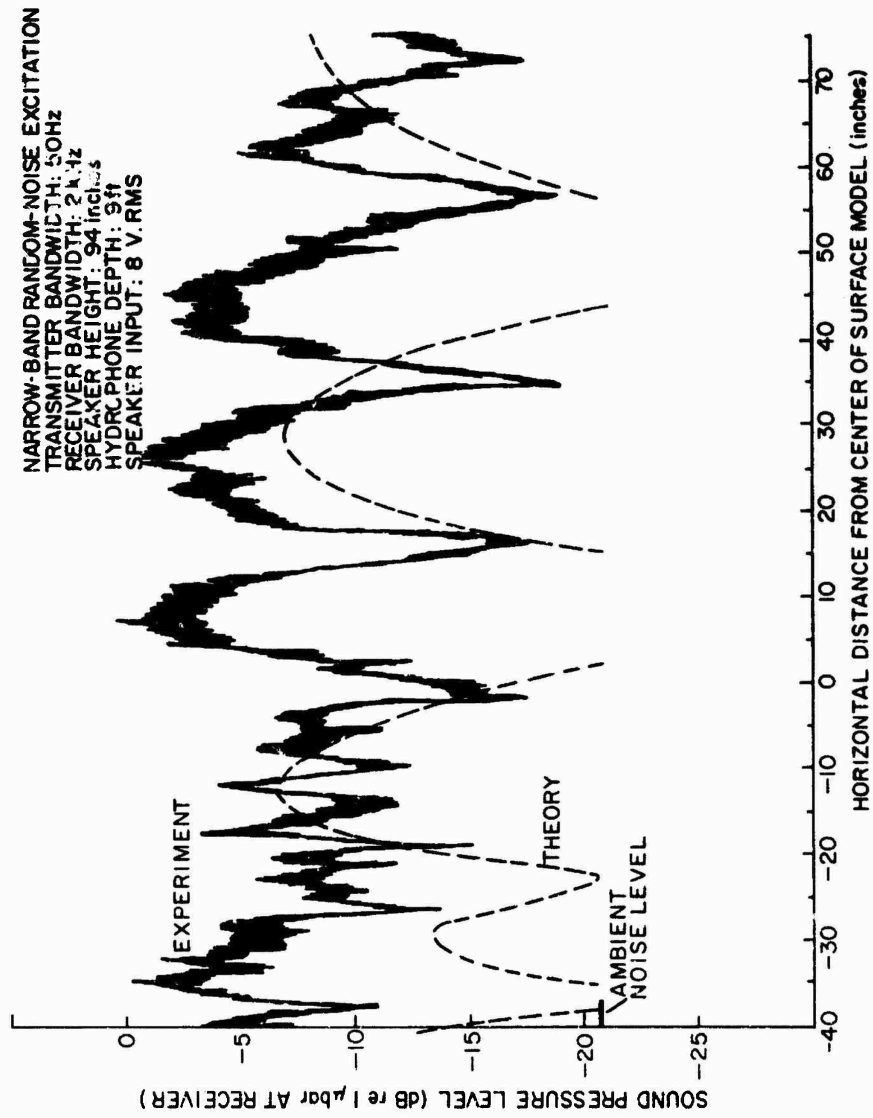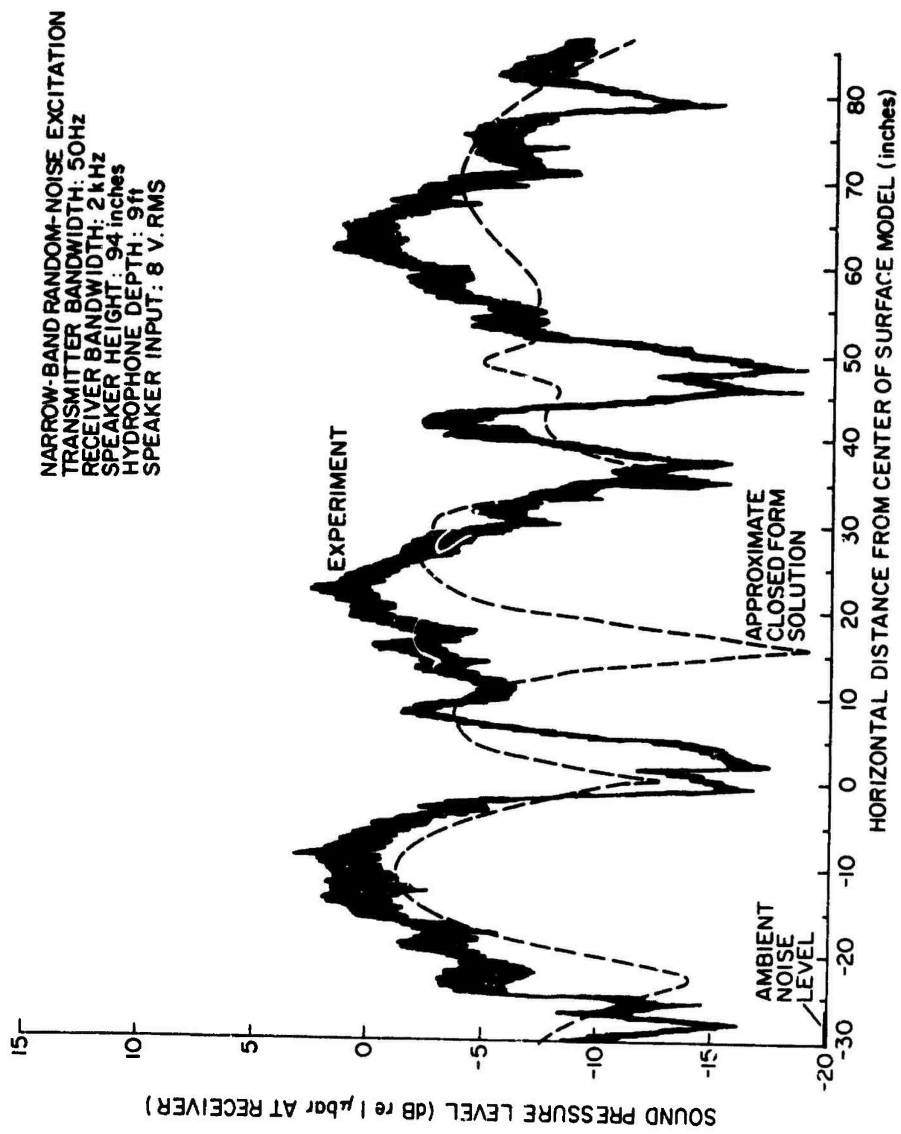Figure 52. Underwater Sound Field Beneath Surface Model
No. 3 (Transmitter Frequency: 20 kHz, Speaker
Angle: 3 deg.)
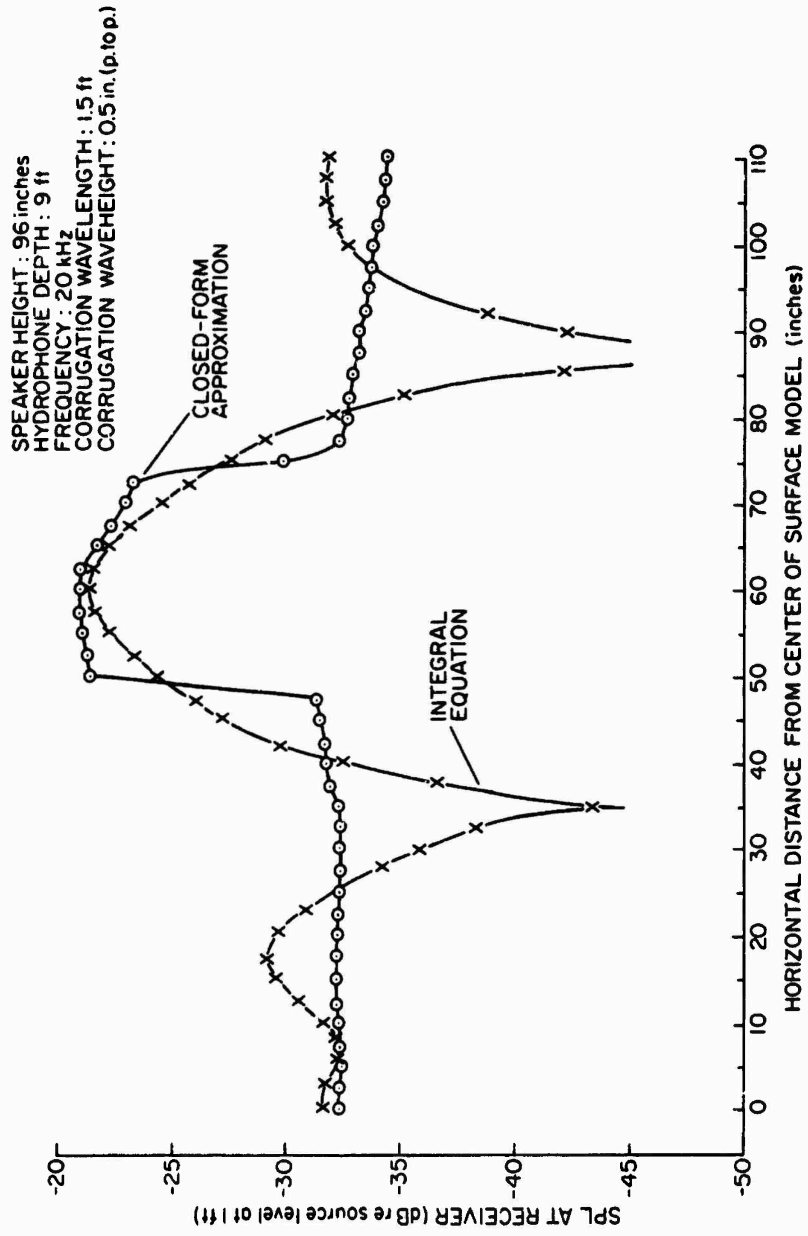
Figure 53. Comparison of Data Between Integral Equation
and Approximate Closed-Form Solution
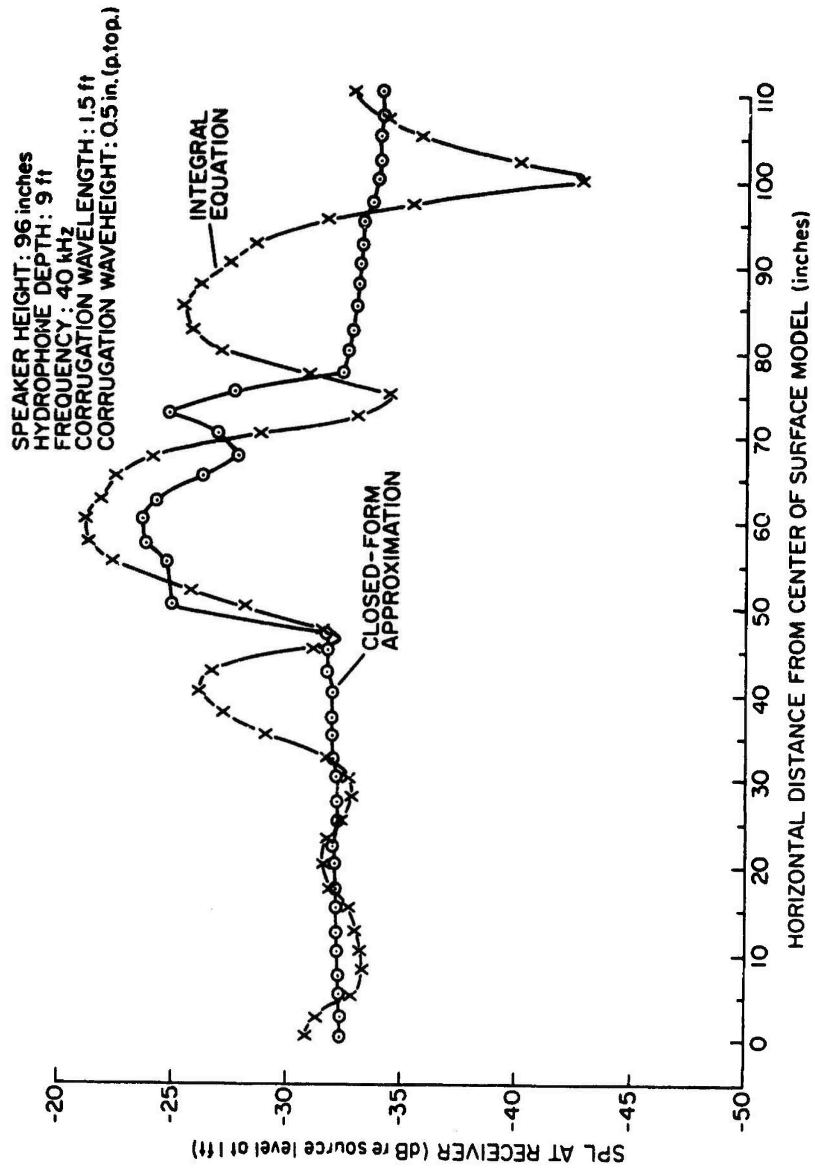
Figure 54. Comparison of Data Between Integral Equation and Approximate Closed-Form Solution
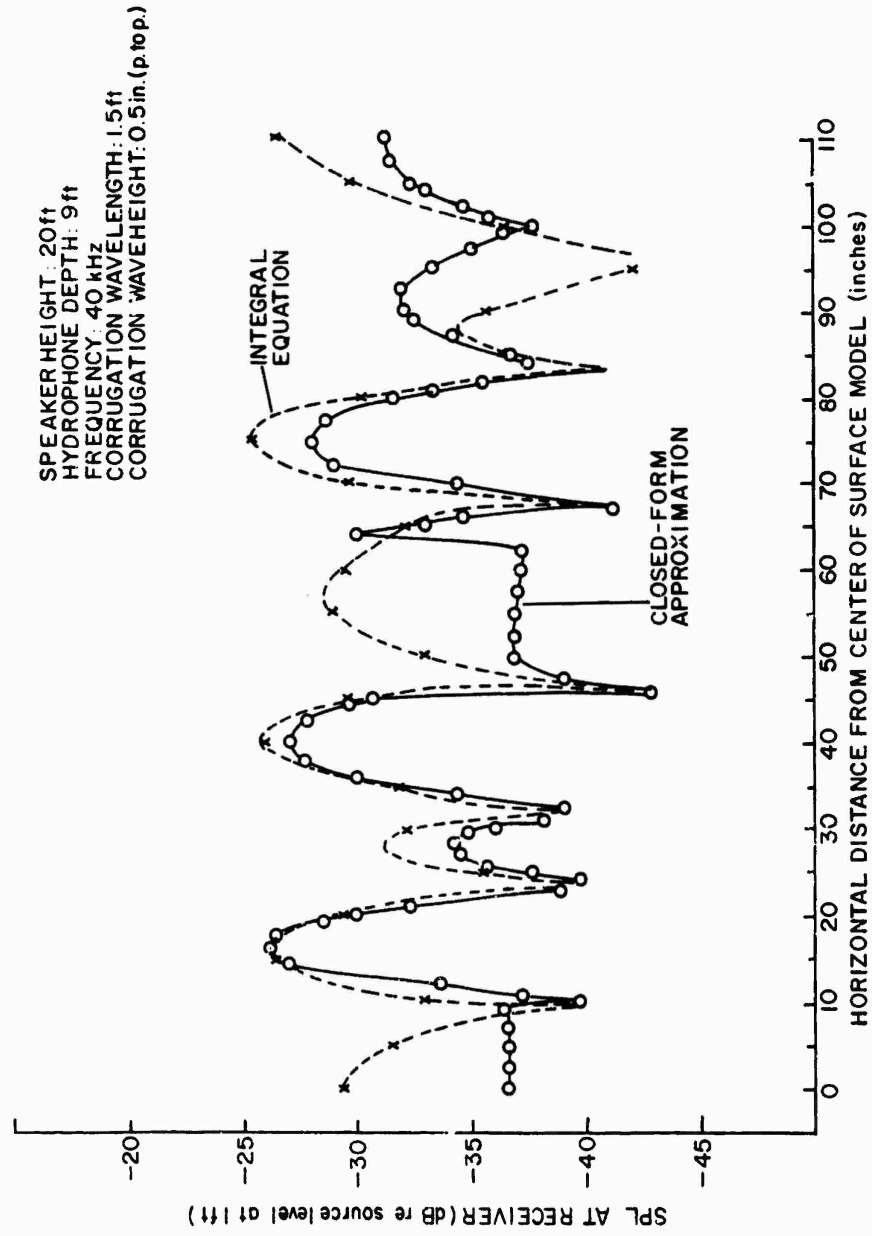
Figure 55. Comparison of Data Between Integral Equation and Approximate Closed-Form Solution

REFERENCES

1. Asano, S., "Reflection and Refraction of Elastic Waves at a Corrugated Interface," Bulletin of the Seismological Society of America, Vol. 56, No. 1, pp. 201-221, Feb., 1966.

2. Brekhovskikh, L. M., Waves in Layered Media, (Academic Press, New York, 1960.)

3. Hudimac, A. A., "Ray Theory Solution for the Sound Intensity in Water Due to a Point Source Above It," JASA, Vol. 29, No. 8, August, 1957, pp. 916-917.

4. Jackson, J. D., Classical Electrodynamics, (John Wiley and Sons, New York, 1966.)

5. Lysanov, Iu. P., "Theory of the Scattering of Waves at Periodically Uneven Surfaces," Soviet Physics-Acoustics, Vol. 4, No. 1, January-March, 1958, pp. 1-10.

6. Mashashvili, E. S. And Urusovskii, I. A., "Wave Diffraction at a Periodically Uneven Interface," Soviet Physics-Acoustics, Vol. 15, No. 1, July-September, 1969, pp. 79-85.

7. Park, B. K. and Erteza, A., "Reflection and Transmission of Dipole Radiation in Presence of an Extended Boundary, Rough and Smooth," University of New Mexico, Bureau of Engineering Research, Technical Report EE-159 (69), NASA - 027, March, 1969.

8. Strutt, J. W., (Lord Rayleigh), Theory of Sound, (Dover Publications, New York, 1945), Second Edition, Vol. II, p. 89.

9. Urusovskii, I. A., "Diffraction by a Periodic Surface", Soviet Physics-Acoustics, Vol. 10, No. 3, January-March, 1965, pp. 287-293.

10. Weinstein, M. S., "Wave Solution for Air-to-Water Sound Transmission", JASA, Vol. 37, No. 5, May, 1965, pp. 899-901.

APPENDIX A

EVALUATION OF AN INTEGRAL BY THE STATIONARY PHASE METHOD

Consider the integral

$$I = \int\int_{-\infty}^{\infty} \exp\left[\frac{i}{2}\left[\frac{\partial^2 \psi}{\partial k_{1x}^2}\right]_0 (k_{1x} - k_{1x}')^2 + \left[\frac{\partial^2 \psi}{\partial k_{1z}^2}\right]_0 (k_{1z} - k_{1z}')^2 \right.$$

$$\left. + 2\left[\frac{\partial^2 \psi}{\partial k_{1x}\partial k_{1z}}\right]_0 (k_{1x} - k_{1x}')(k_{1z} - k_{1z}')\right] dk_{1x} dk_{1z} \quad .$$

Making the substitutions

$$a = \left[\frac{\partial^2 \psi}{\partial k_{1x}^2}\right]_0 \qquad\qquad \alpha = k_{1x}'$$

$$b = \left[\frac{\partial^2 \psi}{\partial k_{1z}^2}\right]_0 \qquad\qquad B = k_{1z}'$$

and

$$c = \left[\frac{\partial^2 \psi}{\partial k_{1x}\partial k_{1z}}\right]_0 \qquad\qquad x = k_{2x}$$

$$y = k_{2z}$$

it can be rewritten as

$$I = \int\int_{-\infty}^{\infty} \exp\left[\frac{ia}{2}(x-a)^2 + \frac{b}{a}(y-B)^2 + 2\frac{c}{a}(x-a)(y-B)\right] dx dy \quad .$$

Completing the square within the braces and rearranging the result gives:

$$I = \int_{-\infty}^{\infty} \exp \frac{i}{2} \left[(y-B)^2 (b- \frac{c^2}{a}) \right] dy \int_{-\infty}^{\infty} \exp \frac{ia}{2} \left[(x-\alpha) + \frac{c}{a} (y-B) \right]^2 dx \; .$$

In the rightmost integral, make the substitution:

$$u = (x-\alpha) + \frac{c}{a} (y-B)$$

and the integral may be rewritten as

$$\int_{-\infty}^{\infty} e^{\frac{iau^2}{2}} du = 2 \int_{0}^{\infty} \left[\cos \frac{a}{2} u^2 + i \sin \frac{a}{2} u^2 \right] du$$

$$= 2 (1+i) \int_{0}^{\infty} \cos \frac{a}{2} u^2 \, du$$

$$= (1+i) \left(\frac{\pi}{a} \right)^{1/2} \; .$$

Substituting into the original equation, we have:

$$I = (1+i) \left(\frac{\pi}{a} \right)^{1/2} \int_{-\infty}^{\infty} \exp \frac{i}{2} \left[(y-B)^2 (b- \frac{c^2}{a}) \right] dy \quad .$$

In this equation, let

$$\frac{1}{2} (b- \frac{c^2}{a}) = \gamma$$

and introduce the change of variables

$$u = y-B \qquad ;$$

then

$$I = (1+i) \left(\frac{\pi}{a}\right)^{1/2} \int_{-\infty}^{\infty} e^{i\gamma u^2} \, du \qquad ,$$

which is

$$I = 2\pi i \, (2a\gamma)^{-1/2} \qquad ,$$

or, in terms of the original variables,

$$I = 2\pi i \left\{ \left[\frac{\partial^2 \psi}{\partial k_{1x}^2}\right]_0 \left[\frac{\partial^2 \psi}{\partial k_{1z}^2}\right]_0 - \left[\frac{\partial^2 \psi}{\partial k_{1x}\partial k_{1z}}\right]_0^2 \right\}^{-1/2} \qquad .$$

APPENDIX B

COMPUTER PROGRAM FOR NUMERICAL INTEGRATION
OF THE TRANSMISSION INTEGRAL

The digital program included in this Appendix was written to provide a means for numerically integrating the transmission integral (2.31). The method employed is that of carrying out the double summation suggested by the integral, using small x and y intervals whose size is set by specification of the parameter DELTA. The successive contributions to the final result are summed within the double DO loop using double precision arithmetic. Within the inner DO loop, the sign of the quantity in the Snell's law radical is checked and solutions representing negative values of this quantity are cast out since they represent cases in which incident rays make an angle with the normal to the surface which exceeds the critical angle.

One difficulty which can be foreseen with the use of this version of the program is the loss of accuracy which can occur when the "ray path lengths" $(k_1 R_0 + k_2 R_2)$ become very large. In such cases, it is well to restructure the computations made to account for relative phase delays at the receiver in order to avoid loss of precision in summing the various contributions to the magnitude of the total transmitted potential (or pressure).

```
C          NUMERICAL EVALUATION OF TRANSMISSION INTEGRAL
C
C
C          CALCULATION OF RATIO OF TRANSMITTED PRESSURE TO INCIDENT PRESSURE
C          FOR THE SOLUTION OF THE PROBLEM OF SOUND TRANSMITTED FROM A
C          MONOPOLE SOURCE THROUGH A CORRUGATED FLUID BOUNDARY
C               J.MACALUSO  URL   10/17/69  VERSION 3
C
C
C          INPUT UNITS ARE TO BE SUPPLIED IN FT,LBS,FT/SEC,LBS/FT**2,KHZ &
C          DEGREES. APPROPRIATE UNIT CONVERSIONS ARE MADE BY THE PROGRAM.
C
C                  LIST OF SYMBOLS FOR PRINCIPAL VARIABLES
C
C
C               SYMBOL                  DESCRIPTION OR EQUATION
C
C               ANS             RECEIVED PRESSURE AMP RE SOURCE AMP
C               ANS1            20*LOG(ANS)
C               C1              VELOCITY OF PROPOGATION-MEDIUM 1
C               C2              VELOCITY OF PROPOGATION-MEDIUM 2
C               DELTA           X AND Y INTERVAL SIZE
C               FREQ            FREQUENCY OF SOURCE
C               GAMMA           CORRUGATION PHASE ANGLE
C               H               CORRUGATION AMPLITUDE
C               NX              NUMBER OF GRID POINTS IN X DIRECTION
C               NZ              NUMBER OF GRID POINTS IN Z DIRECTION
C               PHASE           SOURCE TO RECEIVER PHASE CHANGE
C               RHO1            DENSITY OF MEDIUM 1
C               RHO2            DENSITY OF MEDIUM 2
C               RO              DISTANCE FROM SOURCE TO INTERFACE
C               R2              DISTANCE FROM INTERFACE TO RECEIVER
C               SRCHT           SOURCE HEIGHT
C               T               PERIOD OF CORRUGATION
C               WS              = TWOPI/T
C               XI,ZI           VARIABLES OF INTEGRATION
C               XSTRT           INITIAL VALUE OF X
C               YZERO           = H*COS(WS*XI-GAMMA)
C               X2,Y2,Z2        RECEIVER COORDINATES
C               ZSTRT           INITIAL VALUE OF Z
C
C
      REAL K1,K2
      REAL*8 TMAG1,TMAG2
      NAMELIST/DATIN/RHO1,C1,RHO2,C2,H,T,GAMMA,SRCHT,DELTA,XSTRT,ZSTRT,
     1FREQ,NX,NZ/RCVRPT/X2,Y2,Z2,X2IN,Y2IN,Z2IN/OUT/ANS,ANS1,TMAG1,TMAG2
     2,EPHSE
    1 READ(5,2) RHO1,C1,RHO2,C2,H,T,GAMMA,SRCHT,DELTA,XSTRT,ZSTRT,FREQ,
     1NX,NZ
    2 FORMAT(12F5.1,2I5)
      WRITE(6,DATIN)
      TWOPI=2.*3.1415926
      FREQ=FREQ*1000.
      WS= TWOPI/T
      GAMMA= GAMMA*(TWOPI/360.)
      CRATIO= C2/C1
    3 READ(5,4)X2,Y2,Z2
    4 FORMAT(3F10.3)
      X2IN=X2*12.
      Y2IN=Y2*12.
      Z2IN=Z2*12.
```

```
      WRITE(6,RCVRPT)
  5  IF(Y2.EO.0.) STOP
      K1= (TWOPI*FREO)/C1
      K2= (TWOPI*FREO)/C2
  6  TMAG1=0.
      TMAG2=0.
  7  DO 8 I=1,NX
      XI= XSTRT + I*DELTA-DELTA/2.
      YZERO = H*COS(WS*XI-GAMMA)
      DYZRO= WS*H*SIN(WS*XI-GAMMA)
      FCTR1= (SRCHT-YZERO-XI*DYZRO)
      FCTR1P = FCTR1**2
      DO 8 J=1,NZ
      ZI= ZSTRT + J*DELTA-DELTA/2.
      RO2= (XI**2+ZI**2+(YZERO-SRCHT)**2)
      R2 = SORT((X2-XI)**2+(Z2-ZI)**2+(Y2-YZERO)**2)
      RO=SORT(RO2)
      FCTR2= RO2*(1.+DYZRO**2)
      RADICL= (1.-CRATIO**2)*(FCTR2/FCTR1P)+ CRATIO**2
      IF(RADICL.LT.0. )GO TO 8
      FCTR3= RHO2*C2+ RHO1*C1*SORT(RADICL)
      FCTR4=  (FCTR1/(RO*SORT(1.+DYZRO**2)))+ 1.0
      DELMG= ((FCTR4*(DELTA**2))/(RO*R2*FCTR3))*SORT(1.+DYZRO**2)
      PHASE = K1*RO+ K2*R2
      PHASE= AMOD(PHASE,TWOPI)
      TMAG1= TMAG1+ DELMG*COS(PHASE)
      TMAG2= TMAG2 + DELMG*SIN(PHASE)
  8  CONTINUE
      FPHSE= TMAG2/TMAG1
      FPHSE= ATAN(FPHSE)
      FPHSE= AMOD(FPHSE,TWOPI)
      FPHSE=FPHSE*(360./TWOPI)
      ANS=  RHO2*FREO*DSORT(TMAG1**2+TMAG2**2)
      ANS1= (ALOG10(ANS))*20.
      WRITE(6,OUT)
      GO TO 3
      END
```

APPENDIX C

COMPUTER PROGRAM FOR EVALUATION OF
APPROXIMATE CLOSED-FORM SOLUTION OF
TRANSMISSION INTEGRAL

The digital program included in this Appendix was written to facilitate evaluation of the roots of the stationary phase relations, Equation (2.39) and (2.40), for the specific case $z_2=0$ and thereby to compute the transmitted pressure. This particular program obtains the stationary phase points in two stages or steps. First, an estimate of the locations of the roots is found by checking the sign of the result for Equation (2.39) as x_m is varied from a starting value, XSTRT, to its final value, XSTOP, at intervals of DELTAX. Possible real roots are indicated, and their values stored in vector ROOTS(I), when particular successive values of x_m cause the left-hand side of Equation (2.39) to vanish or to alternate in sign. After all the possible approximate roots are catalogued in this way, these roots are more closely approximated by the use of subroutine RTWI as the second step in their evaluation. After locating all the points of stationary phase, the program evaluates the total potential at the observation point $(x_2, y_2, 0)$ by summing the individual contributions using Equation (2.41). Finally, the total transmitted pressure is calculated in decibels and presented as output.

```
C      EVALUATION OF POINT-SOURCE CORRUGATED INTERFACE SOLUTION BY
C      GEOMETRICAL OPTICS APPROXIMATION OF TRANSMISSION INTEGRAL
C      SURFACE EQUATION IS   YO=H*COS(WS*X-GAMMA)
C      SOURCE POSITIONED DIRECTLY OVER ORIGIN
C      RECEIVER IN X-Y PLANE
C      J.MACALUSO  ORL  11/20/69  VERSION 3  MOD 1 11/22/69
C
C                         LIST OF SYMBOLS FOR PRINCIPAL VARIABLES
C
C          SYMBOL                     DESCRIPTION OR EQUATION
C
C          C1                    VELOCITY OF MEDIUM 1
C          C2                    VELOCITY OF MEDIUM 2
C          D                     RECEIVER DEPTH
C          DELTAX                INCREMENT OF X FOR ROOT SEARCH
C          F                     FREQUENCY
C          GAM                   CORRUGATION PHASE ANGLE(DEG)
C          GAMMA                 CORRUGATION PHASE ANGLE(RAD)
C          H                     HEIGHT OF CORRUGATION
C          ITER                  NUMBER OF ITERATIONS IN RTWI
C          K1                    WAVENUMBER IN MEDIUM 1
C          K2                    WAVENUMBER IN MEDIUM 2
C          NN                    C2/C1
C          PHASE                 SOURCE TO REC PHSE ANGLE FOR XM
C          PHITOT                TOTAL (REL) PRESSURE AT RECEIVER
C          PHIRE                 INTERMEDIATE VALUE OF POTENTIAL(RE PT)
C          PHIIM                 INTERMEDIATE VALUE OF POTENTIAL(IM PT)
C          RHO1                  DENSITY OF MEDIUM 1
C          RHO2                  DENSITY OF MEDIUM 2
C          ROM                   DISTANCE FROM SOURCE TO STAT PHSE PT
C          ROOT(I)               I'TH APPROXIMATE ROOT
C          R2M                   DISTANCE FROM RECEIVER TO STAT PHSE PT
C          SRCHT                 SOURCE HEIGHT
C          T                     PERIOD OF CORRUGATION
C          WS                    2*PI/T
C          XMP                   TRIAL VALUE OF X IN ROOT SEARCH
C          XM                    MOST ACCURATE VALUE FOR I'TH ROOT
C          XSTRT                 STARTING VALUE OF X FOR ROOT SEARCH
C          XSTOP                 FINAL VALUE OF X FOR ROOT SEARCH
C          YZERO                 VALUE OF Y AT CCORDINATE XM
C
       DIMENSION ROOTS(50)
       REAL K1,K2,NN,NN2
       COMMON NN,WS,H,GAMMA,SRCHT,D,X2
       EXTERNAL  FCT
       NAMELIST/DATIN/RHO1,C1,RHO2,C2,T,H,SRCHT,D,F,  GAM  ,ITER ,XSTRT,
      1XSTOP,DELTAX,X2
     1 READ(5,2)RHO1,C1,RHO2,C2,T,H,SRCHT,F,GAM  ,ITER
     2 FORMAT(9F5.1,2I5)
     3 IF(RHO1.EQ.0.)STOP
       PI=3.1415926
       GAMMA=GAM*(PI/180.)
   301 READ(5,300) D,XSTRT,XSTOP,DELTAX,X2
   300 FORMAT(5E10.3)
       WRITE(6,DATIN)
       IF(D.EQ.0.) GO TO 1
       TWOPI= 2.*PI
       WS=TWOPI/T
       B=(WS**2)*H
       K1= (TWOPI*F*1000.)/C1
```

```
      K2= (TWOPI*F*1000.)/C2
      NN=C2/C1
      NN2=NN**2
      PHIRE=0.
      PHIIM=0.
      IDX=0
      NX=(XSTOP-XSTRT)/DELTAX +1.
      XMP=XSTRT-DELTAX
      DO 100 I=1,NX
      XMP=XMP+DELTAX
      XMPP1=XMP+DELTAX
      Y1=FCT(XMP)
      Y2=FCT(XMPP1)
      IF((XMP-Y1)*(XMPP1-Y2))101,101,100
  101 IDX=IDX+1
      ROOTS(IDX)=XMP+DELTAX/2.
      IF(IDX.EQ.1)GO TO 100
      IF(ROOTS(IDX)-ROOTS(IDX-1).GT.1.5*DELTAX)GO TO 100
      IDX=IDX-1
      ROOTS(IDX)=ROOTS(IDX)+DELTAX/2.
  100 CONTINUE
      DO 105 KK=1,IDX
  105 WRITE(6,106) KK,ROOTS(KK)
  106 FORMAT(1H ,I3,'APPROXIMATE ROOT FOUND AT XM=',E10.3)
      DO 8 J=1,IDX
      XMP=ROOTS(J)
      CALL RTWI(XM,VAL,FCT,XMP,1.E-06,ITER,IER)
      IER=IER+1
      GO TO(501,502,503),IER
  502 WRITE(6,512)XM,XMP
  512 FORMAT(1H0,'NO CONVERGENCE, XM=',E10.3,'XMP=',E10.3)
      GO TO 410
  503 WRITE(6,513)
  513 FORMAT(1H0,'DENOMINATOR=0.,I.E. FNCN DERIVATIVE=1,CANNOT CONTINUE
     1GO TO NEXT RECEIVER POINT')
      GO TO 301
  501 WRITE(6,511) VAL,XM,XMP
  511 FORMAT(1H ,'VAL OF X-F(X) AFTER CONVERGENCE=',E10.3,'XM=',E10.3,
     1'XMP=',E10.3)
      HT=SRCHT-H*COS(WS*XM -GAMMA)
  411 XM2=XM**2
      DD=D+H*COS(WS*XM-GAMMA)
      ROM2= XM2+HT**2
      R2M2=(X2-XM)**2+DD**2
      ROM=SQRT(ROM2)
      R2M=SQRT(R2M2)
      YZERO=H*COS(WS*XM-GAMMA)
      YP=WS*H*SIN(WS*XM-GAMMA)
      YP2=YP**2
      RADICL=  (((1.-NN2)*ROM2*(1.+YP2))/((    HT-XM*YP)**2))+NN2
      IF(RADICL.GE.0.) GO TO 11
  410 PHITOM=0.
      GO TO 12
   11 RADICL= SQRT(RADICL)
      FCTR1= RHO2*C2+RHO1*C1*RADICL
      FCTR2= (1.+(    HT-XM*YP)/(ROM*SQRT(1.+YP2)))*SQRT(1.+YP2)
      FCTR3=(NN/ROM)*(1.+HT*YZERO*(WS**2)+YP2-((XM+HT*YP)**2)/ROM2)
      FCTR4=(1.-DD*(WS**2)*YZERO+YP2-((XM-X2-DD*YP)**2)/R2M2)/R2M
      D2BDX= FCTR3+FCTR4
      D2BDZ = NN/ROM + 1./R2M
```

```
      FCTR5 = D2BDX*D2BDZ
      FCTR5= ABS(FCTR5)
      FCTR5= SQRT(FCTR5)
      PHITOM = (RHO1*C2*FCTR2)/(FCTR1*FCTR5*ROM*R2M)
    9 PHASE = K1*ROM+K2*R2M
      PHASE = AMOD(PHASE,TWOPI)
      PHIRE= PHITOM*COS(PHASE) + PHIRE
      PHIIM= PHITOM*SIN(PHASE) + PHIIM
   12 PHITOT= SQRT(PHIRE**2+PHIIM**2)
      IF(PHITOT.NE.0.)GO TO 10
      PHITOT=-9.99E+09
      GO TO 401
   10 PHITOT = 20.*ALOG10((RHO2*PHITOT)/RHO1)
  401 WRITE(6,6)  J,PHITOT
    6 FORMAT(1H0,'REL PRESS LVL WITH',I5,'ORDER CORRECTION TERM IS',
     1E10.3,'DB'///)
      IF(H.EQ.0.) GO TO 301
    8 CONTINUE
      GO TO 301
      END
      REAL FUNCTION FCT(X)
      REAL K1,K2,NN,NN2
      COMMON NN,WS,H,GAMMA,SRCHT,D,X2
      HPRME= SRCHT-H*COS(WS*X-GAMMA)
      DPRME=-D-H*COS(WS*X-GAMMA)
      ROMP=SQRT(X**2+HPRME**2)
      R2MP=SQRT((X2-X)**2+DPRME**2)
      YPRME=WS*H*SIN(WS*X-GAMMA)
      FCTR1=-(NN*HPRME*YPRME*R2MP)/(NN*R2MP+ROMP)
      FCTR2=(DPRME*YPRME*ROMP)/(NN*R2MP+ROMP)
      FCTR3=(X2*ROMP)/(NN*R2MP+ROMP)
      FCT=FCTR1-FCTR2 +FCTR3
      RETURN
      END
```

1. ORIGINATING ACTIVITY (Corporate author)	2a. REPORT SECURITY CLASSIFICATION
Ordnance Research Laboratory	UNCLASSIFIED
University Park, Pennsylvania	2b. GROUP ___

3. REPORT TITLE

ON THE TRANSMISSION OF SOUND FROM A MONOPOLE SOURCE THROUGH A FINITE, CORRUGATED BOUNDARY BETWEEN FLUID MEDIA

4. DESCRIPTIVE NOTES (Type of report and inclusive dates)

Technical Memorandum, February 9, 1970

5. AUTHOR(S) (First name, middle initial, last name)

J. A. Macaluso

6. REPORT DATE	7a. TOTAL NO. OF PAGES	7b. NO. OF REFS
February 9, 1970	124	10

8a. CONTRACT OR GRANT NO.	9a. ORIGINATOR'S REPORT NUMBER(S)
N00017-70-C-1407	TM 214-02
b. PROJECT NO.	
c.	9b. OTHER REPORT NO(S) (Any other numbers that may be assigned this report)
d.	None

10. DISTRIBUTION STATEMENT

Distribution of this document is unlimited

11. SUPPLEMENTARY NOTES	12. SPONSORING MILITARY ACTIVITY
Ph. D. Thesis	Office of Naval Research (Code 461) Department of the Navy

13. ABSTRACT

 This investigation was undertaken with the objective of developing techniques for solving the problem of sound transmission from a harmonic monopole source through a finite, corrugated boundary between fluid media and to corroborate these techniques by means of laboratory data obtained for the important case of air-to-water sound transmission.

 Using a form of the Kirchoff radiation integral, expressions were derived describing both the reflected and transmitted acoustic potentials due to the scattering of monopole sound at a corrugated boundary between fluids.

 For the case of sound transmission through the boundary, the integral expression was reduced to an approximate closed-form solution which is valid in the limit of geometrical optics and for extended interface geometries for which the tangent plane approximation is applicable.

 Empirical data was obtained using four different laboratory models of corrugated (sinusoidal) surface sections designed to float on the surface of an anechoic tank so as to simulate different corrugated air-water boundaries. Numerous comparisons of theoretical results with experimental data obtained by loudspeaker insonification of these model surfaces demonstrated the suitability of the theory and illustrated the inaccuracies which arise in cases for which the tangent plane approximation is unsuitable.

DD FORM 1473, 1 NOV 65

14. KEY WORDS	LINK A		LINK B		LINK C	
	ROLE	WT	ROLE	WT	ROLE	WT
Acoustics	8					
Boundary layer	8					
Calibration	8					
Integral equations	8					
Numerical integration	8					
Optics	8					
Reflection	8					
Scattering	8					
Sound transmission	8					
Surface properties	8					
Underwater sound	8					